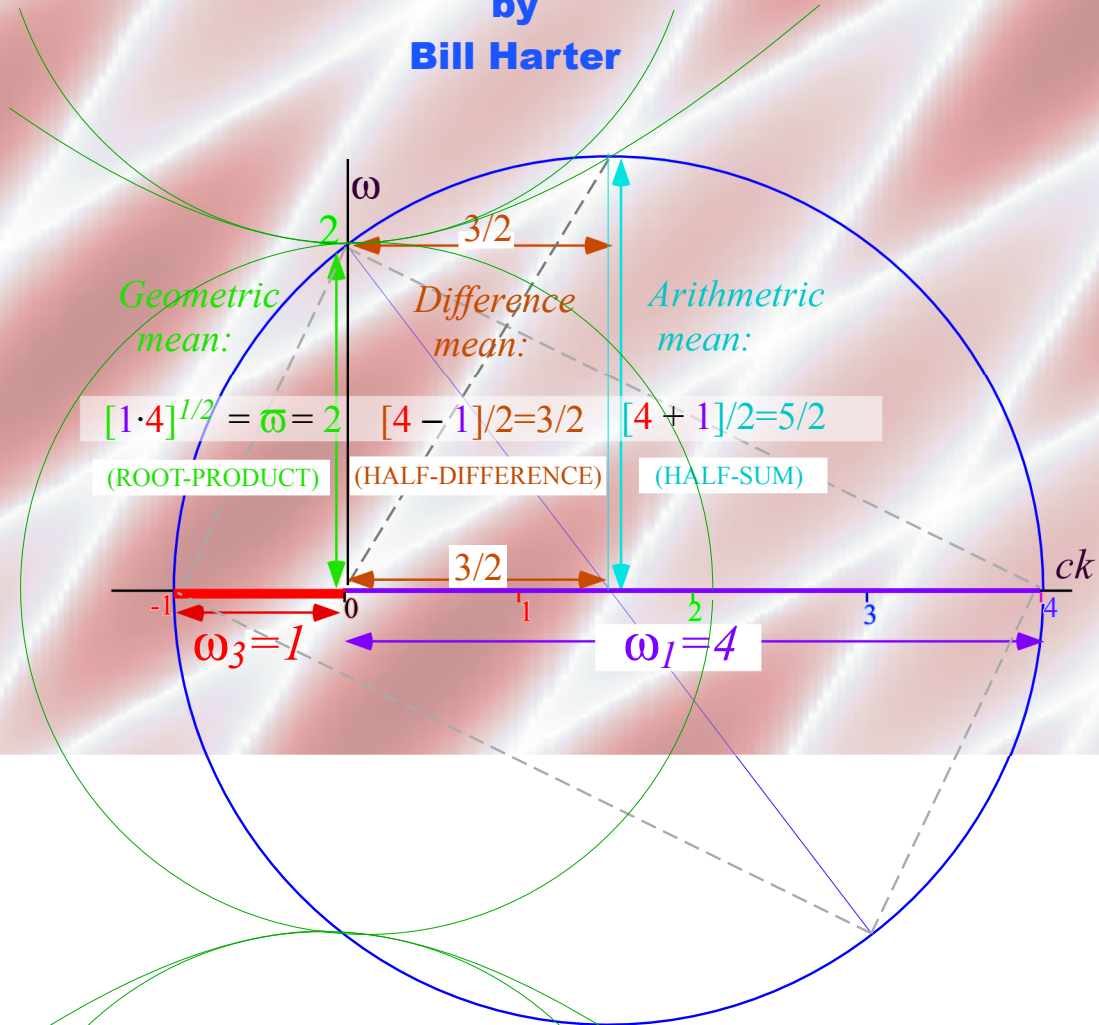


# Unit 8. Relativity and Quantum Theory

**Classical Mechanics with a Bang!**

by  
**Bill Harter**

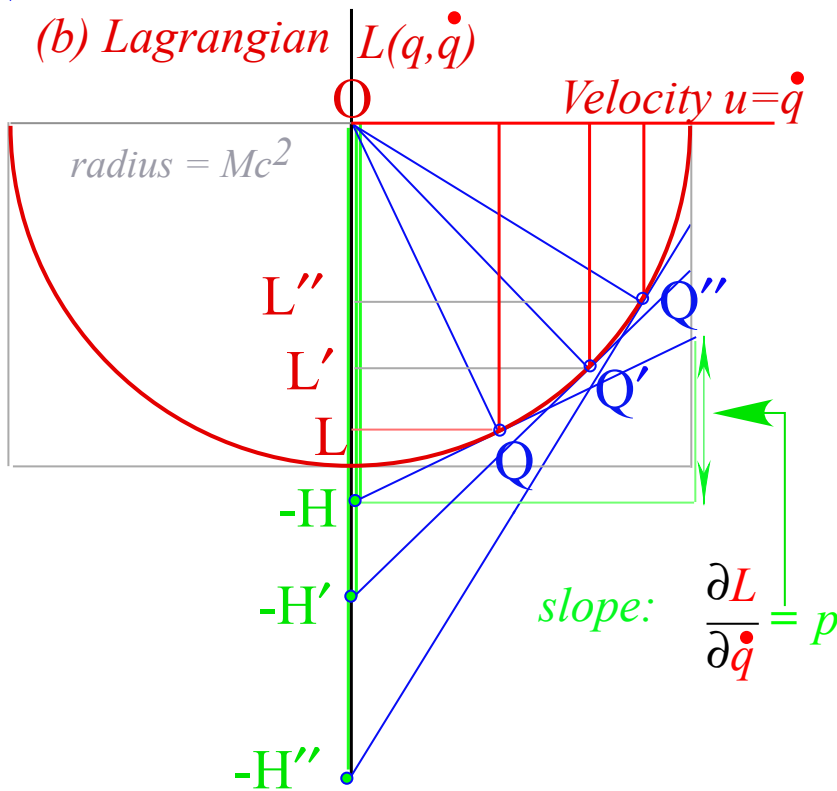
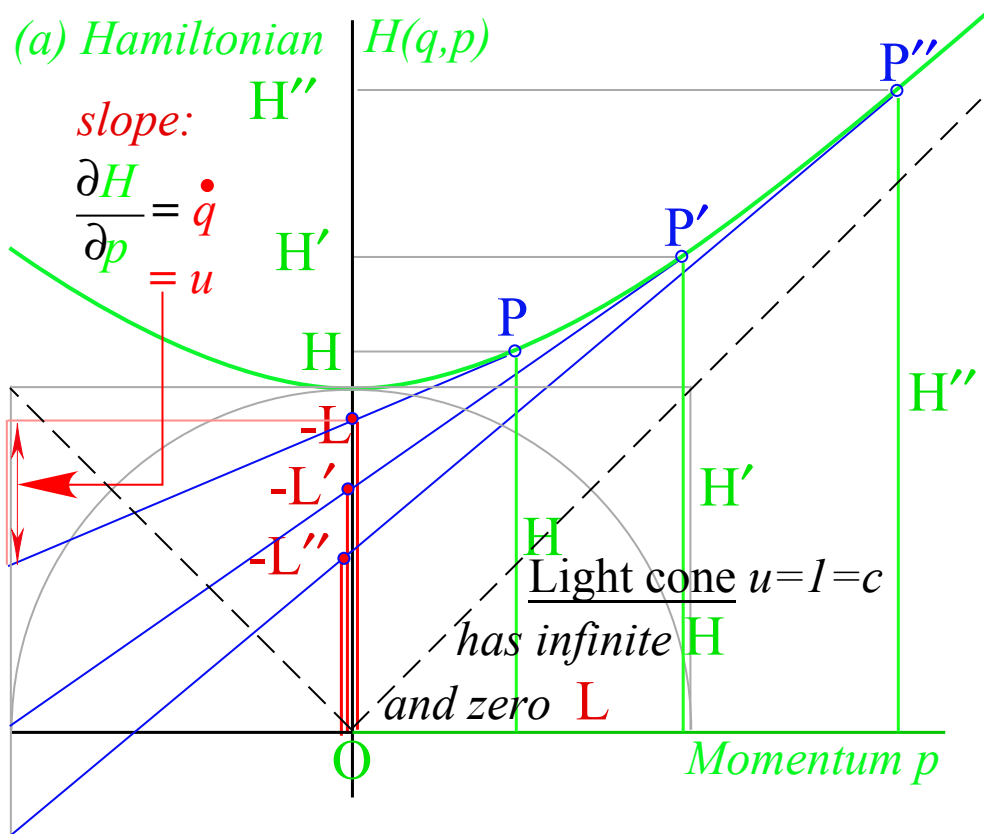


**Department of Physics - University of Arkansas - Fayetteville**

*Hardware and Software by*

**HARTER - Soft**

*Elegant Educational Tools Since 2001*



Legendre contact transformation for relativistic mechanics

Classical Mechanics with a BANG! – Unit 8 Table of Contents

**UNIT 8. RELATIVITY AND QUANTUM THEORY .....5**

**Introduction .....5**

    Review and plan of attack: Relativity of pairs.....6

**Chapter 1 Continuous Wave (CW) vs. Pulse Wave (PW) functions.....9**

    Phase velocity for 1-CW .....9

    Axioms for light: 2-CW vs. 2-PW.....9

        Astronomical view of CW axiom .....11

        Spectroscopic view of CW axiom .....11

        Time reversal axiom .....13

        Phase invariance axioms viewed in a classical way .....13

        CW squares vs. PW diamonds in space-time plots.....15

        CW wave-zeros vs. PW pulse paths.....15

        Comparing wave-like vs particle-like behavior.....16

    Wave-zero (WZ) and pulse-peak (PP) space-time coordinate grids.....18

**Chapter 2 When Light Waves Collide: Relativity of waves in spacetime.....23**

    CW-Doppler derivation of relativity.....23

        First things first.....25

        Lorentz-Einstein transformations .....27

        Geometry of Lorentz-Einstein contraction-dilation.....27

**Chapter 3. Invariance and Relative Phase: Galileo’s revenge.....29**

    Geometry of relative phase.....30

    Geometry of Doppler factors .....31

    Doppler rapidity and Euclid means business.....33

    Invariance of proper time (age) and frequency (rate of aging).....35

**Chapter 4. Mechanics based on CW axioms.....41**

    Quantized cavity modes and “fuzzy” hyperbolas .....42

    Alternative definitions of wave mass.....43

    Absolute vs. relative phases: Method in madness .....44

**Chapter 5. Classical vs. quantum mechanics.....47**

    Contact transformation geometry of a relativistic Lagrangian.....48

    Geometry of circular and hyperbolic functions.....51

        Hyper-circular contacts.....53

    Transverse vs. longitudinal Doppler: Stellar aberration .....55

        Graphical wave 4-vector transformation .....57

        Symmetry and conservation principles.....59

        1st and 2nd Quantization: phase vs. amplitude.....60

**Chapter 6. Variation and quantization of optical amplitudes .....61**

    Maxwell amplitudes and energy.....65

    Quantized optical fields .....65

    Relativistic 1-CW covariance of Poynting flux.....66

Relativistic 2-CW invariance of cavity quanta .....	66
N-Photon vs Coherent- $\alpha$ -states .....	69
Fuzzy hyperbolas vs. fuzzy coordinates .....	69
Deeper symmetry aspects of pair creation .....	70
<b>Chapter 7. Compton Effects and Optical Transitions.....</b>	<b>71</b>
1-photon kinematics for emission and absorption of light .....	71
The kicker: Recoil shifts .....	71
This is not rocket science! (Or is it?) .....	71
2-photon processes: Rayleigh-Thompson-Compton scattering .....	73
Car 54 where are you? .....	73
Suspended 2-photon diamonds .....	73
Feynman’s Father’s query .....	75
Photo-absorption and Compton effects .....	75
Compton-Doppler staircase .....	77
Compton wavelength sum rule .....	78
Geometric transition series .....	79
Optical PW bounce and accordian-like CW shifts .....	79
<b>Chapter 8. Wave Frame Acceleration .....</b>	<b>81</b>
Chirping and Einstein elevators .....	81
Constant velocity gives constant acceleration .....	84
Wave geometry vs. Newton .....	84
Pair creation and quantum frames. ....	84
References .....	87
Acknowledgements .....	87
-- The Purest Light and a Resonance Hero – Ken Evenson (1932-2002) -- .....	88

## Unit 8. Relativity and Quantum Theory

### Introduction

Preceding Units 1 thru 4 on mechanics and wave resonance are prerequisites to modern physics of *spacetime relativity* and *quantum wave mechanics* introduced here in Unit 8. A wave based geometric approach helps to understand special relativity (SR) and quantum mechanics (QM) while it shows that these two pillars of modern physics are actually belong to *the same subject!*

SR and QM have been treated in separate texts as different and even inimical subjects. (SR is most often found in E&M texts.) While advanced quantum field theory treatments do integrate special relativity they do it in a mathematical way that lacks lucidity and physical intuition. The present development seeks to improve the situation by appealing to the detailed geometry of wave interference.

Separated introductions to SR and QM lead to misconceptions for professional physicists as well as for their students. In spite of its simple algebra, SR is also regarded as mysterious. Student comments for SR and QM courses are typically, “Well, I didn’t understand it, but neither did the prof!” Comments on a QM and SR derivation by an editor of the *Journal of Modern Optics* in 2003 illustrate the problem:

“Even Schrodinger probably never claimed to have a derivation, and *we* certainly don't tell *our* students that *we* have one. (A) *Hand-waving, inspired guess is more like it.*”

A key problem has been a failure to clarify wave mechanics. Consider the editor’s next comment.

“It is quite arbitrary how one defines envelope and carrier parts of a wave. Usually this is done only when all frequencies are nearby and all k-vectors are nearby. Then something like the analytic signal formulation can be used to arrive at unique but still arbitrary definition.”

This statement exposes a pernicious blind spot in conventional wave analysis. Its resolution uses Unit 4 *expo-cosine* relations in (4.3.30) to clearly separate a wave envelope from its “carrier” phase.

$$\begin{aligned} \psi_+ &= e^{ia} + e^{ib} \\ &= e^{\frac{i(a+b)}{2}} \left( e^{\frac{i(a-b)}{2}} + e^{-\frac{i(a-b)}{2}} \right) \quad (4.3.30) \text{ repeat } a \\ &= 2e^{\frac{i(a+b)}{2}} \cos \frac{a-b}{2} \end{aligned} \qquad \begin{aligned} \psi_- &= e^{ia} - e^{ib} \\ &= e^{\frac{i(a+b)}{2}} \left( e^{\frac{i(a-b)}{2}} - e^{-\frac{i(a-b)}{2}} \right) \quad (4.3.30) \text{ repeat } b \\ &= 2ie^{\frac{i(a+b)}{2}} \sin \frac{a-b}{2} \end{aligned}$$

These are true regardless of how “nearby” are arguments  $a=(k_ax-\omega_at)$  or  $b=(k_bx-\omega_bt)$  or their constituent frequency-time  $\omega_{a,b}t$  and wavevector-space  $k_{a,b}x$  terms. Identities (4.3.30) separate a wave’s *modulus* or *group envelope* embodied by the cosine or sine factor that defines the outside envelope or “skin” of a wave sketched in the figure below. The modulus is the factor that remains in the expression  $\psi^*\psi$  for intensity while the phase part  $e^{i(a+b)/2}$  of  $\psi$  cancels the  $e^{-i(a+b)/2}$  of  $\psi^*$  leaving real intensity  $|\psi|^2$  or MOD  $|\psi|$ .

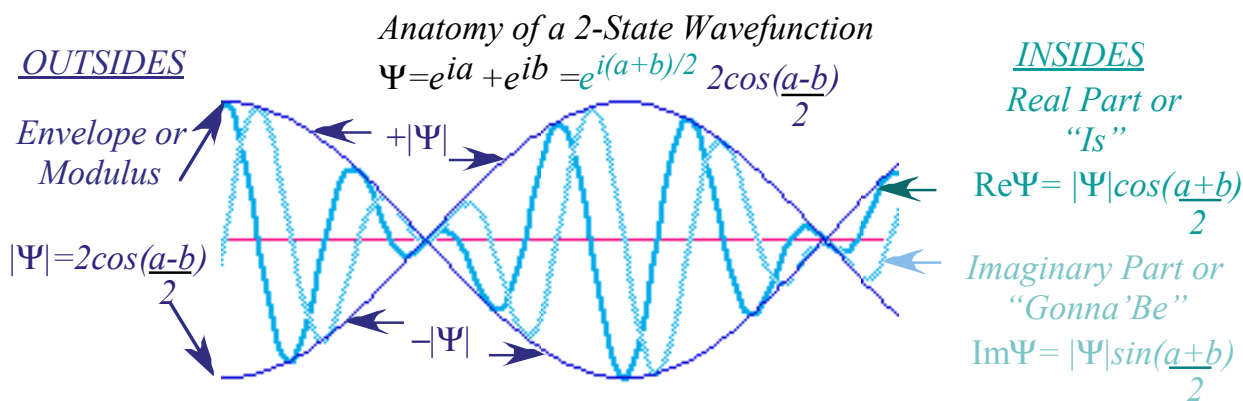
$$MOD(\psi_{\pm}) = |\psi_{\pm}| = \sqrt{\psi_{\pm}^* \psi_{\pm}} = \begin{cases} \cos\left(\frac{a-b}{2}\right) & \text{for } \psi_+ \\ \sin\left(\frac{a-b}{2}\right) & \text{for } \psi_- \end{cases}$$

Envelope is thus distinguished from a wave’s *argument* or *overall phase* held by exponential factor  $e^{i(a+b)/2}$ .

$$ARG(\psi_{\pm}) = ATN \frac{\text{Im}\psi_{\pm}}{\text{Re}\psi_{\pm}} = \begin{cases} \left(\frac{a+b}{2}\right) & \text{for } \psi_+ \\ \left(\frac{a+b}{2} + \frac{\pi}{2}\right) & \text{for } \psi_- \end{cases}$$

The latter governs real (Re  $\psi$ ) and imaginary (Im  $\psi$ ) “carrier” parts that are the inside “guts” of the wave shown in the sketches below. (One may imagine a boa constrictor that has swallowed live prey.)

The speed of the  $MOD(\psi_{\pm})$  wave factor is called *group velocity*. This external “skin” of the wave is the only part visible to probability or intensity measurements of  $\psi^* \psi$ . Meanwhile the speed of exponential phase factor inside the envelope is called *mean phase velocity* or just plain *phase velocity*. Internal phase “guts” may oscillate very rapidly and be difficult or impossible to measure directly.



*Review and plan of attack: Relativity of pairs*

Our plan of attack in Unit 3 for relativity and quantum theory has similar philosophy to that of Unit 1 for classical Newtonian mechanics and Unit 4 for resonance. The idea is to develop the axioms, rules, or laws of physics using *relativity of elementary pairs*. It is a kind of Occam-razor philosophy.

In Unit 1 we began with collisions between a pair of cars or a pair of bouncing super-balls and developed the rules of classical mechanics. In Unit 4 we used a pair of coupled pendulums to establish the rules of resonant energy transfer. Here in Unit 8 we use a pair of light waves to find the rules of relativity and quantum mechanics. Geometry is a key part of this analysis as before.

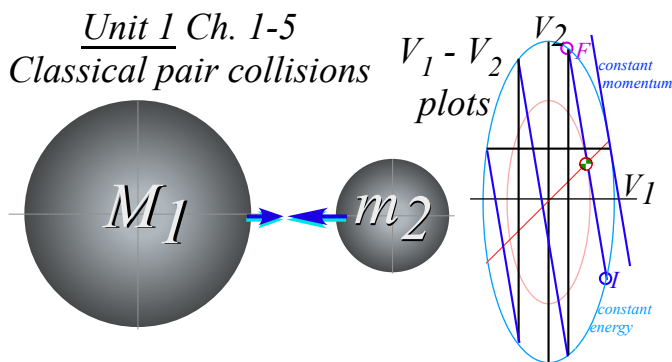
At first, the approach seems almost childish in simplicity. Who hasn’t seen (or been) a child who puts two beetles together to see if they will fight (or whatever)? Relation between pairs is something that first comes to mind when we see new things. Unfortunately, human egocentricity steers us toward a more complicated pair, a *single* thing and *you*. That’s the *adult* analytic approach, isn’t it?

Conventional “adult” mechanics books begin with axioms for a single mass or “particle” acted on by “outside forces” (presumably *you*) to move according to Newton laws 1 thru 3. Detailed treatment of all these laws at the start is usually not a favorite pastime for either instructor or student. The algebra or calculus is tedious and it is difficult at first to arrange neat compelling and demonstrative experiments.

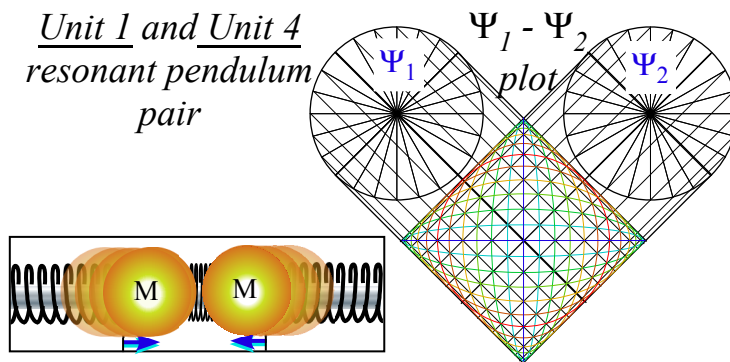
In contrast, Unit 1 starts off with just a single axiom (Newton law-1 of momentum conservation) for particle-*pair* mechanics and derives collision kinematics by simple geometry using velocity-velocity  $V_1$ - $V_2$  plots. This clearly exposes Galilean relativity symmetry and the logic of  $m_1V_1+m_2V_2$  conservation. An almost child-like geometric simplicity of particle-*pair* relativity economizes the logic.

Pair relativity easily finds results for neat first-day experiments by ignoring (until later) the “you” and your “outside force.” Energy conservation is then proved using  $V_1$ - $V_2$  geometry and time symmetry. An autonomous one-pair-at-a-time mechanics leads later to multi-mass force and potential relations that also have an Occam-cut-to-the-chase logic that may be derived using plane geometry.

Unit 1 Ch. 1-5  
Classical pair collisions

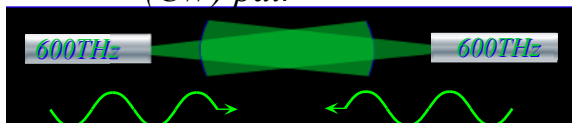


Unit 1 and Unit 4  
resonant pendulum pair

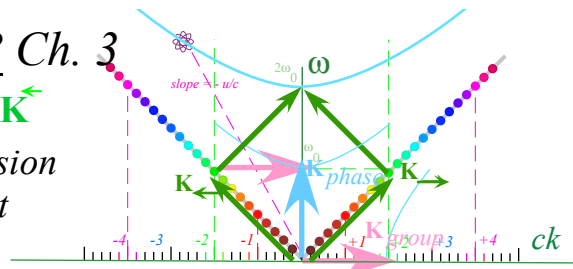


In Unit 4, resonance mechanics is based on autonomous pairs of coupled pendulums described by phasor-pair plots of  $x_1$ - $V_1$  versus  $x_2$ - $V_2$  or complex  $\Psi_1$  versus  $\Psi_2$  plots. Again, the key idea is *pair-relative*. Energy transfer rate is the product ( $|\Psi_1||\Psi_2|\sin \rho$ ) of phasor amplitudes and sine of *relative* phase angle  $\rho$ . Autonomous one-phasor-pair-at-a-time mechanics have a direct cut-to-the-chase geometric logic that then leads to multi-phasor wave mechanics, Fourier spectral analysis, and dispersion relations. Very important is a logic for complex pairs of numbers and for  $U(2)$  pairs of complex phasors in the study of resonance.

Unit 8 Ch. 1  
laser continuous wave  
(CW) pair



Unit 8 Ch. 3  
 $\vec{K} - \vec{K}$   
dispersion plot



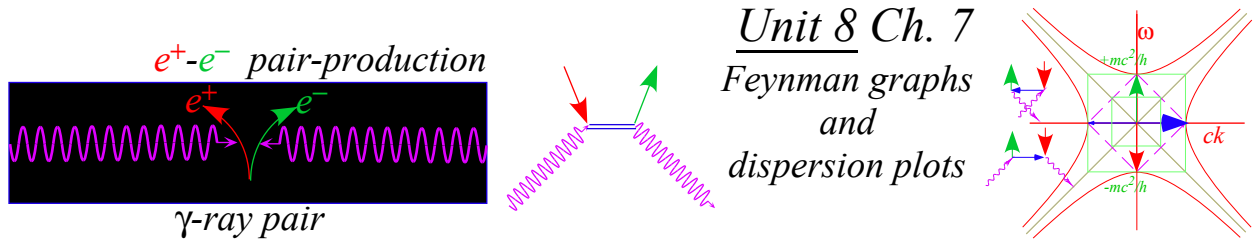
In Unit 8, the protagonists are a pair of colliding (counter-propagating) laser continuous waves (CW). Here we contemplate what happens at the micron level in the collision region of two bluish green beams of  $600 THz$  dye laser, and arrive at an extraordinary claim. A pair of CW light beams can show the rules of classical mechanics, quantum mechanics, and special relativity.

What a claim! These green beams can expose the fundamental logic of three hard physics courses CM, QM, and SR all for a fraction of the price one of them. And, like the late night TV ad, that’s not all! For just a little more you can get EM (electro-magnetism) thrown into the bargain.

How can it be possible to conjure rules about mechanics of mass *particles* from light *waves*? A 1939 theory by Dirac and a 1950 experiment by Anderson provide some advance motivation for such thought-experimentation. What Dirac theorized and Anderson demonstrated are results of colliding two high-energy light beams. Crossing two gamma-( $\gamma$ )-ray beams can convert light to matter *plus anti-matter* in  $\gamma + \gamma$  *electron-positron pair production* reactions. This primal chemistry is denoted as follows.

$$\gamma + \gamma \leftrightarrow e^- + e^+$$

The idea that  $0.51\text{MeV}$   $\gamma$ -rays can produce positronium pairs is taken for granted by many high-energy physicists, but it should be a mind-boggling Genesis-moment for any thinking student of physics.



Unit 8 Ch. 7  
Feynman graphs  
and  
dispersion plots

Now green  $600\text{ THz}$  lasers do not produce positronium matter. The  $\gamma$ -frequency  $mc^2/h = 0.1\text{ ExaHz}$  is about a million times more than our lasers can go. (That’s just as well given current world politics!) But, *any* two lasers can produce something that obeys *symmetry conditions* for matter waves, and it is those symmetry “laws” and geometry that underlie *all* our mechanics whether classical, quantum, relativistic, or electromagnetic. CW laser beams may not *be* matter but they do expose some of its kinematics.

Ideal CW-laser pairs help us derive fundamental relativistic or quantum concepts and formulas by ruler and compass in just a few steps. A number of concepts, quantities, and relations are exposed in Unit 3 by wave geometry. These include longitudinal Doppler shifts, Einstein-Lorentz-Minkowski frames, time dilation, length contraction, stellar aberration, transverse Doppler effects, mass-energy-momentum dispersion relations, Legendre-Lagrange-Hamilton-Poincare relativistic contact transformations, Compton recoil shifts, Compton scattering, polarization and spin transformation, acceleration by frequency chirps, Einstein wave-elevators, and quantum count-rate covariance.

According to a historical footnote given to me by Dudley Herschbach, Einstein became fascinated with ruler and compass geometry when he was just five years old. We can only guess the age Euclid was when he first picked up a Babylonian compass. In any case, a ruler and compass is child’s play, first and foremost, and therein lies a certain pedagogical power.

We cannot know if either of these gentlemen would welcome a geometric approach to relativity and quantum theory. I would like to think so, but it’s possible they might have taken a Bourbakian view and found all these pictures to be just so childish. If so then it’s their loss and our gain!

## Chapter 1 Continuous Wave (CW) vs. Pulse Wave (PW) functions

The standard units of time  $t$  and space  $x$  are *seconds* and *meters*. Pure waves are labeled by inverse units that count waves *per-time* or *frequency*  $\nu$ , which is *per-second* or *Hertz* ( $1\text{Hz}=1\text{ s}^{-1}$ ) and waves *per-meter* that is called *wavenumber*  $\kappa$  whose old units were *Kaiser* ( $1\text{ K}=1\text{ cm}^{-1}=100\text{ m}^{-1}$ ). Inverting back gives the *period*  $\tau=1/\nu$  or *time for one wave* and *wavelength*  $\lambda=1/\kappa$  or the *space occupied by one wave*.

Physicists like angular or radian quantities of *radian-per-second* or *angular frequency*  $\omega=2\pi\nu$  and *radian-per-meter* or *wavevector*  $k=2\pi\kappa$  in plane *continuous wave (CW)* functions  $\psi$ .

$$\langle k, \omega | x, t \rangle = \psi_{k, \omega}(x, t) = e^{i(kx - \omega t)} = \cos(kx - \omega t) + i \sin(kx - \omega t). \tag{1.1a}$$

Sine or cosine are circular functions of wave *phase* ( $kx - \omega t$ ) given in radians and defined here.

$$\tau = \frac{2\pi}{\omega} = \frac{1}{\nu} \tag{1.1b} \qquad \lambda = \frac{2\pi}{k} = \frac{1}{\kappa} \tag{1.1c}$$

They relate time  $\tau$  and space  $\lambda$  parameters to *per-time*  $\omega$  or  $\nu$  and *per-space*  $k$  or  $\kappa$  wave parameters.

### Phase velocity for 1-CW

Spacetime plots of the real field  $\text{Re}\psi_{k\omega}(x, t)$  for one CW laser light are shown in Fig. 1.1. The left-to-right moving wave  $e^{i(kx - \omega t)}$  in Fig. 1.1(a) has a positive wavevector  $k$  while  $k$  is negative for right-to-left moving wave  $e^{i(-kx - \omega t)}$  in Fig. 1.1(b). Light and dark lines mark time paths of crests, zeros, and troughs of  $\text{Re}\psi_{k\omega}(x, t)$ . A zero-phase line (where  $kx - \omega t$  is zero) or crest line has slope  $c = V_{\text{phase}}$ .

$$kx - \omega t = 0, \quad \text{or:} \quad \frac{x}{t} = V_{\text{phase}} = \frac{\omega}{k} = \nu\lambda \tag{1.1d}$$

Each white line in Fig. 1.1 has a phase is an odd multiple ( $N=1, 3, \dots$ ) of  $\pi/2$  and marks a  $\lambda/2$ -interval.

$$kx - \omega t = \pm N \frac{\pi}{2}, \quad \text{or:} \quad x = V_{\text{phase}}t \pm N \frac{\pi}{2k} = V_{\text{phase}}t \pm N \frac{\lambda}{4}$$

Slope or *phase velocity*  $V_{\text{phase}}$  of all lightwave phase line is a *universal constant*  $c=299,792,548\text{m/s}$ . (Note tribute to Ken Evenson’s  $c$ -measurement in Unit 4.) Velocity is a ratio of space to time ( $x/t$ ) or a ratio of per-time to per-space ( $\nu/\kappa$ ) or  $(\omega/k)$ , or a product of per-time and space ( $\nu\lambda$ )= $1/(\tau\kappa)$ .

The standard wave quantities of (1.1) are labeled for a long wavelength example (infrared light) in the lower part of Fig. 1.1. Note that the  $\text{Im}\psi_{k\omega}(x, t)$  wave precedes the  $\text{Re}\psi_{k\omega}(x, t)$  wave. A simple mnemonic is helpful, “*Imagination precedes reality by one quarter.*” and applies to combined waves, too.

### Axioms for light: 2-CW vs. 2-PW

Beginning relativity courses paraphrase Einstein’s light speed axiom as in Fig. 1.2a, “*Speed of a lightning flash is  $c$  according to passengers of any train,*” or simply, “*Pulse wave (PW) speed  $c$  is invariant.*” For critically thinking students, that is a show-stopper. It boggles the mind that something of finite speed cannot *ever* be caught up to, indeed, cannot even *begin* to be caught.<sup>1</sup>

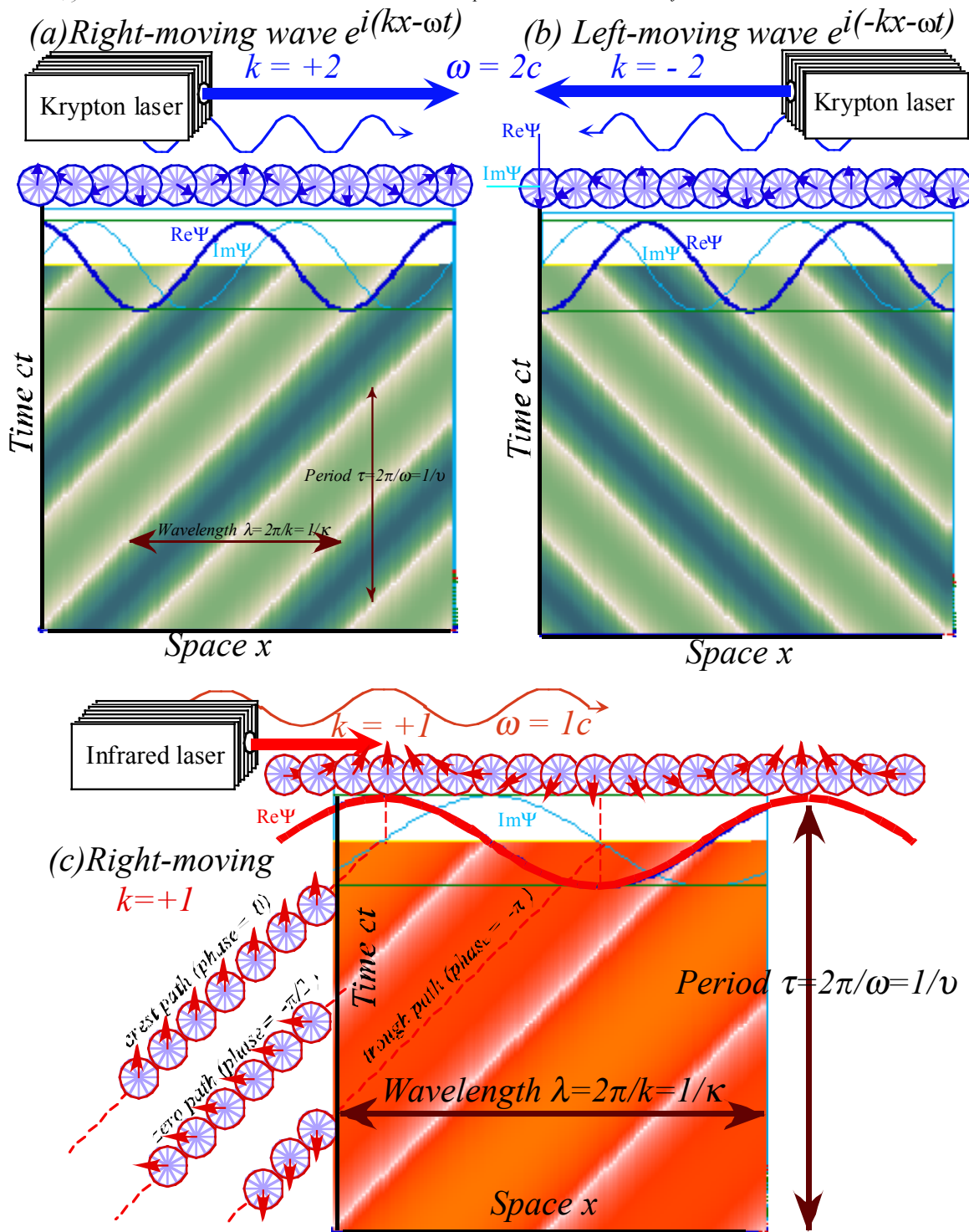


Fig. 1.1 Phasor and spacetime plots of moving CW laser waves. (a) Left-to-right. (b) Right-to-left.

Occam’s razor can dissect the  $c$ -axiom into a less mind-boggling form. As Evenson viewed a frequency chain of multiple “colors” of continuous wave (CW) laser beams, he assumed that, “All colors have speed  $c$ .” Had Einstein imagined trains viewing a 600THz (green) laser as in Fig. 1.2b, his  $c$ -axiom might be, “CW speed is  $c$  according to passengers of any train while frequency and wavelength vary by a Doppler effect that depends on velocity of the train,” or more simply, “All colors go  $c$ .”

A CW spectral component of a PW has a color variation with observer speed that a “white” PW does not. A colored wave (CW) will blue-shift if you approach its source or a red-shift if you run away from it. Doppler’s

theory of acoustical wave frequency shift existed 200 years before radar, masers, and lasers showed the ultra-precise 1<sup>st</sup>-order Doppler sensitivity of a coherent optical CW.

Also an optical Doppler shift depends on *one* relative velocity of source and observer while acoustical Doppler depends on *three* absolute (or three relative) velocities involving source, observer, and a “wind.” This single-velocity simplicity of *en vacuo* optical Doppler shifts is crucial for relativity.

Consider a 600THz green wave from a 600THz source. One may ask, “Is it distinguishable from another 600THz green wave sent by a 599THz source approaching or a 601THz source departing at just the right speed? Or, could 600THz light, seen as we approach a fixed 599THz source, ever differ in speed from 600THz light seen as we depart a fixed 601THz source? How many kinds of 600THz light exist?”

Evenson’s axiom follows if one answers, “There is only one kind of each frequency (color) and only one speed independent of source or observer velocity.” An undesirable alternative is to have many different kinds of each color, corresponding to many ways to make each color by tuning source up (or down) while moving out (or in). (In fact, one color illuminating a gas, liquid, or solid may involve two or many varieties of mode dispersion with wave speeds ranging above or below  $c$ .) Evenson’s axiom demands that light in a vacuum be one speed for all frequency. In short, light is *dispersion-free*.

If so, a PW must move rigidly at the speed  $c$  shared by its component CW colors. In this way one derives Einstein’s PW law as a *theorem* arising from Evenson’s CW *axiom*. Occam wins one!

#### *Astronomical view of CW axiom*

It also relates to appearance of distant nebulae and the night sky. If any colors were even a fraction of a percent slower than other frequencies, they would show up thousands or millions of years later with less evolved images than neighboring colors. We might then enjoy a sky full of blurry colorful streaks but would lose the clarity of Hubble astronomical images of colliding galaxies billions of light years away.

#### *Spectroscopic view of CW axiom*

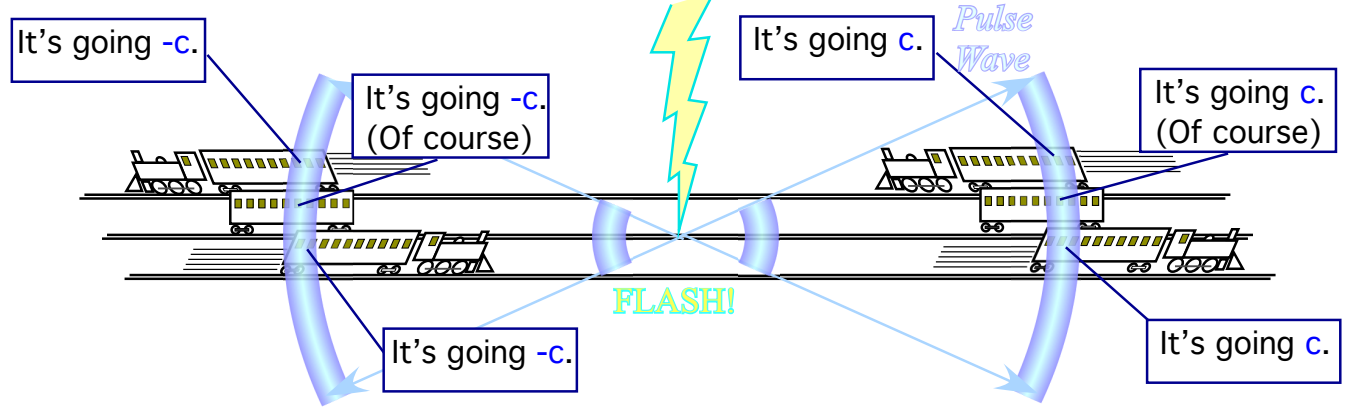
Astronomy is just one dependent of Evenson’s CW axiom. Spectroscopy is another. Laser atomic spectra are listed by frequency  $\nu$  ( $s^{-1}$ ) or period  $\tau=1/\nu$  (s) while early tables list atomic lines from gratings by wavenumber  $\kappa$  ( $m^{-1}$ ) or wavelength  $\lambda=1/\kappa$  (m). The equivalence of time and space listings is a tacit assumption in Evenson’s axiom. The axiom may be stated by the following summary of (1.1a-d).

$$c = \nu \cdot \lambda = \lambda/\tau = \nu/\kappa = 1/(\kappa \cdot \tau) = c = 299,792,548m/s \quad (1.1)_{summary}$$

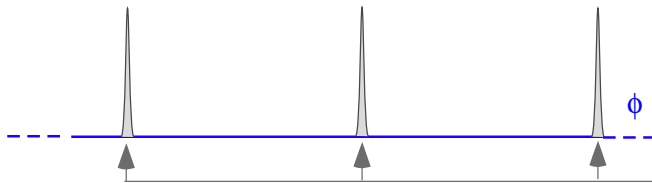
An atomic resonance is *temporal* and demands a precise *frequency*. Sub-nanometer atomic radii are thousands of times smaller than micron-sized wavelengths of optical transitions. Optical wavelength is not a key variable in atomic dipole approximations that ignore spatial dependence of light.

However, optical grating diffraction demands precise *spatial* fit of micron-sized *wavelength* to micron grating slits. Optical frequency is not a key variable for time independent Bragg or Fraunhofer laws. Spatial geometry of a spectrometer grating, cavity, or lattice directly measures wavelength  $\lambda$ , and then frequency  $\nu$  is determined indirectly from  $\lambda$  by axiom (1.1). That is valid if the light speed  $c = \nu \cdot \lambda$  is invariant throughout the spectrum (and throughout the universe.)

(a) Einstein Pulse Wave (PW) Axiom: *PW speed seen by all observers is  $c$*

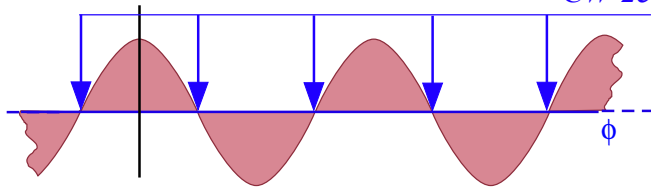


*Pulse wave (PW) train*



*PW peaks precisely locate places where wave is.*

*Continuous wave (CW) train*



*CW zeros precisely locate places where wave is not.*

(b) Evenson Continuous Wave (CW) axiom: *CW speed for all colors is  $c$*

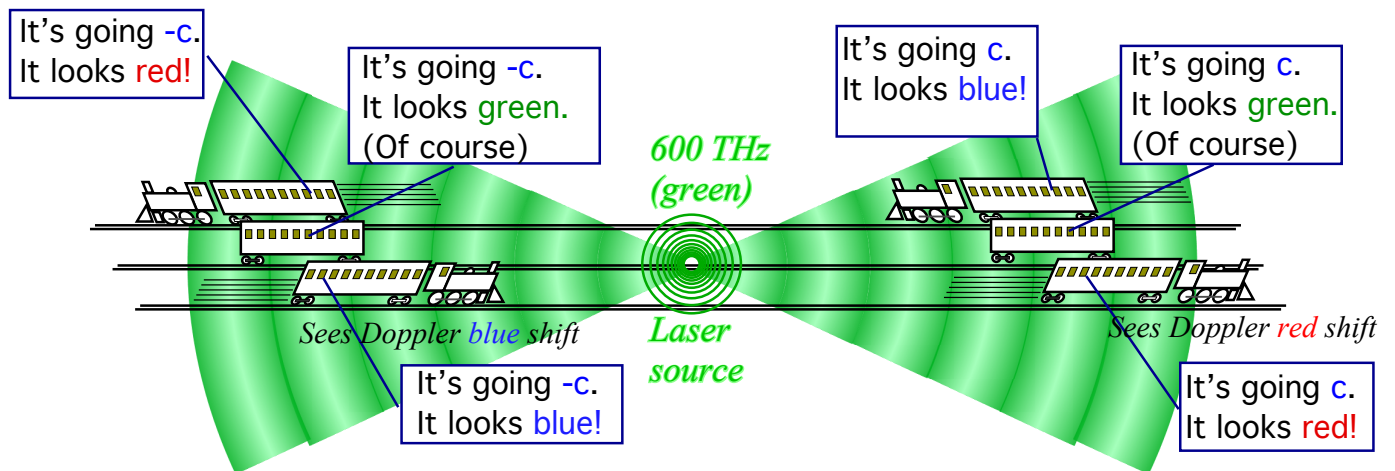


Fig. 1.2 Comparison of wave archetypes and related axioms of relativity.

(a) *Pulse Wave (PW) peaks locate where a wave is. Their speed is  $c$  for all observers.*

(b) *Continuous Wave (CW) zeros locate where it is not. Their speed is  $c$  for all colors (or observers.)*

A spectroscopist expects an atomic laser cavity resonating at a certain atomic spectral line in one rest frame to do so in *all* rest frames. Each  $\lambda$  or  $\nu$  value is a *proper quantity* to be stamped on the device and officially

tabulated for its atoms. Passersby may see output  $\nu$  Doppler red shifted to  $r\nu$  or blue shifted to  $b\nu$ . Nevertheless, all can agree that the device and its atoms are actually lit up and working!

Moreover, Evenson’s CW axiom demands that  $\nu$  and  $\lambda$  must Doppler shift *inversely* one to the other so that the product  $\nu \cdot \lambda$  is always a constant  $c=299,792,458 \text{ m}\cdot\text{s}^{-1}$ . The same applies to  $\tau$  and  $\kappa$  for which  $\kappa \cdot \tau=1/c$ . Also, there is an inverse relation that exists between Doppler blue and red shifts seen before and after passing a source. This is our second CW axiom. It involves time reversal symmetry.

*Time reversal axiom*

Atoms behave like tiny radio transmitters, or just as well, like receivers. Unlike macroscopic radios, atoms are time-reversible in detail since they have no resistors or similarly irreversible parts. Suppose an atom  $A$  broadcasting frequency  $\nu_A$  resonates an approaching atom  $B$  tuned to receive a blue shifted frequency  $\nu_B = b\nu_A$ . If time runs backwards all velocity values change sign. Atom  $B$  becomes a *transmitter* of its tuned frequency  $\nu_B = b\nu_A$  that is *departing* from atom  $A$  who is a *receiver* tuned to its frequency  $\nu_A = (1/b)\nu_B$ . Atom  $A$  sees  $\nu_A$  red-shifted from  $B$ ’s frequency  $\nu_B$  by an *inverse* factor  $r=1/b$ .

$$b=1/r \tag{1.2}$$

*Phase invariance axioms viewed in a classical way*

Optical CW axioms may be based on deeper phase invariance principles. Elementary CW function  $\Psi=A \exp i(k\cdot x-\omega\cdot t)$  or its real part  $\text{Re}\Psi=A \cos(k\cdot x-\omega\cdot t)$  has a phase angle  $\Phi=(k\cdot x-\omega\cdot t)$  that is regarded as an invariant or proper quantity. Our rationale is that each space-time point of the wave has a phase clock or *phasor* ( $\text{Re}\Psi, \text{Im}\Psi$ ) turning at *angular* frequency  $\omega=2\pi\cdot\nu$ . Each phasor reading  $\Phi$  could be stamped or “officially” tabulated. All observers should agree on  $\Phi$  even if Doppler shifts change frequency  $\omega=2\pi\cdot\nu$  and *wavevector*  $k=2\pi\kappa$  to new values  $(\omega',ck')$  or if space  $x$  and time  $t$  also transform to  $x',t'$ .

$$k\cdot x-\omega\cdot t = \Phi = k'\cdot x'-\omega'\cdot t' \tag{1.3}$$

(Lorentz-Einstein transformations for both space-time  $x,t$  to  $x',t'$  and inverse space-time  $(\omega,ck)$  to  $(\omega',ck')$  are derived in Ch. 2 using CW axioms (1.1) and (1.2) in a few algebraic or ruler-and-compass steps.)

Historically, invariance (1.3) relates to classical Legendre contact transforms of Lagrangian  $L$  to energy  $E$  or Hamiltonian  $H$ . Differential  $Ldt$  is Poincare’s *action invariant*  $dS$  or phase  $d\Phi$  with an  $\hbar$  factor.

$$L = p \cdot \dot{x} - H \tag{1.4a}$$

$$\hbar d\Phi = dS = Ldt = p \cdot dx - Hdt \tag{1.4b}$$

Connecting (1.3) to (1.4b) requires quantum scaling relations  $p=\hbar k$  of DeBroglie and  $E=\hbar\omega$  of Planck. Ch. 3 shows how such relations arise from CW axioms (1.1-2). Exact relativistic quantum and classical mechanical relations are found in a few algebraic<sup>ii</sup> or ruler-and-compass steps. Elegant wave-geometric<sup>iii</sup> interpretations of momentum, mass, energy, and Poincare’s invariant are exposed in Ch. 4 and Ch. 5.<sup>iv</sup>

We surmised that Einstein might have liked geometric derivations since a compass first caught his theoretical attention at an age of five.<sup>v</sup> Perhaps, it might also appeal to Poincare who also discovered relativity

around the time of Einstein’s 1905 *annus mirabilis*. Poincare phase invariance (1.3) underlies both CW lightspeed axiom (1.1) and time reversal axiom (1.2). Consider the  $\Phi=0$  point.

$$k \cdot x - \omega \cdot t = 0 \tag{1.5a}$$

Solving gives phase velocity  $x/t$  (*meters-per-second*) equal by (1.1) to  $v/\kappa$  (*per second*)-*per*-(*per meter*).

$$\frac{x}{t} = \frac{\omega}{k} = \frac{v}{\kappa} = c \tag{1.5b}$$

Doppler shift ( $\omega \rightarrow b\omega$  and  $k \rightarrow bk$ ) leaves phase velocity invariant. Phase  $\Phi=(k \cdot x - \omega \cdot t)$  itself is invariant to time reversal ( $(\omega \rightarrow -\omega)$  and  $(t \rightarrow -t)$ ) and that supports (1.2), the inverse-Doppler relation  $b=1/r$ .

We find relativistic and quantum derivations based on classical mechanical laws to be clumsy at best and wrong-way-to at worst. Simple wave interference with axioms (1.1-2) can unite relativity and quantum theory. At the wave-phaser or “gauge” level, Nature may be seen as a big wave trick!

*Comparing pulsed and continuous wave trains*

It is instructive to contrast two opposite wave archetypes, the *Pulse Wave* (PW) train sketched in Fig. 1.2a and the *Continuous Wave* (CW) train sketched in Fig. 1.2b. A CW is the more elementary theoretical entity, indeed the *most* elementary entity in classical optics since it has just one value of angular frequency  $\omega=2\pi \cdot v$ , one value of wavevector  $k=2\pi\kappa$ , and one amplitude  $A$ .

$${}^{CW}\Psi_{k,\omega}(x,t) = Ae^{i(kx-\omega t)} = \langle k, \omega | x, t \rangle \tag{1.6}$$

The real part is the cosine wave  $A \cos(kx - \omega t)$  shown in Fig. 1.2(b). Acronym CW fits cosine wave, as well. If frequency  $v$  is in the visible 400-750THz range, then CW could also stand for colored wave.

In contrast, the PW is a *less* elementary wave function and contains  $N$  harmonic terms of CW functions where bandwidth  $N$  is as large as possible. Fig. 1.3 shows an example with  $N=12$ .

$${}^{PW}\Psi_{N(k,\omega)}(x,t) = A(1 + e^{i(kx-\omega t)} + e^{i2(kx-\omega t)} + e^{i3(kx-\omega t)} \dots + e^{iN(kx-\omega t)}) \tag{1.7}$$

An infinite- $N$  PW is a train of Dirac  $\delta(x-a)$ -functions each separated by fundamental wavelength  $\lambda=2\pi/k$ . The  $\delta$ -spikes march in lockstep at light speed  $c=\omega/k$  because of Evenson’s CW axiom (1.1).

$${}^{PW}\Psi_{N(k,\omega)}(x,t) \xrightarrow{N \rightarrow \infty} A \sum_{n=-\infty}^{\infty} \delta(x - ct - n\lambda)$$

Delta functions have infinite frequency bandwidth and are thus impractical. Realistic PW trains apply cutoff or tapering amplitudes  $a_n$  to the harmonic so as to restrict frequency to a finite bandwidth  $\Delta$ .

$${}^{PW}\Psi_{\Delta}(x,t) = \sum_{n=0}^{\infty} a_n e^{in(kx-\omega t)} = \sum_{n=-\infty}^{\infty} G(x - ct - n\lambda) \quad \text{where: } a_n \ll 1 \text{ for } n > \Delta \tag{1.8}$$

One choice is the Gaussian taper  $a_n = e^{-(n/\Delta)^2}$  that gives Gaussian PW functions  $G(\theta) = e^{-(\theta \cdot \Delta)^2}$ .

PW functions (1.8) involve an unlimited number of amplitude parameters  $a_n$  in addition to fundamental frequency  $\omega$ , while a CW function has a single amplitude parameter  $A$ . Thus, theory based on CW properties is closer to an Occam ideal for axiomatic simplicity than one based on PW.

*CW squares vs. PW diamonds in space-time plots*

However, with regard to counter-propagating or colliding beams the PW *appear* in Fig. 1.4a to have simpler properties than CW in Fig. 1.4b. PW have a simple classical Boolean OFF (0) over most of space-time with an occasional ON (1) at a sharp pulse. On the other hand CW range gradually between +1 and –1 over most of space-time, but have sharp zeros (0) in between crest and trough. (A PW is *designed* to make precise peaks that show where it *is*. A CW *naturally* has precise zeros that show where it is *not*.)

Interference between two colliding CW makes a square (P, G)-zero-grid that is subtler and sharper than the left-right moving (L,R)-peak-diamond grid made by two colliding PW. One should understand how this wave interference works to make these two archetypical types of wave space-time geometry.

Interference of colliding PW in Fig. 1.4a or Fig. 1.5b is *wysiwyge* (*What you see is what you expect*). The pattern of interference for the sum of colliding CW in Fig. 1.4b and Fig. 1.5a is subtler. PW paths in space-time ( $x, ct$ ) resemble baseline *diamonds* in Fig. 1.5b like paths in the American baseball sport. Meanwhile, CW zeros form Cartesian space-time *squares* in Fig. 1.5a with horizontal  $x$ -axial fixed time-lines ( $ct = \dots 1, 2, \dots$ ) and vertical temporal  $ct$ -axial lines of fixed location ( $x = \dots 1, 2, \dots$ ).

PW peak diamonds seem simple but hide intricate networks of zeros near each peak. CW squares make truly simple and precise lattices of standing wave zeros of given by (1.9), which is just a factored sum of two equal-but-opposite colliding CW. Note that the *group envelope* factor ( $\cos(kx)$ ) is zero on lines ( $kx/\pi + 1/2 = \dots 0, 1, 2, \dots$ ) parallel to the  $ct$ -axis. The *phase* factor ( $e^{-i\omega t}$ ) has a zero real part on lines of *simultaneous time* ( $ct/\pi + 1/2 = \dots 0, 1, 2, \dots$ ) parallel to the  $x$ -axis. (At lattice corners, *both* factors are zero.)

$${}^{CW}\Psi_{k,\omega} + {}^{CW}\Psi_{-k,\omega} = A\left(e^{i(kx-\omega t)} + e^{i(-kx-\omega t)}\right) = 2Ae^{-i\omega t}(\cos(kx)) \tag{1.9}$$

*CW wave-zeros vs. PW pulse paths*

Phase and group wave *zeros* of 2-CW interference define a space-time wave-zero (P,G)-coordinate grid for light waves in Fig. 1.5 and more general waves in Fig. 1.6. Vector **P** points along a *phase zero path* and vector **G** points along a *group zero path*. They complement PW pulse peak or peak-path (L,R)-grid based on vector **L** that points along a *left moving peak path* and a vector **R** that points along a *right moving peak path*. The half-sum-and-difference relation of (P,G) to (L,R) is as follows.

$$\mathbf{P} = \frac{1}{2}(\mathbf{L} + \mathbf{R}) \tag{1.10a}$$

$$\mathbf{L} = (\mathbf{P} + \mathbf{G}) \tag{1.10c}$$

$$\mathbf{G} = \frac{1}{2}(\mathbf{L} - \mathbf{R}) \tag{1.10b}$$

$$\mathbf{R} = (\mathbf{P} - \mathbf{G}) \tag{1.10d}$$

The Sum-and-differences are due to phase sum-and-differences. (Recall discussion of (4.8.21) in Unit 4.)

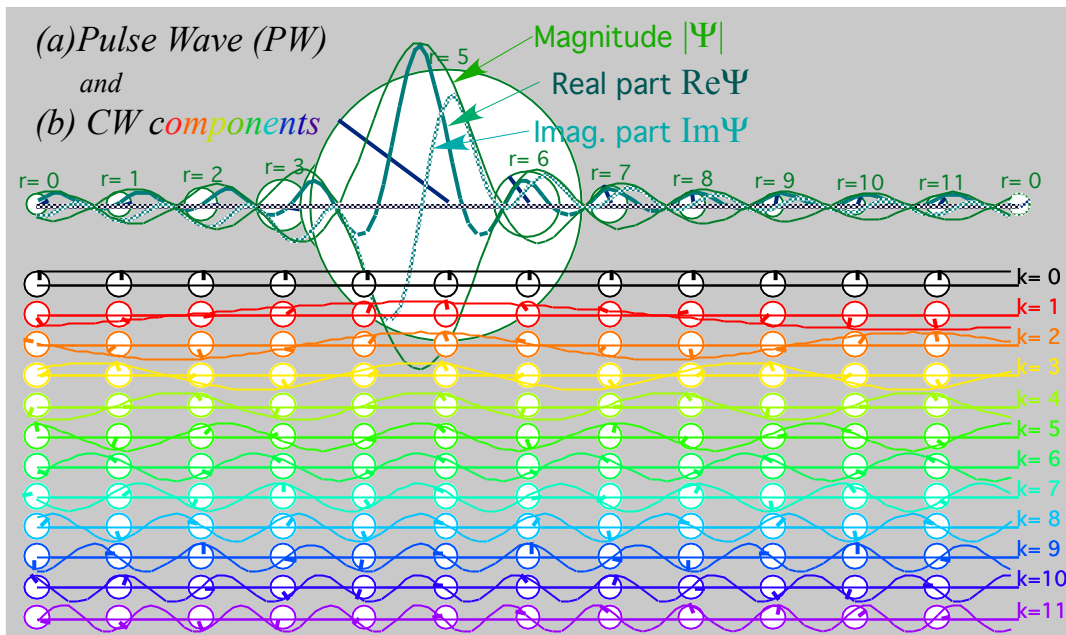


**Fig. 1.3.** Pulse Wave (PW) as a sum of 12 Fourier CW's

(a) PW parts: real  $Re\Psi$  imaginary  $Im\Psi$ , and magnitude  $|\Psi|$ .  
 (b) CW phasor clock plot real vs. imaginary

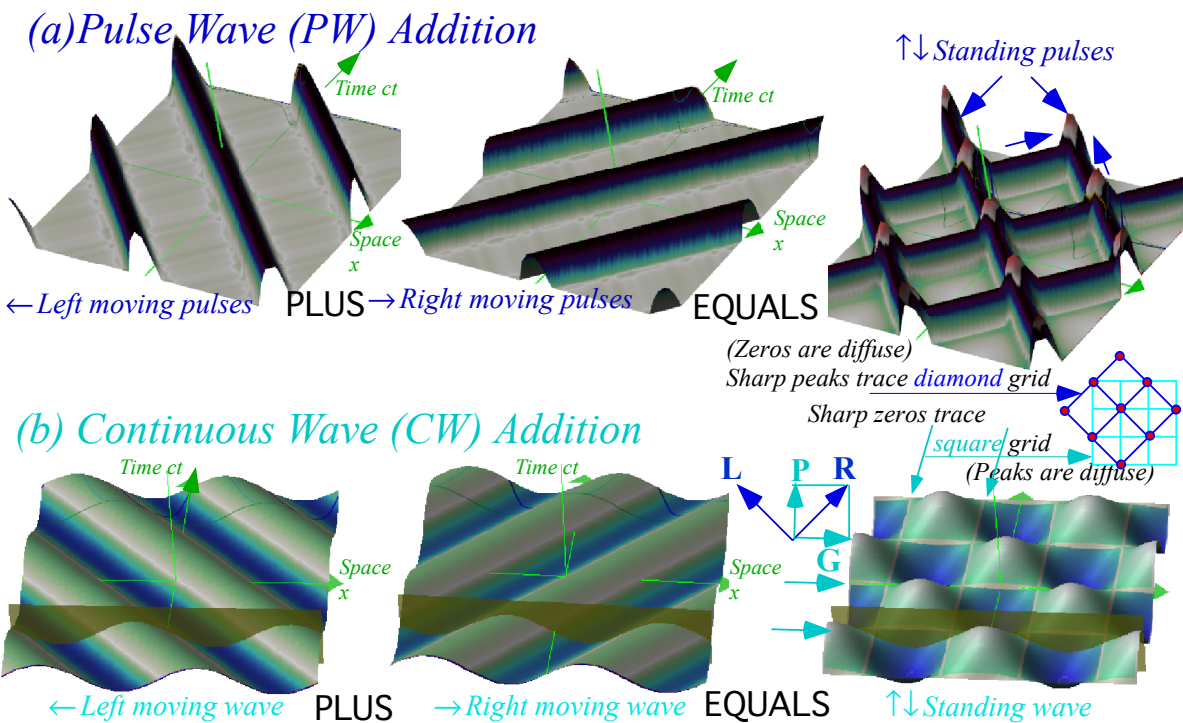


**Fig. 1.4** Wave Add

(a) 2-PW Su Boolean bin sum has 4 vertices (0,0), (0,1), (1,0), (1,1) and diamond of peak path a plane of zeros.  
 (b) 2-CW Su Interference value continuous and square; of zeros.

**Comparing wave-like vs particle-like behavior**

Relations (1.10) highlight *wave-particle duality*. First, Newton saw light as particle-like. Then Young and Maxwell showed its wave-like nature. Finally, Planck, Einstein, and Compton found particle-like behavior of “photon” quanta. The label “photon” is reserved for quantum field eigenstates having decidedly more complicated behavior than is shown in semi-classical wave plots in Fig. 1.6 or colliding light waves in Fig. 1.5. Still the diamond left-and-right moving PW (L,R)-peak paths in Fig. 1.5b might be thought of as paths of fictitious particles or “photon bunches” that are well localized in space-time as they move at  $\pm c$  in either direction. Each PW laser “spits” pulses (*patooy! patooy!...*) at 600Thz.

Optical pulse peaks do move like particles in between the points where “collisions” occur (with very complicated wave interference). After that the “particles” seem to pass through each other or recoil elastically. Newton wrote about optical interference behavior as crazy “light having fits.”

Square 2-CW (**P,G**) zero-paths in Fig. 1.5a are due to counter-propagating 600THz CW waves interfering wherever they exist in space-time. The wave between the zeros is delocalized in space-time compared to the PW peaks but the square white zero-lines are extremely sharp as are vectors  $\mathbf{L}=(ck, \omega)$  and  $\mathbf{R}=(-ck, \omega)$  that determine motion of left and right CW component laser beams while vectors  $\mathbf{P}=(0, \omega)$  and  $\mathbf{G}=(\omega, 0)$  determine the real wave-zero lattice of their 2-CW interfering sum.

It is important to note that these vectors, appropriately scaled, describe both time-vs-space  $(x,t)$ -plots and Fourier inverse *per-time-space* or *reciprocal space-time* plots of frequency-vs-wavevector  $(\omega,k)$ . A general example of this is derived and shown in a following Fig. 1.6 where the two kinds of plots may be superimposed. We will see that a  $(\omega,ck) \rightleftharpoons (ck,\omega)$  switch or else an  $(x,ct) \rightleftharpoons (ct,x)$  switch to the Newtonian format is needed in order to make a CW lattice and reciprocal PW lattice coincide and that entails a  $(\mathbf{P,G}) \rightleftharpoons (\mathbf{P,G})$  switch. This is indicated in Fig. 1.5a to the right of the square space-time lattice.

PW (**L,R**)-peak paths are “particle-like” and stand out in space-time for  $N$ -CW wave trains. Then interference “fits” between pulses die off (to make Newton comfortable again.) But, CW (**P,G**)-zero paths, in contrast, are “wave-like” with very sharp lines in space-time for maximally interfering 2-CW beats.

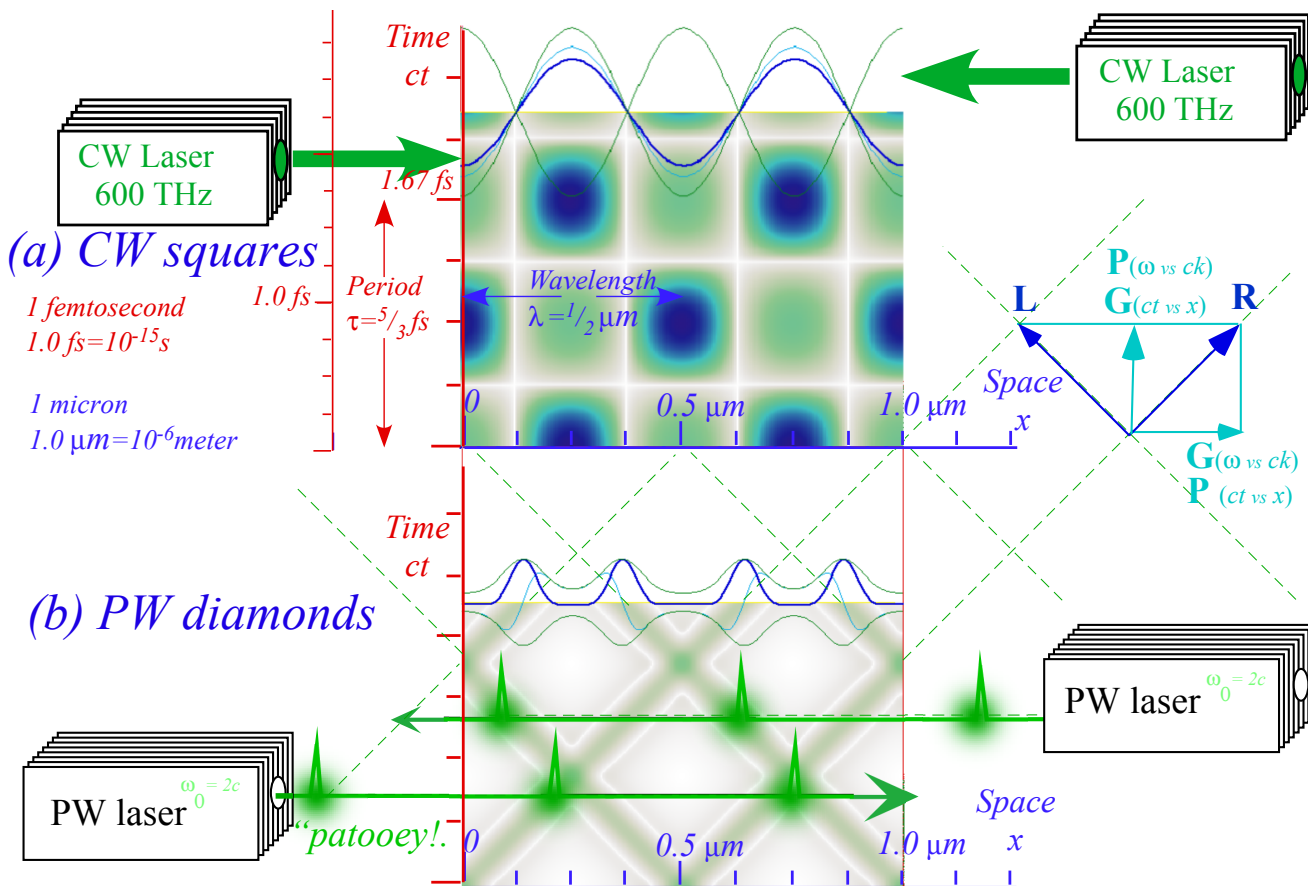


Fig. 1.5 Space-time grids (a) 2-CW standing-wave-zero squares. (b) 2-PW diamond pulse peak paths.

### Wave-zero (WZ) and pulse-peak (PP) space-time coordinate grids

The following Fig. 1.6 and Fig. 1.7 compare and superimpose time-vs-space  $(x,t)$ -plots of group and phase waves, on one hand, with their inverse *per-time-space* or *reciprocal space-time* plots of frequency-vs-wavevector  $(\omega,k)$ , on the other, and thereby mesh  $(x,t)$ -plots with their Fourier transforms.

The plots apply to all waves and not just to light. The example in Fig. 1.6 begins by picking four random numbers, say, 1,2,4, and 4 to insert into frequency-wavevector  $\mathbf{K}_2 = (\omega_2, k_2) = (1, 2)$  of a mythical *source-2* and frequency-wavevector  $\mathbf{K}_4 = (\omega_4, k_4) = (4, 4)$  of another mythical *source-4*. Velocity  $c_2 = \omega_2/k_2 = 1/2$  of *source-2* and  $c_4 = \omega_4/k_4 = 1$  of *source-4* are unequal. For light waves in Fig. 1.7,  $c_2$  equals  $c_4$  as required by an important axiom discussed in the following Chapter 2.

Let the continuous waves (CW) from the two sources interfere in a 2-CW sum.

$$\Psi^{2-CW} = (e^{i(k_4 x - \omega_4 t)} + e^{i(k_2 x - \omega_2 t)}) / 2 \quad (1.11a)$$

To solve for zeros of this sum we first factor it into a phase-wave  $e^{ip}$  and a group-wave  $\cos g$  factor.

$$\begin{aligned} \Psi^{2-CW} &= e^{i\left(\frac{k_4+k_2}{2}x - \frac{\omega_4+\omega_2}{2}t\right)} \left( e^{i\left(\frac{k_4-k_2}{2}x - \frac{\omega_4-\omega_2}{2}t\right)} + e^{-i\left(\frac{k_4-k_2}{2}x - \frac{\omega_4-\omega_2}{2}t\right)} \right) / 2 \\ &= e^{i(k_p x - \omega_p t)} \cos\left(k_g x - \omega_g t\right) \equiv e^{ip} \cos g \end{aligned} \quad (1.11b)$$

Phase factor  $e^{ip}$  uses the half-sum  $(\omega,k)$ -vector  $\mathbf{K}_{phase} = (\mathbf{K}_4 + \mathbf{K}_2)/2$  in its argument  $p = k_p x - \omega_p t$ . Group factor  $\cos g$  has the half-difference  $(\omega,k)$ -vector  $\mathbf{K}_{group} = (\mathbf{K}_4 - \mathbf{K}_2)/2$  in its argument  $g = k_g x - \omega_g t$ .

$$\begin{aligned} \mathbf{K}_{phase} &= \frac{\mathbf{K}_4 + \mathbf{K}_2}{2} = \frac{1}{2} \begin{pmatrix} \omega_4 + \omega_2 \\ k_4 + k_2 \end{pmatrix} & \mathbf{K}_{group} &= \frac{\mathbf{K}_4 - \mathbf{K}_2}{2} = \frac{1}{2} \begin{pmatrix} \omega_4 - \omega_2 \\ k_4 - k_2 \end{pmatrix} \\ &= \begin{pmatrix} \omega_p \\ k_p \end{pmatrix} = \frac{1}{2} \begin{pmatrix} 4+1 \\ 4+2 \end{pmatrix} = \begin{pmatrix} 2.5 \\ 3.0 \end{pmatrix} & & = \begin{pmatrix} \omega_g \\ k_g \end{pmatrix} = \frac{1}{2} \begin{pmatrix} 4-1 \\ 4-2 \end{pmatrix} = \begin{pmatrix} 1.5 \\ 1.0 \end{pmatrix} \end{aligned} \quad (1.11c) \quad (1.11d)$$

The  $(\omega,k)$ -vectors  $\mathbf{K}_n$  define paths and coordinate lattices for pulse peaks and wave zeros in Fig. 1.6a.

Real zeros ( $\text{Re}\Psi=0$ ) have velocity  $V_{phase}$  on  $\mathbf{K}_{phase}$  paths. Group zeros ( $|\Psi|=0$ ) move at  $V_{group}$  on  $\mathbf{K}_{group}$ .

$$V_{phase} = \frac{\omega_p}{k_p} = \frac{\omega_4 + \omega_2}{k_4 + k_2} = \frac{2.5}{3.0} = 0.83 \quad (1.12a) \quad V_{group} = \frac{\omega_g}{k_g} = \frac{\omega_4 - \omega_2}{k_4 - k_2} = \frac{1.5}{1.0} = 1.5 \quad (1.12b)$$

Zeros of phase factor real part  $\text{Re} e^{ip} = \text{Re} e^{i(k_p x - \omega_p t)} = \cos p$  lie on *phase-zero paths* where angle  $p$  is  $N(\text{odd}) \cdot \pi/2$ .

$$k_p x - \omega_p t = p = N_p \pi / 2 \quad (N_p = \pm 1, \pm 3 \dots)$$

Zeros of group amp-factor  $\cos g = \cos(k_g x - \omega_g t)$  lie on *group-zero* or *nodal paths* where angle  $g$  is  $N(\text{odd}) \cdot \pi/2$ .

$$k_g x - \omega_g t = g = N_g \pi / 2 \quad (N_g = \pm 1, \pm 3 \dots)$$

Both factors are zero at *wave zero (WZ) lattice points*  $(x,t)$ . This defines the lattice vectors in Fig. 1.6a.

$$\begin{pmatrix} k_p & -\omega_p \\ k_g & -\omega_g \end{pmatrix} \begin{pmatrix} x \\ t \end{pmatrix} = \begin{pmatrix} p \\ g \end{pmatrix} = \begin{pmatrix} N_p \\ N_g \end{pmatrix} \frac{\pi}{2} \tag{1.13a}$$

Solving gives *spacetime*  $(x,t)$  zero-path lattices that are white lines in Fig. 1.6a. Each lattice intersection point is an odd-integer  $(N_p, N_g)$  combination of wave-vectors  $\mathbf{P} = \pi \mathbf{K}_{phase} / 2D$  and  $\mathbf{G} = \pi \mathbf{K}_{group} / 2D$ .

$$\begin{pmatrix} x \\ t \end{pmatrix} = \frac{\begin{pmatrix} -\omega_g & \omega_p \\ -k_g & k_p \end{pmatrix} \begin{pmatrix} p \\ g \end{pmatrix}}{\omega_p k_g - \omega_g k_p} = \frac{-p \begin{pmatrix} \omega_g \\ k_g \end{pmatrix} + g \begin{pmatrix} \omega_p \\ k_p \end{pmatrix}}{\omega_p k_g - \omega_g k_p} = \frac{\pi}{2D} (-N_p \mathbf{K}_{group} + N_g \mathbf{K}_{phase}) \tag{1.13b}$$

So *space-time* lattice points reuse the base lattice vectors  $\mathbf{K}_{group}$  and  $\mathbf{K}_{phase}$  of reciprocal *per-space-time*!

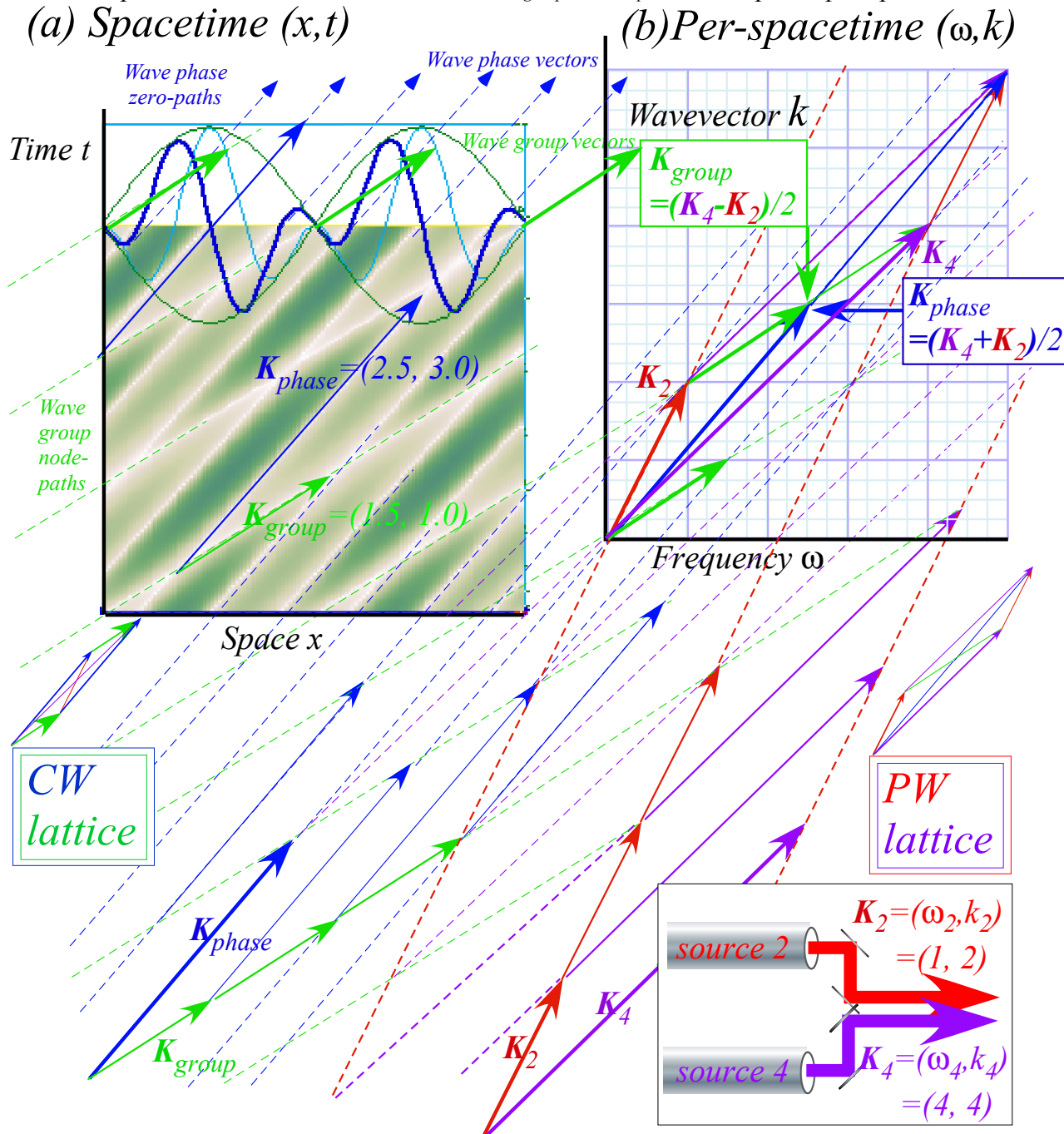


Fig. 1.6 “Mythical” sources and their wave coordinate lattices in (a) Spacetime and (b) Per-spacetime. CW lattices of phase-zero and group-node paths intermesh with PW lattices of pulse, packet, or “particle” paths.

Scaling factor  $2D/\pi = 2(\omega_p k_g - \omega_g k_p) / \pi$  converts (*per-time, per-space*) vectors  $\mathbf{K}_{group}$  or  $\mathbf{K}_{phase}$  into (*space, time*) vectors  $\mathbf{P} = \begin{pmatrix} x \\ t \end{pmatrix}_p$  or  $\mathbf{G} = \begin{pmatrix} x \\ t \end{pmatrix}_g$ . (Plot units are set so  $2D/\pi = 1$  or  $D = \pi/2$ . *This works only if D is non-zero.*)

Fig. 1.6b is a lattice of source vectors  $\mathbf{K}_2$  and  $\mathbf{K}_4$  (the difference and sum of  $\mathbf{K}_{group}$  and  $\mathbf{K}_{phase}$ ).

$$\mathbf{K}_2 = \mathbf{K}_{phase} - \mathbf{K}_{group} = \begin{pmatrix} \omega_2 \\ k_2 \end{pmatrix} = \begin{pmatrix} 1 \\ 2 \end{pmatrix} \quad (1.14a)$$

$$\mathbf{K}_4 = \mathbf{K}_{phase} + \mathbf{K}_{group} = \begin{pmatrix} \omega_4 \\ k_4 \end{pmatrix} = \begin{pmatrix} 4 \\ 4 \end{pmatrix} \quad (1.14b)$$

Source-2 has phase speed  $c_2$  on  $\mathbf{K}_2$  paths of slope  $c_2$ . Source-4 has speed  $c_4$  on  $\mathbf{K}_4$  paths of slope  $c_4$ .

$$c_2 = \frac{\omega_2}{k_2} = \frac{1}{2} = 0.5 \quad (1.15a)$$

$$c_4 = \frac{\omega_4}{k_4} = \frac{1}{1} = 1.0 \quad (1.15b)$$

One may view the  $\mathbf{K}_2$  and  $\mathbf{K}_4$  paths from a classical or semi-classical viewpoint if pulse waves (PW) were wave packets (WP) that mimic particles. Newton took a hard-line view of nature and ascribed reality to “corpuscles” but viewed waves as illusory. He misunderstood light if it exhibited interference phenomena and complained that its particles or “corpuscles” were having “fits.”

Newtonian corpuscular views are parodied here by imagining that frequency  $\nu_2 = \omega_2/2\pi$  (or  $\nu_4 = \omega_4/2\pi$ ) is the rate at which source-2 (or 4) emits “corpuscles” of velocity  $c_2$  (or  $c_4$ ). Then the wavelengths  $\lambda_2 = 2\pi/k_2$  (or  $\lambda_4 = 2\pi/k_4$ ) are just inter-particle spacing of  $\mathbf{K}_2$  (or  $\mathbf{K}_4$ ) lines in Fig. 1.6a.

Since wavelength  $\lambda_2$  ( $\lambda_4$ ) separates  $\mathbf{K}_2$  ( $\mathbf{K}_4$ ) lattice lines in Fig. 1.6b, one can imagine them as “corpuscle paths.” The paths are *diagonals* of the  $\mathbf{K}_{group}(\mathbf{K}_{phase})$  wave-zero lattice in time vs space  $(x,t)$  of Fig. 1.6a.

This development shows wave-particle, wave-pulse, and CW-PW duality in the cells of each CW-PW wave lattice. Each  $(\mathbf{K}_2, \mathbf{K}_4)$ -cell of a PW lattice has a CW vector  $2\mathbf{P}$  or  $2\mathbf{G}$  on each diagonal, and each  $(\mathbf{P}, \mathbf{G})$ -cell of the CW lattice has a PW vector  $\mathbf{K}_2$  or  $\mathbf{K}_4$  on each diagonal. This is due to sum and difference relations (1.11d) or (1.14b) between  $(\mathbf{P}, \mathbf{G}) = (\mathbf{K}_{phase}, \mathbf{K}_{group})$  and  $(\mathbf{K}_2, \mathbf{K}_4)$ .

In order that space-time  $(x,t)$ -plots can be superimposed on frequency-wavevector  $(\omega, k)$ -plots or  $(\nu, \kappa)$ -plots, it is necessary to switch axes for one of them. The space-time  $t(x)$ -plots in Fig. 1.6a follow the convention adopted by most relativity literature for a vertical time ordinate (*t-axis*) and horizontal space abscissa (*x-axis*) that is quite the opposite of Newtonian calculus texts that plot  $x(t)$  horizontally. However, the frequency-wavevector  $k(\omega)$ -plots in Fig. 1.6b switch axes from the usual  $\omega(k)$  convention so that  $t(x)$  slope due to space-time velocity  $x/t$  or  $\Delta x/\Delta t$  (*meter/second*) in Fig. 1.6a matches that of equal per-time-per-space wave velocity  $\omega/k$  or  $\Delta\omega/\Delta k$  (*per-second/per-meter*) in Fig. 1.6b.

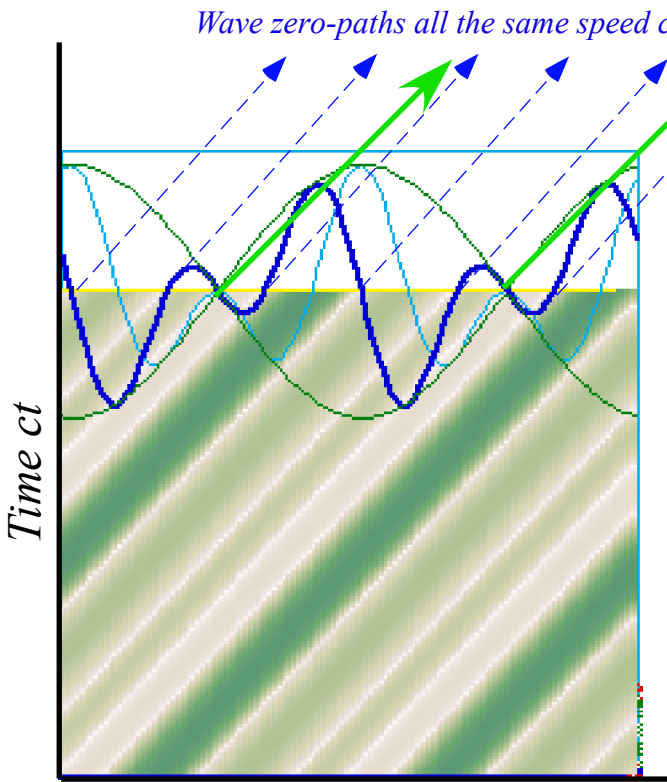
Superimposing  $t(x)$ -plots onto  $k(\omega)$ -plots also requires that the latter be rescaled by the scale factor  $\pi/2D$  derived in (1.13b), but rescaling fails if cell-area determinant factor  $D$  is zero.

$$D = \omega_p k_g - \omega_g k_p = \left| \mathbf{K}_{phase} \times \mathbf{K}_{group} \right| \quad (1.16)$$

Co-propagating light beams  $\mathbf{K}_2 = (\omega_2, k_2) = (2c, 2)$  and  $\mathbf{K}_4 = (\omega_4, k_4) = (4c, 4)$  in Fig. 1.7b have  $D=0$  since all  $\mathbf{K}$ -vectors including  $\mathbf{K}_{phase} = (\omega_p, k_p) = (3c, 3)$  and  $\mathbf{K}_{group} = (\omega_g, k_g) = (c, 1)$  lie on one  $c$ -baseline of speed  $c$  that has unit slope ( $\omega/ck=1$ ) if we rescale  $(\omega, k)$ -plots to  $(\omega, ck)$  and  $(x, t)$ -plots to  $(x, ct)$ .

In summary, *co-propagating* light waves absolutely fail to make coordinate grids! However, *counter-propagating* (right-left) light waves are another “matter” altogether.

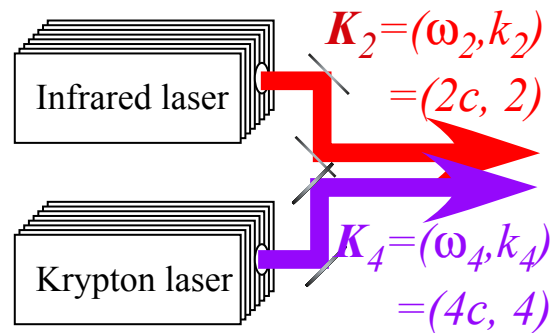
(a) Spacetime  $(x, ct)$



Space  $x$



Replaced by:



(b) Per-spacetime  $(\omega, ck)$

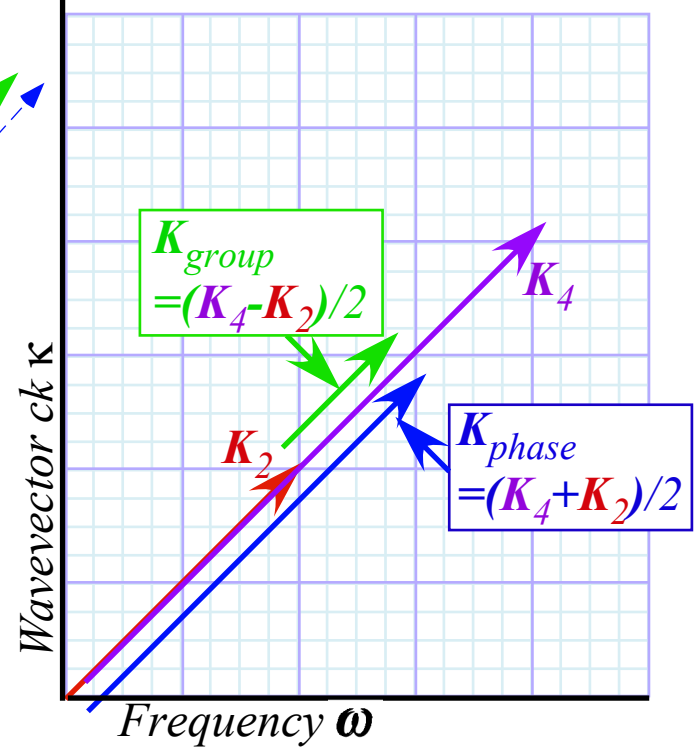


Fig. 1.7 Co-propagating laser beams produce a collapsed wave lattice since all parts have same speed  $c$ .

In Ch. 2 *counter-propagating* (right-left) light wave vectors  $(\mathbf{R}, \mathbf{L}) = (\mathbf{K}_2, -\mathbf{K}_4)$  are used to make CW bases  $(\mathbf{P} = \mathbf{K}_{phase}, \mathbf{G} = \mathbf{K}_{group})$  with a non-zero value for area  $D = |\mathbf{G} \times \mathbf{P}|$ . Opposing PW base vectors are sum and difference  $(\mathbf{R}, \mathbf{L}) = (\mathbf{P} + \mathbf{G}, \mathbf{P} - \mathbf{G})$  of CW bases so a PW cell area  $|\mathbf{R} \times \mathbf{L}|$  is twice that of CW cell  $|\mathbf{G} \times \mathbf{P}|$ .

$$|\mathbf{R} \times \mathbf{L}| = |(\mathbf{P} + \mathbf{G}) \times (\mathbf{P} - \mathbf{G})| = 2|\mathbf{G} \times \mathbf{P}| \tag{6.22}$$

Wave cell areas due to colliding CW are key geometric invariants for relativity and quantum mechanics.



## Chapter 2 When Light Waves Collide: Relativity of waves in spacetime

Let us represent counter-propagating frequency- $\omega$  laser beams by a baseball diamond in Fig. 2.1a spanned by CW vectors for waves moving left-to-right (**R** on 1<sup>st</sup> base) and right-to-left (**L** on 3<sup>rd</sup> base).

$$\mathbf{R}=\mathbf{K}_1=(ck_1,\omega_1)=\omega(1,1) \quad (2.1a)$$

$$\mathbf{L}=\mathbf{K}_3=(ck_3,\omega_3)=\omega(-1,1) \quad (2.1b)$$

Fig. 2.1 uses conventional  $(ck,\omega)$ -plots for per-space-time and  $(x,ct)$ -plots for space-time. Both beams have frequency  $\nu=\omega/2\pi=600THz$ (green), the unit scale for  $\omega$  and  $ck$  axes. For the **L**-beam,  $ck$  equals  $-\omega$ .

Phase vector  $\mathbf{P}=\mathbf{K}_{phase}$  and group vector  $\mathbf{G}=\mathbf{K}_{group}$  are also plotted in  $(\omega,ck)$ -space in Fig. 2.1b.

$$\begin{aligned} \mathbf{K}_{phase} &= \frac{\mathbf{K}_1 + \mathbf{K}_3}{2} = \frac{1}{2} \begin{pmatrix} ck_1 + ck_3 \\ \omega_1 + \omega_3 \end{pmatrix} \\ &= \mathbf{P} = \begin{pmatrix} ck_p \\ \omega_p \end{pmatrix} = \frac{\omega}{2} \begin{pmatrix} 1-1 \\ 1+1 \end{pmatrix} = \omega \begin{pmatrix} 0 \\ 1 \end{pmatrix} \end{aligned} \quad (2.2a)$$

$$\begin{aligned} \mathbf{K}_{group} &= \frac{\mathbf{K}_1 - \mathbf{K}_3}{2} = \frac{1}{2} \begin{pmatrix} ck_1 - ck_3 \\ \omega_1 - \omega_3 \end{pmatrix} \\ &= \mathbf{G} = \begin{pmatrix} ck_g \\ \omega_g \end{pmatrix} = \frac{\omega}{2} \begin{pmatrix} 1+1 \\ 1-1 \end{pmatrix} = \omega \begin{pmatrix} 1 \\ 0 \end{pmatrix} \end{aligned} \quad (2.2b)$$

Phase and group velocities of counter-propagating light waves may vary from  $c$ . These surely do!

$$\frac{V_{phase}}{c} = \frac{\omega_1 + \omega_3}{ck_1 + ck_3} = \frac{2}{0} = \infty \quad (2.3a)$$

$$\frac{V_{group}}{c} = \frac{\omega_1 - \omega_3}{ck_1 - ck_3} = \frac{0}{2c} = 0 \quad (2.3b)$$

The extreme speeds account for the square (Cartesian) wave-zero (WZ) coordinates plotted in Fig. 2.1c. As noted for Fig. 1.5, the group zeros or wave nodes are stationary and parallel to the time  $ct$ -axes, while the real-zeros of the phase wave are parallel to the space  $x$ -axes. The latter instantly appear and disappear periodically with infinite speed (2.3a) while standing wave nodes have zero speed (2.3b).

Fig. 2.1d shows 2-way pulse wave (2-PW) trains for comparison with the 2-CW WZ grid in Fig. 2.1c. As noted for Fig. 1.3, a PW function is an  $N$ -CW combination that suppresses its amplitude through *destructive* interference between pulse peaks that owe their enhancement to *constructive* interference.

Colliding PW's show no mutual interference in destroyed regions. Generally one PW is alone on its diamond path going  $+c$  parallel to 1<sup>st</sup> baseline  $\mathbf{R}=\mathbf{K}_1$  or going  $-c$  parallel to 3<sup>rd</sup> baseline  $\mathbf{L}=\mathbf{K}_3$ .

$$\frac{V_1}{c} = \frac{\omega_1}{ck_1} = \frac{1}{1} = 1 \quad (2.4a)$$

$$\frac{V_3}{c} = \frac{\omega_3}{ck_3} = \frac{1}{-1} = -1 \quad (2.4b)$$

But wherever two PW peaks collide, each of the CW pairs will be seen trying to form a square coordinate grid that 2-CW zeros would make by themselves. This begins to explain the tiny square “bases” seen at the corners of the space-time “baseball diamonds” in Fig. 2.1d simulation.

### CW-Doppler derivation of relativity

Evenson's CW razor-cut of Einstein's PW axiom improves relativity development. However, quantifying Einstein's popular (and still common) derivation is difficult as is a step-by-step count for the CW derivation that

follows. Let us just say that *several* steps are reduced to *fewer* and *clearer* steps. Most important is the wave-natural insight that is gained and the wave mechanics that follows.

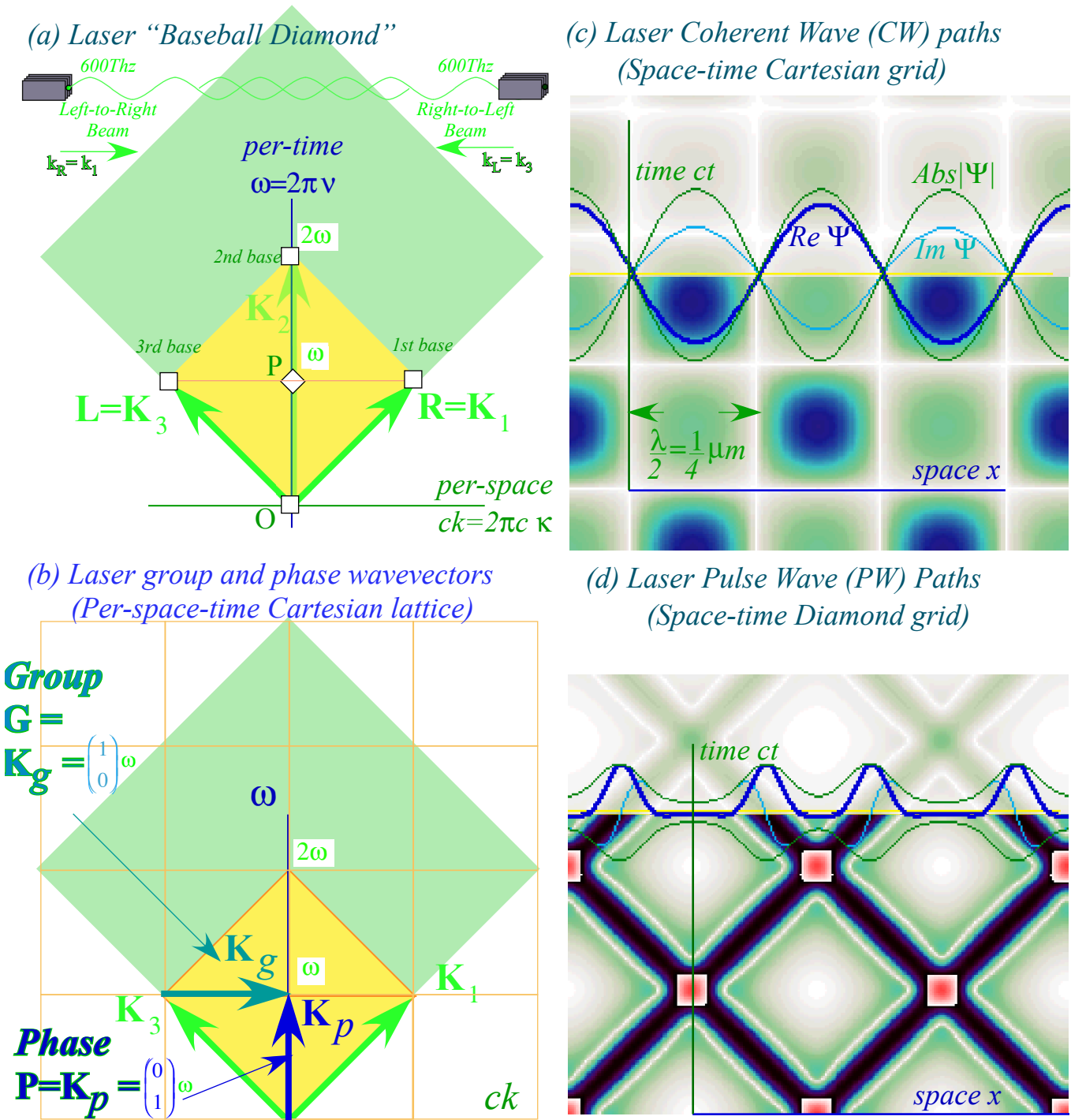
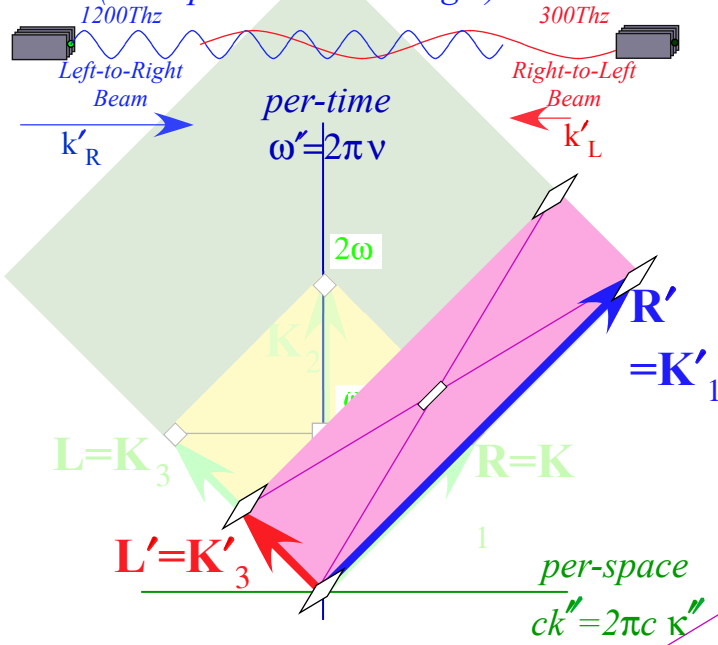


Fig. 2.1. Laser lab view of 600Thz CW and PW light waves in per-space-time (a-b) and space-time (c-d).

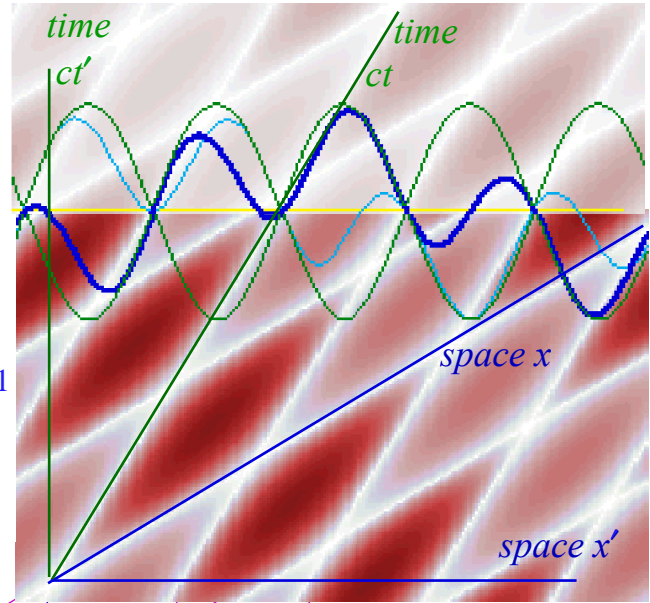
In fact, we could claim that a CW derivation takes *zero* steps. It is already done by a 2-CW wave pattern in Fig. 2.2c that automatically produces an Einstein-Lorentz-Minkowski<sup>vi</sup> grid of space-time coordinates. Still we need logical steps drawn in Fig. 2.2a-b that redo the Cartesian grid in Fig. 2.1 just by Doppler shifting each baseline one octave according to *c*-axiom (1.1) (“*Stay on baselines!*”) and *t*-reversal axiom (1.2) (“*If 1<sup>st</sup> base increases by one octave, 3<sup>rd</sup> base decreases by the same.*”)



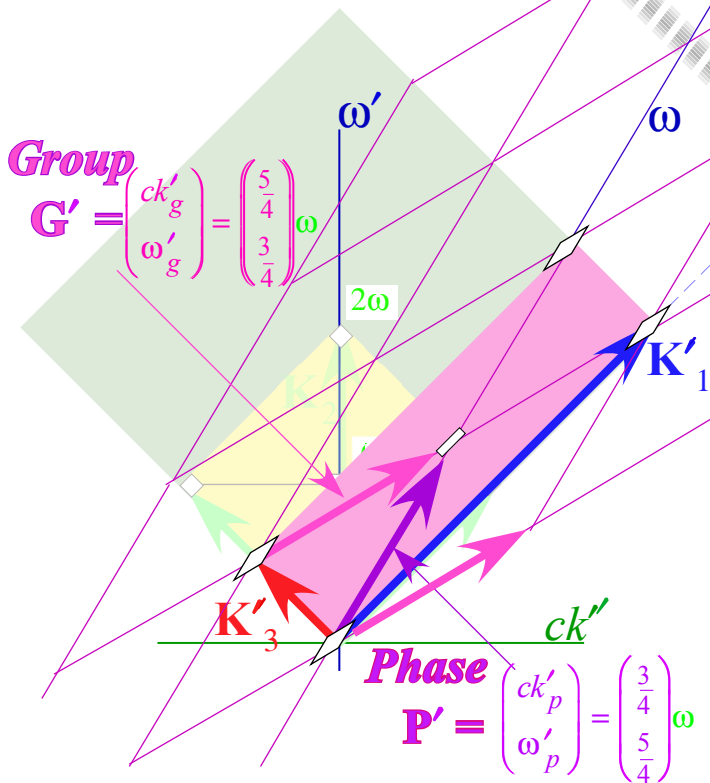
(a) Boosted Laser “Baseball Diamond”  
(Per-space-time rectangle)



(c) ( $u=3c/5$ )-Boosted CW paths  
(Space-time Minkowski grid)



(b) Boosted group and phase wavevectors  
(Per-space-time Minkowski lattice)



(d) Boosted PW Paths  
(Rectangular grid)

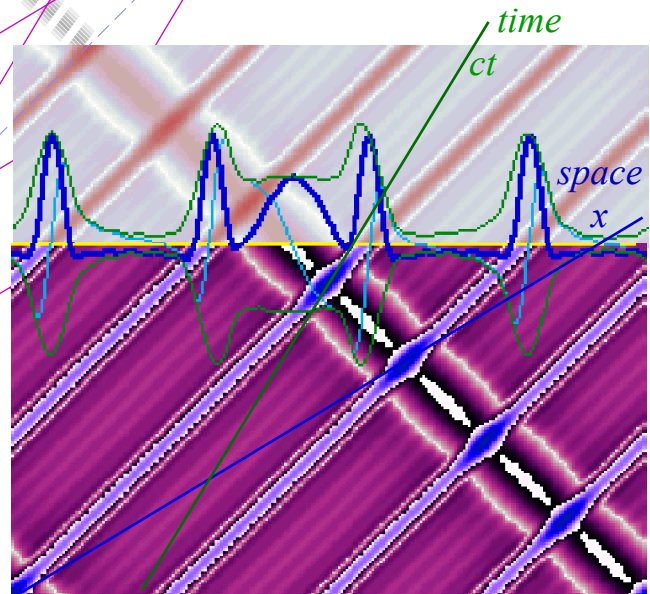


Fig. 2.2 Atom view of 600Thz CW and PW light waves in per-spacetime (a-b) and space-time (c-d) boosted to  $u=3c/5$ .

Einstein’s PW axiom “PW speed  $c$  is invariant,” might give the impression that pulses themselves are invariant, but finite- $\Delta$  pulses in Fig. 2.2d clearly deform. Pulse speed is invariant but each CW square in Fig. 2.3a deforms into a Minkowski-like rhombus in Fig. 2.3b simply due to Doppler detuning beats.

### Lorentz-Einstein transformations

The Lorentz<sup>vii</sup>-Einstein<sup>viii</sup> per-spacetime and spacetime transformations follow from **K**-vectors (2.9).

$$\begin{pmatrix} \omega' \\ ck' \end{pmatrix} = \begin{pmatrix} 1 & u/c \\ \sqrt{1-u^2/c^2} & \sqrt{1-u^2/c^2} \\ u/c & 1 \\ \sqrt{1-u^2/c^2} & \sqrt{1-u^2/c^2} \end{pmatrix} \begin{pmatrix} \omega \\ ck \end{pmatrix} \quad (2.10a) \quad \begin{pmatrix} x' \\ ct' \end{pmatrix} = \begin{pmatrix} 1 & u/c \\ \sqrt{1-u^2/c^2} & \sqrt{1-u^2/c^2} \\ u/c & 1 \\ \sqrt{1-u^2/c^2} & \sqrt{1-u^2/c^2} \end{pmatrix} \begin{pmatrix} x \\ ct \end{pmatrix} \quad (2.10b)$$

Wave **K**-vectors are bases for space-time *and* per-space-time. One symmetric LE matrix, invariant to axis-switch  $(\omega, ck) \rightleftharpoons (ck, \omega)$ , applies to both. Conventional  $\omega$ -ordinate vs.  $ck$ -abscissa per-space-time and  $ct$ -ordinate vs.  $x$ -abscissa space-time plots are used in Fig. 2.2 where  $\hat{\omega} = \mathbf{P} = \mathbf{K}_{phase}$  and  $\hat{ck} = \mathbf{G} = \mathbf{K}_{group}$  vectors serve as  $x$ -space and  $ct$ -time bases, respectively, and then also serve as  $\omega$ -and- $ck$ -bases.

The left and right pulse wave (PW) vectors **L** and **R** in per-space-time Fig. 2.2a also define left and right PW paths in space-time Fig. 2.2d. This holds in either convention because **L** and **R** lie on 45° reflection planes that are eigenvectors of an axis-switch  $(\omega, ck) \rightleftharpoons (ck, \omega)$  with eigenvalues  $+1$  and  $-1$  while half-sum-and-difference vectors  $\mathbf{P} = (\mathbf{L} + \mathbf{R})/2$  and  $\mathbf{G} = (\mathbf{L} - \mathbf{R})/2$  simply switch ( $\mathbf{P} \rightleftharpoons \mathbf{G}$ ).

### Geometry of Lorentz-Einstein contraction-dilation

Fig. 2.3 compares wave path space-time coordinate lines for the laser lab in top figure (a) and for the atom going right-to-left at speed  $u=3c/5$  in bottom figure (b).

The fast wave-phase zeros define the space- $x$  axis and gridlines in either view where they go at a speed of  $5c/3$  in the atom view and at infinite speed  $\infty$  in the lab view.

The slow wave-group zeros define the time- $ct$  axis and gridlines in either view where they go at a speed of  $3c/5$  in the atom view and at zero speed  $0$  in the lab view.

The spatial separation of the slow wave-group zeros in Fig. 2.2c is  $4/5$  of the original  $1/4\mu\text{m}$  shown separating the stationary wave zeros in Fig. 2.1c or Fig. 1.5a. That is the *Lorentz contraction factor*  $1/d$ .

$$1/d = \sqrt{1-u^2/c^2} \quad (2.11)$$

The well-known *Einstein time dilation factor*  $d$  is inverse to Lorentz contraction.

$$d = \sqrt{1-u^2/c^2} \quad (2.12)$$

Here this inverse time dilation factor  $d=5/4$  is the vertical height of the new “pitcher’s mound”  $P$  in Fig. 2.2a that was originally of unit height in Fig. 2.1a. In space-time diamond of Fig. 1.5b the pitcher’s mound is  $5/6 fs$  from origin or “home plate” and that dilates by factor  $d=5/4$  to  $25/24 fs$  in Fig. 2.2c.

The invariant hyperbolas that determine space-time scaling in Fig. 2.4 are among the most important topics in the following chapters 3 and 4. More detailed geometry of relativistic quantities is given in later figures. (Fig. 5.1, 5.4, and 5.5.)



### Chapter 3. Invariance and Relative Phase: Galileo’s revenge

Einstein relativity shows Galilean relativity, based on simple velocity sums and differences, to be a 400 year-old approximation that fails utterly at high speeds. Einstein also dethrones *infinite* velocity that is the one invariant velocity shared by Galilean observers regardless of their (finite) velocity. In its place reigns a finite velocity limit  $c=299,792,458ms^{-1}$  that is now the Einstein-Maxwell-Evenson invariant speed.

So it is remarkable that frequency sums and differences (1.10) simplify relativity by using Galilean-like rules for *angular* velocities  $\omega_A = \dot{\phi}_A$  of light phases  $\phi_A$ . Frequency sums or differences  $\omega_A \pm \omega_B$  from interference terms like  $\psi_A \psi_B^* = ABe^{-i(\omega_A - \omega_B)t}$  between wave pairs  $\psi_A = Ae^{-i\omega_A t}$  and  $\psi_B = Be^{-i\omega_B t}$  are *relative* frequencies (beat notes, overtones, etc.) subject only to simple addition and subtraction rules that are like Galileo’s rules for linear velocity. Simple angular phase principles deeply underlie modern physics, and so far there appears to be no  $c$ -like speed limit for an angular velocity  $\omega$ .

Phase principles have electromagnetic origins. Writing oscillatory wave functions using real and imaginary parts is used to study AC phenomena or harmonic oscillators in Unit 4. Real part  $q$  of oscillator amplitude  $q+ip = Ae^{-i\omega t}$  is its *position*  $q = A\cos\omega t$ . Imaginary part  $p = A\sin\omega t$  is oscillator *velocity*  $v = -A\omega\sin\omega t$  in units of angular frequency  $\omega$ . Positive  $\omega$  gives a clockwise rotation like that of classical phase space or analog clocks, so a minus sign in a conventional  $Ae^{-i\omega t}$  phasor serves to remind us that wave frequency  $\omega$  *defines* our clocks and wavevector  $k = \omega/c$  *defines* our meter sticks. (Recall Fig. 1.10.5 and Fig. 4.2.1.)

A plane wave of wavevector  $k$  in Fig. 3.1 is drawn as a phasor array, one  $A = |A|e^{ikx}$  for each location  $x$ . A plane wave advances in time according to  $|A|e^{i(kx - \omega t)}$  at phase velocity  $V = \omega/k$ . Similar convention and notation are used for light waves and for quantum matter waves, but only light waves have physical units, vector potential  $\mathbf{A}$  and electric  $\mathbf{E}$ -field, defining their real and imaginary parts. While classical laser wave phase is observable, only *relative* phase of a quantum wave  $\psi$  appears to be so.

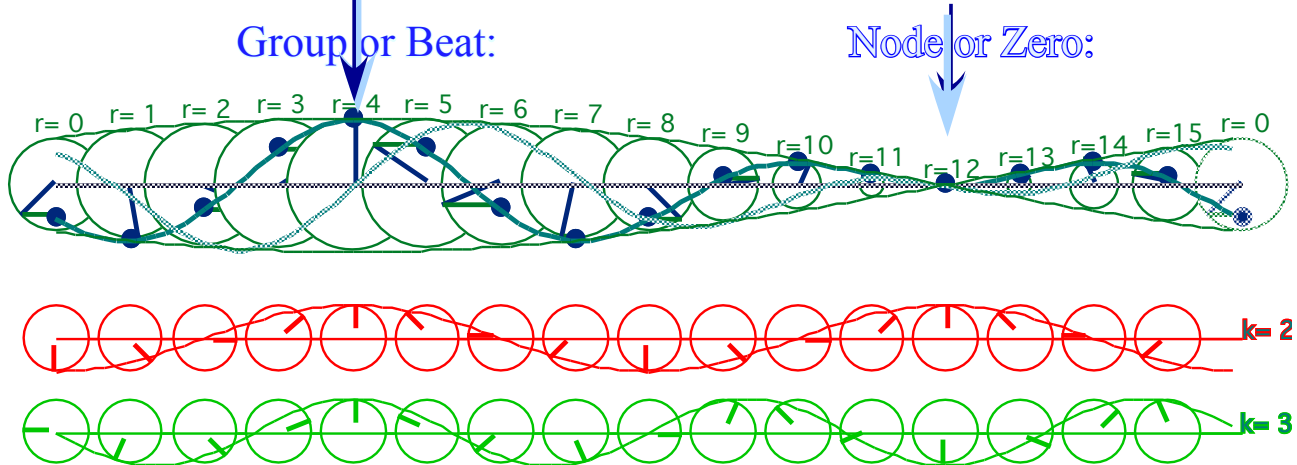
The concept of relative phase (and frequency) arises in classical or quantum interference where a sum of two waves  $\psi_A = Ae^{i\phi_A}$  and  $\psi_B = Be^{i\phi_B}$  may be represented at each position  $x$  by a vector sum of a phasor-A with a phasor-B as in Fig. 3.1a. (Fig. 3.1 has a sum of 12 phasors, one for each  $x$ -point.) The result is a clockwise race around a track between the faster one, say A-phase  $\phi_A = k_A x - \omega_A t$  of angular speed  $-\omega_A$ , and the slower B-phase  $\phi_B = k_B x - \omega_B t$  of angular speed  $-\omega_B$  as sketched in Fig. 3.1b.

Galilean relativity of phase angular velocity holds if the phase wave is governed by linear equations of motion such as Maxwell’s equations. Very precise measurements of *en vacuo* light have verified this so far and Einstein relativity is a consequence. You might say this is Galileo’s revenge!

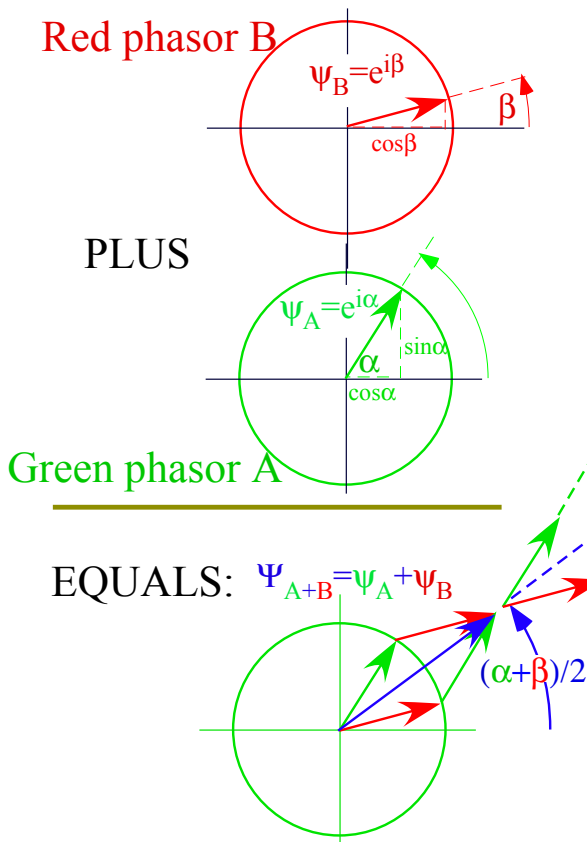
#### Geometry of relative phase

When A passes B the sum is a maximum or *beat* that then subsides to a minimum or *node* when A is on the opposite side of the track from B. If amplitude magnitudes  $|A|$  and  $|B|$  are equal as they are in Fig. 3.1, then the wave node is a wave *zero* that defines one of the group  $\mathbf{G}$ -lines in WZ coordinates of Fig. 1.4 through Fig. 2.2.

(a) Sum of Wave Phasor Array



(b) Typical Phasor Sum:



(c) Phasor-relative views

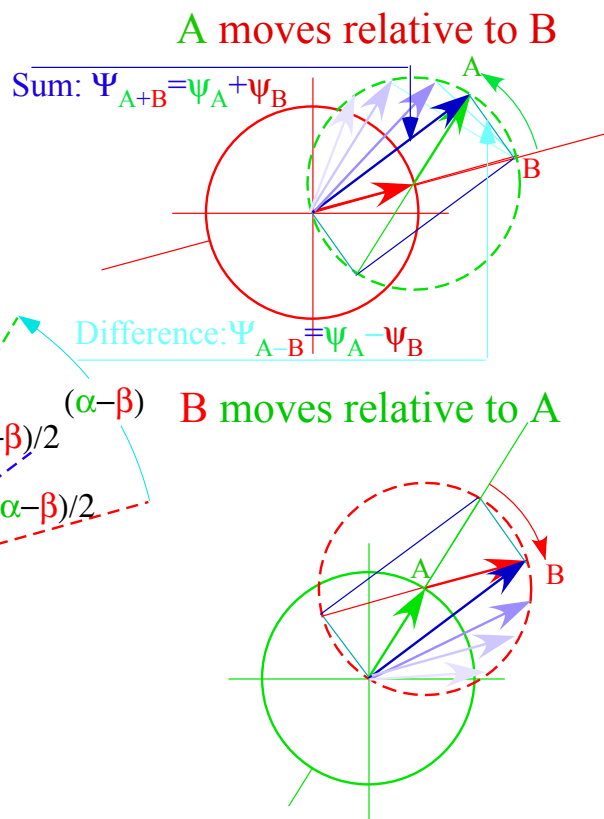


Fig. 3.1 Wave phasor addition. (a) Each phasor in a wave array is a sum (b) of two component phasors. (c) In phasor-relative views either A or else B is fixed. An evolving sum-and-difference rectangle is inscribed in the (dashed) circle of the phasor moving relative to the fixed one.

The relative angular velocity  $\Delta = \omega_A - \omega_B$  (beat angular frequency) is the angular rate at which A passes B. A-B passings occur  $\delta$  times (per sec.) where  $\delta$  is  $\Delta$  divided by track length  $2\pi$ .

$$\delta_{beat} = \Delta / 2\pi = \nu_A - \nu_B \tag{3.1}$$

If one could ride in an angular Galilean frame of phasor-B, then A would be seen passing at angular speed  $\Delta$  with frequency  $\delta$ . Suppose instead, one could ride at their *average* angular speed  $\bar{\Omega}$ .

$$\bar{\Omega} = \frac{1}{2} (\omega_A + \omega_B) \quad (3.2)$$

Then Galilean arithmetic (which lasers given no reason to doubt in these matters) implies that phasor A or B would each appear with a relative speed of plus-or-minus *half* their relative velocity.

$$\pm \frac{1}{2} \Delta = \pm \frac{1}{2} (\omega_A - \omega_B) \quad (3.3)$$

A point of view relative to phasor B is shown by the first of Fig. 3.1c. A dashed circle represents moving phasor A with  $\psi_A$  on one diagonal of an inscribed rectangle whose sides are the resultant sum  $\psi_A + \psi_B$  and difference  $\psi_A - \psi_B$ . The other diagonal  $\psi_B$  appears fixed. A companion figure has  $\psi_A$  appear fixed instead. Resultants in either figure begin and end on a dashed circle traced by the phasor that is moving relative to the other. A rectangle-in-circle is a key Euclidian element of wave physics and is a key feature of a later figure (Fig. 3.3) that shows the essence of wave interference geometry.

The half-sum and half-difference angles in Fig. 3.1b and frequencies (3.2) and (3.3) appear in the interference formulas (1.10) that lead to relativistic Lorentz-Einstein coordinate relations (2.10) and their WZ grid plots of Minkowski coordinates in Fig. 2.2c. One key is the *arithmetic mean*  $(\alpha + \beta)/2$  of phases that gives the *geometric mean*  $(\psi_A \psi_B)^{1/2} = A e^{i(\alpha+\beta)/2}$  of wave phasor amplitudes. The other key is the *difference mean*  $(\alpha - \beta)/2$  and that is the phase angle of a *cross mean*  $(\psi_A \psi_B^*)^{1/2} = A e^{i(\alpha-\beta)/2}$ .

Euclidian means and rectangle-in-circle constructions underlie relativistic wave geometry as is shown below. This geometry also leads to the geometry of contact transformations in classical mechanics that exposes relations between classical and quantum mechanics in Ch. 5.

### *Geometry of Doppler factors*

Any number  $N$  of transmitter-receivers (“observers” or “atoms” previously introduced) may each be assigned a positive number  $b_{11}, b_{21}, b_{31}, \dots$  that is its Doppler shift of a standard frequency  $\omega_l$  broadcast by atom-1 and then received as frequency  $\omega_{m1} = b_{m1} \omega_l$  by an atom- $m$ . By definition a transmitter’s own shift is unity. ( $1 = b_{11}$ ) Also, coefficient  $b_{m1}$  is independent of frequency since such *geometric* relations work as well on 1THz or 1Hz waves as both waves march in lockstep to the receiver by Evenson’s CW axiom (1.1). The production times of a single wavelength of the 1Hz-wave and  $10^{12}$  wavelengths of the 1THz wave must be the same (*1sec.*), and so must be reception time for the two waves since they arrive in lock step, even if  $\tau$  is shortened geometrically by  $1/b_{m1}$ . Doppler is a *geometric* and *multiplicative* effect.

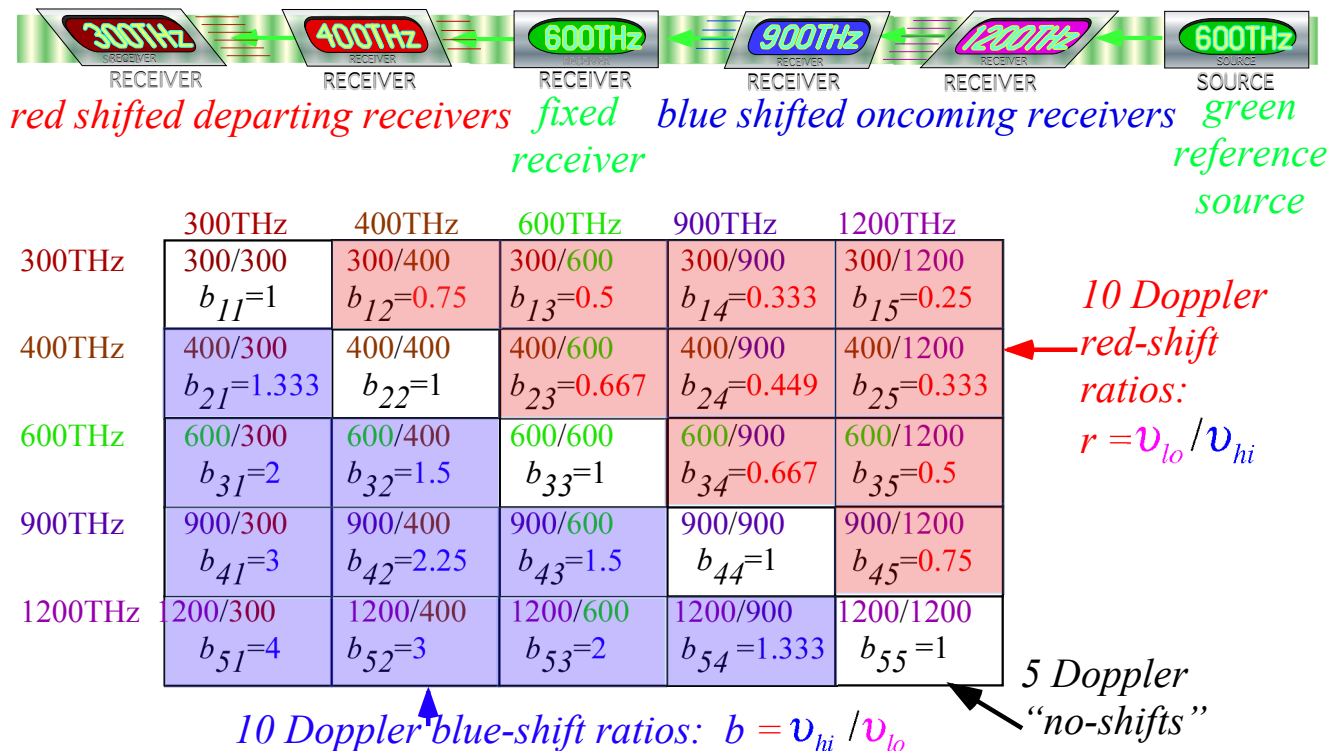


Fig. 3.2 Doppler shift  $b$ -matrix for a linear array of variously moving receiver-sources.

If atoms travel at constant speeds on a straight superhighway, then  $b_{m1}$  in (2.8a) tells what is the relative velocity  $u_{m1}$  of the  $m^{th}$  atomic receiver relative to the number-1 transmitter.

$$u_{m1}/c = (b_{m1}^2 - 1) / (b_{m1}^2 + 1) \tag{3.4}$$

The velocity  $u_{m1}$  is positive if the  $m^{th}$  atom goes toward transmitter-1 and sees a blue ( $b_{m1} > 1$ ) shift, but if it moves away  $u_{m1}$  is negative so it sees a red ( $b_{m1} < 1$ ) shift. Transmitter-1 has no velocity relative to itself. ( $u_{11}=0$ ) Infinite blue (or red) shift  $b_{m1} = \infty$  (or  $b_{m1} = 0$ ) gives  $u_{m1} = c$  (or  $u_{m1} = -c$ ) and this defines the range of parameters. The  $b_{m1}$  are constant until atom- $m$  passes atom-1 so relative velocity flips sign ( $u_{1m} \rightarrow -u_{1m}$ ). Doppler shift then inverts ( $b_{1m} \rightarrow 1/b_{1m}$ ) as is consistent with axiom (1.2).

Suppose now  $b_{12}, b_{22}, b_{32}, \dots$  are Doppler shifts of frequency  $\omega_2$  transmitted by the *second* atom and received by the  $m^{th}$  atom as frequency  $\omega_{m2} = b_{m2} \omega_2$ . (Any atom (say the  $n^{th}$ ) may transmit, too.)

$$\omega_{mn} = b_{mn} \omega_n \tag{3.5a}$$

Recipients don’t notice if atom- $n$  just passes on whatever frequency  $\omega_{nm}$  came from atom- $m$ . If frequency  $\omega_n$  in (3.5a) is  $\omega_{n1} = b_{n1} \omega_1$  that atom- $n$  got from atom-1 then atom- $m$  will not distinguish a direct  $\omega_{m1}$  from a perfect copy  $b_{mn} b_{n1} \omega_1$  made by atom- $n$  from atom-1 and then passed on to atom- $m$ .

$$\omega_{m1} = b_{m1} \omega_1 = b_{mn} b_{n1} \omega_1 \tag{3.5b}$$

A multiplication rule results for Doppler factors and applies to light from atom-1 or any atom- $p$ .

$$\omega_{mp}/\omega_p = b_{mp} = b_{mn} b_{np} \tag{3.5c}$$

An inverse relation results from atom- $p$  comparing its own light to that copied by atom- $n$ .

$$1 = b_{pp} = b_{pn} b_{np} \text{ or: } b_{pn} = 1/b_{np} \tag{3.5d}$$

Notice that copying or passing light means just that and does not include reflection or changing  $+k$  to  $-k$  or any other direction. This presents a problem for a receiver not in its transmitter's  $(+k)$ -beam and certainly for atom- $p$  receiving its own beam. The relations (3.5) depend only on relative velocities and not positions (apart from the problem that a receiver might be on the wrong side of a transmitter).

An obvious solution is to let the receiver overtake its transmitter or failing that delegate a slave transmitter or receiver on its right side. Fig. 3.2 shows  $N=5$  receivers of a  $\omega_3=600THz$  source whose various speeds produce a matrix of  $N(N-1)=20$  Doppler shifted frequencies  $\omega_{mn}$  and factors  $b_{mn}$ .

*Doppler rapidity and Euclid means business*

Composition rules (3.5c) suggest defining Doppler factors  $b=e^\rho$  in terms of *rapidity*  $\rho=\ln b$ .

$$b_{mp}=b_{mn}b_{np} \quad \text{implies: } \rho_{mp}=\rho_{mn}+\rho_{np} \quad \text{where: } b_{ab}=e^{\rho_{ab}} \quad (3.6)$$

Rapidity parameters  $\rho_{mn}$  mimic Galilean addition rules as do phase angles  $\phi$  of wavefunctionss  $e^{i\phi}$ . Both  $\rho$  and  $\phi$  are the parameters that underlie relativity and quantum theory. In fact, by (3.4) rapidity  $\rho_{mn}$  approaches the relative velocity parameter  $u_{mn}/c$  between atom- $m$  and atom- $n$  for speeds much less than  $c$ . Rapidity is also convenient for astronomically large Doppler ratios  $b_{ab}$  since then the numerical value of  $\rho_{ab}=\ln b_{ab}$  is much less than  $b_{ab}$  while  $u_{mn}/c$  approaches 1 in a way that is numerically inconvenient.

At intermediate relativistic speeds the geometric aspects of Doppler factors provide a simple and revealing picture of the nature of wave-based mechanics. Pairs of counter moving continuous waves (CW) have mean values between a **K**-vector  $\mathbf{R}=\mathbf{K}_1=(ck_1,\omega_1)$  going left-to-right and an  $\mathbf{L}=\mathbf{K}_3=(ck_3,\omega_3)$  going right-to-left. A key quantity is the *geometric mean*  $\varpi$  of left and right frequencies.

$$\varpi = \sqrt{\omega_1\omega_3} \quad (3.7)$$

In Fig. 3.2a frequency  $\omega_1=1$  or  $\omega_3=4$  is a blue ( $b=e^{+\rho}=2$ ) or red ( $r=e^{-\rho}=1/2$ ) shift of mean  $\varpi = \sqrt{1 \cdot 4} = 2$ .

$$\omega_1 = b\varpi = e^{+\rho}\varpi \quad (3.8a)$$

$$\omega_3 = r\varpi = e^{-\rho}\varpi \quad (3.8b)$$

In units of  $2\pi \cdot 300THz$ , frequency values  $\omega_3=1$  and  $\omega_1=4$  were used in Fig. 2.2. Their half-sum  $5/2$  is their *arithmetic mean*. That is the radius of the circle in Fig. 3.2b located a *half-difference* ( $3/2$ ) from origin.

$$\frac{\omega_1 + \omega_3}{2} = \varpi \frac{e^{+\rho} + e^{-\rho}}{2} = \varpi \cosh \rho = \varpi \frac{5}{2} \quad (3.9a)$$

$$\frac{\omega_1 - \omega_3}{2} = \varpi \frac{e^{+\rho} - e^{-\rho}}{2} = \varpi \sinh \rho = \varpi \frac{3}{2} \quad (3.9b)$$

By (2.8) the difference-to-sum ratio is the group or *mean frame* velocity-to- $c$  ratio  $u/c=3/5$  for  $b=2$ .

$$\frac{\omega_1 - \omega_3}{\omega_1 + \omega_3} = \frac{\sinh \rho}{\cosh \rho} = \tanh \rho = \frac{u}{c} \quad (3.9c)$$

$$\frac{4-1}{4+1} = \frac{u}{c} = \frac{3}{5} \quad (3.9d)$$

The geometric mean ( $\varpi = \sqrt{1 \cdot 4} = 2$ ) in units of  $2\pi \cdot 300THz$  is the initial  $600THz$  green laser lab frequency used in Fig. 2.1. Diamond grid sections from Fig. 2.2b are redrawn in Fig. 3.3b to connect with the geometry of the Euclidian rectangle-in-circle elements of interfering-phasor addition in Fig. 3.1c.

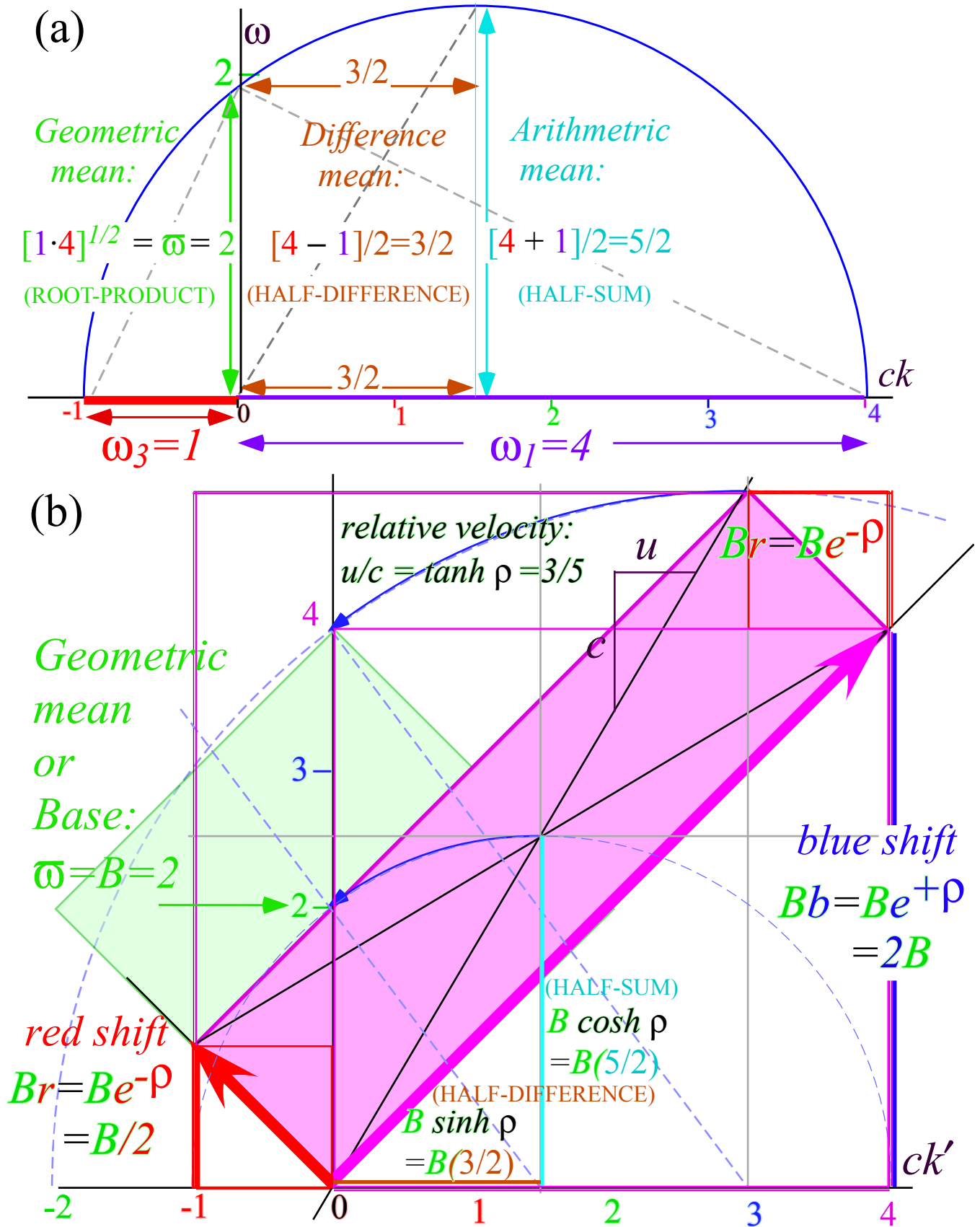


Fig. 3.3a Euclidian mean geometry for counter-moving waves of frequency 1 and 4. (300THz units).

Fig. 3.3b Geometry for the CW wave coordinate axes in Fig. 2.2.

Various observers see the single continuous wave frequencies  $\omega_1$  or  $\omega_3$  shifted to  $\omega'_1=e^{+\rho}\omega_1$  and  $\omega'_3=e^{-\rho}\omega_3$ , that is, to values between zero and infinity. But, because factor  $e^{-\rho}$  cancels  $e^{+\rho}$ , all will agree on the 2-CW mean value  $\varpi =[\omega_1\omega_3]^{1/2}=[\omega'_1\omega'_3]^{1/2}$ . A 2-CW function has an *invariant*  $\varpi$  of its *rest frame* (Recall Fig. 2.2c) seen at velocity  $u=c(\omega_1-\omega_3)/(\omega_1+\omega_3)$ . A single CW has no rest frame or frequency since all observers see it going  $c$  as in Fig. 1.1. To make a home frame, a single CW must marry another one!

**Invariance of proper time (age) and frequency (rate of aging)**

Space, time, and frequency may seem to have an out-of-control fluidity in a wavy world of relativism, so it is all the more important to focus on relativistic invariants. Such quantities make ethereal light billions of times more precise than any rusty old meter bar or clanking cuckoo clock.

It is because of the time-reversal (1.2) and Evenson axiom (1.1) that product  $\omega_1\omega_3=\varpi^2$  is invariant to inverse blue-and-red Doppler shifts  $b=e^{+\rho}$  and  $r=e^{-\rho}$ . It means the blue-red shifted diamond in Fig. 3.3b or Fig. 2.2 has the same area  $\mathbf{R}'\times\mathbf{L}'$  as the original green “home field” baseball diamond area  $\mathbf{R}\times\mathbf{L}$  drawn below it and in Fig. 2.1. Constant products  $\omega_1\omega_3=const.$  give families of hyperbolas.

$$|\mathbf{R}\times\mathbf{L}|=2|\mathbf{G}\times\mathbf{P}|=2|\mathbf{K}_{group}\times\mathbf{K}_{phase}|=2|\varpi^2\cosh^2\rho - \varpi^2\sinh^2\rho|=2\varpi^2$$

One hyperbola in Fig. 3.4a intersects bottom point  $B=\varpi$  (“pitchers’ mound”). The other hits  $2B$  (2<sup>nd</sup> base). Each horizontal  $\mathbf{P}$ -hyperbola is defined by the phase vector  $\mathbf{P}=\mathbf{K}_{phase}$  or some multiple of  $\mathbf{P}$ .

$$\mathbf{K}_{phase} = \frac{\varpi}{2} \begin{pmatrix} e^{\rho} - e^{-\rho} \\ e^{\rho} + e^{-\rho} \end{pmatrix} = \varpi \begin{pmatrix} \sinh \rho \\ \cosh \rho \end{pmatrix} = \begin{pmatrix} ck_p \\ \omega_p \end{pmatrix} \quad \text{on P-hyperbola: } (\omega_p)^2 - (ck_p)^2 = \varpi^2 \quad (3.10a)$$

Each vertical  $\mathbf{G}$ -hyperbola is defined by the wave group vector  $\mathbf{G}=\mathbf{K}_{group}$  or some multiple of  $\mathbf{G}$ .

$$\mathbf{K}_{group} = \frac{\varpi}{2} \begin{pmatrix} e^{\rho} + e^{-\rho} \\ e^{\rho} - e^{-\rho} \end{pmatrix} = \varpi \begin{pmatrix} \cosh \rho \\ \sinh \rho \end{pmatrix} = \begin{pmatrix} ck_g \\ \omega_g \end{pmatrix} \quad \text{on G-hyperbola: } (ck_g)^2 - (\omega_g)^2 = \varpi^2 \quad (3.10b)$$

The  $\mathbf{G}$ -vectors serve as tangents to  $\mathbf{P}$ -hyperbolas and vice-versa. The tangent slope  $\frac{d\omega}{dk}$  to any  $\omega(k)$  curve is a well known definition of group velocity. Fig. 3.4b shows how  $\frac{d\omega}{dk}$  of a  $\mathbf{P}$ -hyperbola is equal to secant slope  $\frac{\Delta\omega}{\Delta k}$  in Fig. 3.4a as defined in the  $u=V_{group}$  equation (2.7b) based on CW axioms.

Phase velocity  $\frac{\omega}{k}=V_{phase}$  and its  $\mathbf{P}$ -vector is an axis-switch  $(\omega,ck) \rightleftharpoons (ck,\omega)$  of  $\frac{\Delta\omega}{\Delta k}$  and its  $\mathbf{G}$ -vector. In conventional  $c$ -units  $V_{group}/c < 1$  and  $1 < V_{phase}/c$  are inverses according to (2.7). ( $V_{phase}\cdot V_{group}=c^2$ )

Features on per-space-time  $(ck,\omega)$  plots of Fig. 3.3-Fig. 3.4 reappear on space-time  $(x,ct)$  plots as noted in Fig. 2.1 and Fig. 2.2. A space-time invariant analogous to (3.10) is called *proper-time*  $\tau$ .

$$(ct)^2 - (x)^2 = (c\tau)^2 = (ct')^2 - (x')^2 \quad (3.11)$$

It conventional to locate oneself at  $(0,ct)$  or presume one’s origin  $x=0$  is located on oneself. Then (3.11) reduces to time axis  $ct=c\tau$ . A colloquial definition of proper time is *age*, a digital readout of one’s computer clock that all observers may note. By analogy,  $\varpi$  is *proper-frequency*, a *rate of aging* or a digital readout on each of the spectrometers in Fig. 3.2. Each reading is available to all observers.

$$(\omega)^2 - (ck)^2 = (\varpi)^2 = (\omega')^2 - (ck')^2 \quad (3.12)$$

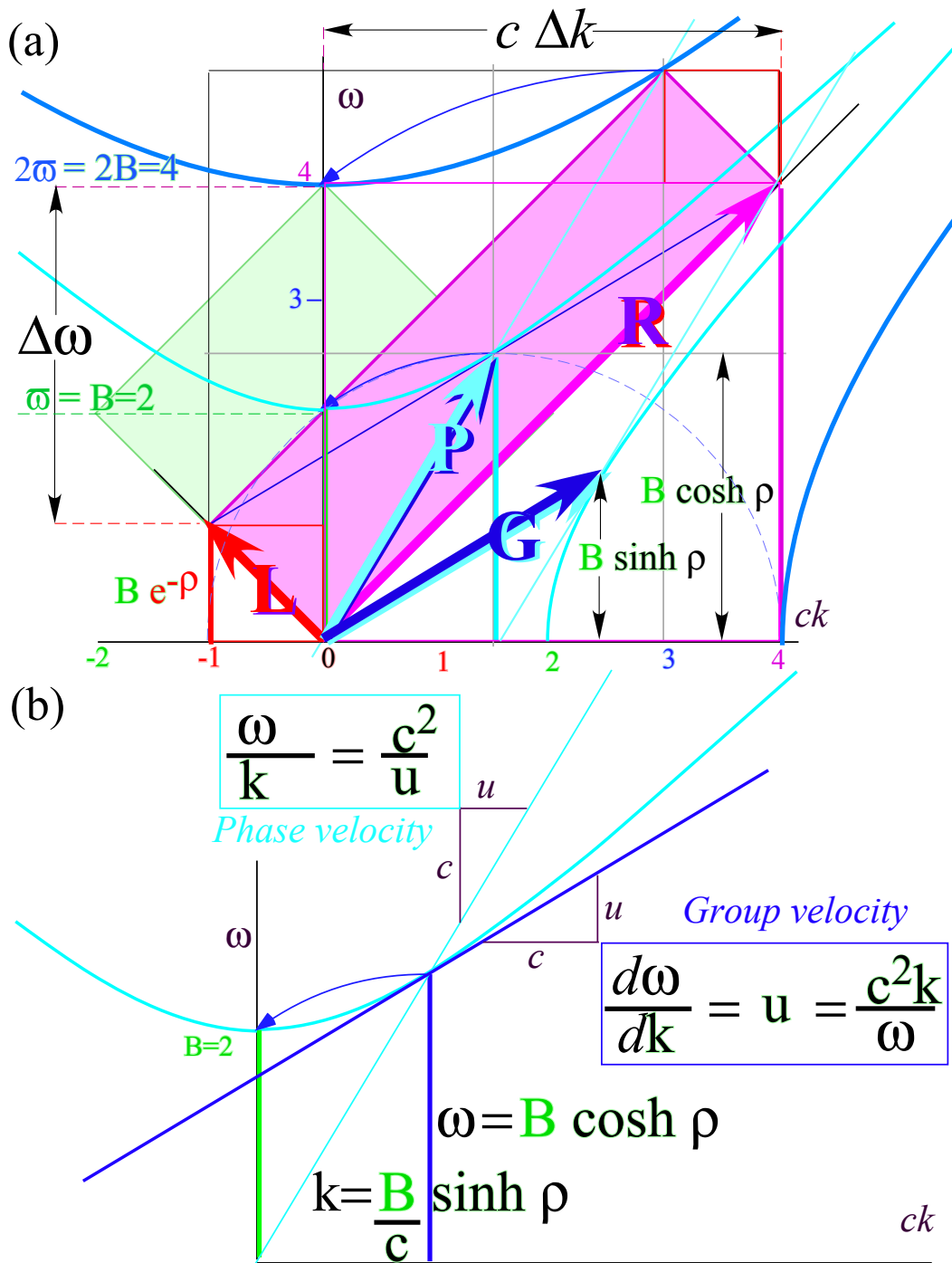


Fig. 3.4 (a) Horizontal G-hyperbolas for proper frequency  $B=\bar{\omega}$  and  $2B$  and vertical P-hyperbolas for proper wavevector  $k$ . (b) Tangents for G-curves are loci for P-curves, and vice-versa. Note: secant  $\Delta\omega/\Delta k$  and tangent  $d\omega/dk$  are always exactly equal.

The same hyperbolas (3.12) mark tics in laser lab  $(\omega, ck)$ , atom frame  $(\omega', ck')$ , or any other frame. The proper frequency of a wave is that frequency observed after one Doppler shifts the wave's kinks away, that is, the special frequency  $\bar{\omega}$  seen in the frame in which its wavevector is zero ( $ck=0$ ) in (3.12). Hence a single CW has a proper frequency that is identically zero ( $\bar{\omega} = 0$ ) by Evenson's axiom ( $\omega=ck$ ), so single CW light cannot age. If we could go  $c$  to catch up to light's home frame then its phasor clocks would appear to stop. Someone moving along a line of phasor clocks in Fig. 1.1c would always see the same reading, but that would be an infinite Doppler shift that one can only approach.

To produce a nonzero proper frequency  $\omega \neq 0$  requires interference of at least two CW entities moving in different directions and this produces a standing wave frame like Fig. 2.1c moving at a speed less than  $c$  as shown in Fig. 2.2c. Matched CW-pairs of **L** and **R** baselines frame a “baseball diamond” for which the phase wavevector  $k_p$  in (2.2a) is zero. Then frame velocity  $u = V_{group}$  in (2.3b) is zero, too.

Fig. 3.5 shows the plots of per-spacetime “baseball diamond” coordinates for comparison of lab and atom frame views. While Fig. 3.5a is a “blimp’s-eye view” of the lab-frame diamond in Fig. 2.1, the atom frame view in Fig. 3.5b looks like the baseball field seen by a spectator sitting in the stands above the dugout. Nevertheless, identical hyperbolas are used to mark grids in either view.

Each point on the lower hyperbola is a bottom point  $\omega' = B = 2$  (600THZ) for the frame whose relative velocity  $u'$  makes it a  $\omega'$ -axis ( $k' = 0$ )-point, and every ( $k' = 0$ )-point on the upper hyperbola is its bottom frequency point  $\omega' = 2B = 4$  (1200THZ), and so on for hyperbolas of any given proper frequency value  $\omega$ . The same applies to space-time plots for which time  $ct'$  takes the place of per-time  $\omega'$  and space  $x'$  takes the place of per-space  $ck'$ . Then bottom points are called proper time or  $\tau$ -values from (3.11).

For single CW light the proper time must be constant since a single CW cannot age. It is a convention to make the baselines or *light cone* intersect at the origin in both time and space. This sets the baseline proper time constant  $\tau$  to zero. Then invariants (3.11) reduce to baseline equations  $x = \pm ct$  or  $x' = \pm ct'$  for all frames. The space-time light cone relations are in direct correspondence with the per-space-time light cone relations  $\omega = \pm ck$  or  $\omega' = \pm ck'$  for zero proper frequency in all frames and are concise restatements of the Evenson CW axiom (1.1).

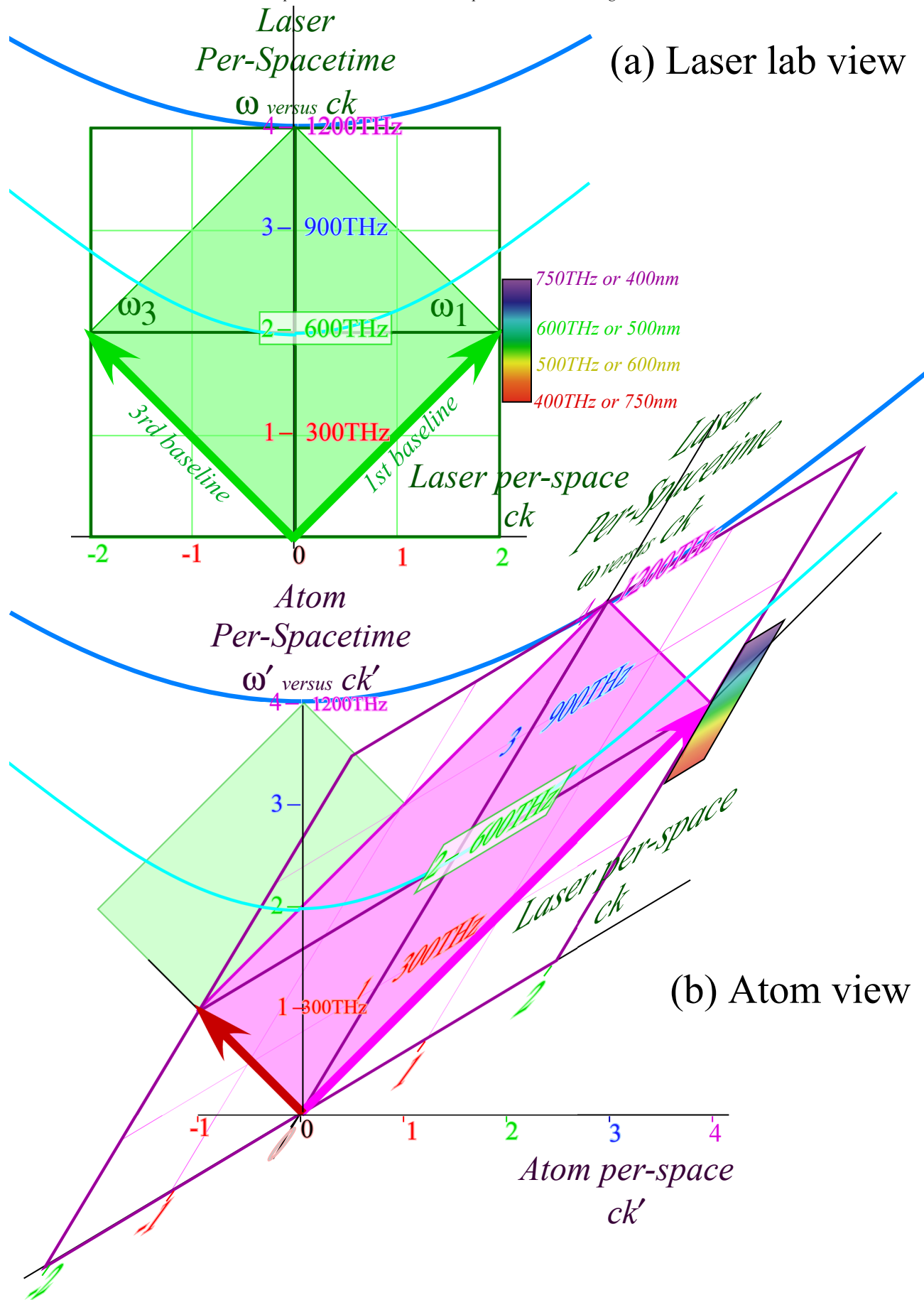


Fig. 3.5 Dispersion hyperbolas for 2-CW interference (a) Laser lab view. (b) Atom frame view.

In preceding Ch. 2, it was shown that objects seen by moving observers appear to be shortened by a factor  $1/d$  (*Lorentz contraction* (2.11)) and have lengthened (dilated) time periods (*Einstein time dialation* (2.12)) by the inverse factor  $d$ . These effects seem quite mysterious. Standard treatments of relativity begin (and often end) with these *2<sup>nd</sup> order* effects. Their algebraic formulas are pretty much all that students have to memorize for GRE testing. (See blue formulas in Fig. 3.6.)

However, it is the far less mysterious *1<sup>st</sup> order Doppler* effects that underlie relativity of the zig-zag waves of Fig. 2.2 and Fig. 2.3. The per-space-time geometry of Fig. 3.3 thru Fig. 3.5 is the same as that of space-time shown in Fig. 3.6. The latter clearly shows how the *2<sup>nd</sup> order* effects arise from wave-zero coordinate intersections with time and space axes. More detailed geometry of relativistic geometry as it applies to mechanics is given in later discussion and figures. (See ahead to Figures 5.1, 5.4, and 5.5.) The invariant hyperbolas that determine per-space-time and space-time scaling in Fig. 3.5 and Fig. 3.6 also serve as the relativistic Hamiltonian mass shell in Fig. 4.1 of the following chapter 4.

So how do things shrink and clocks slow down? Answer: All things are all made of waves, and that is what waves do!

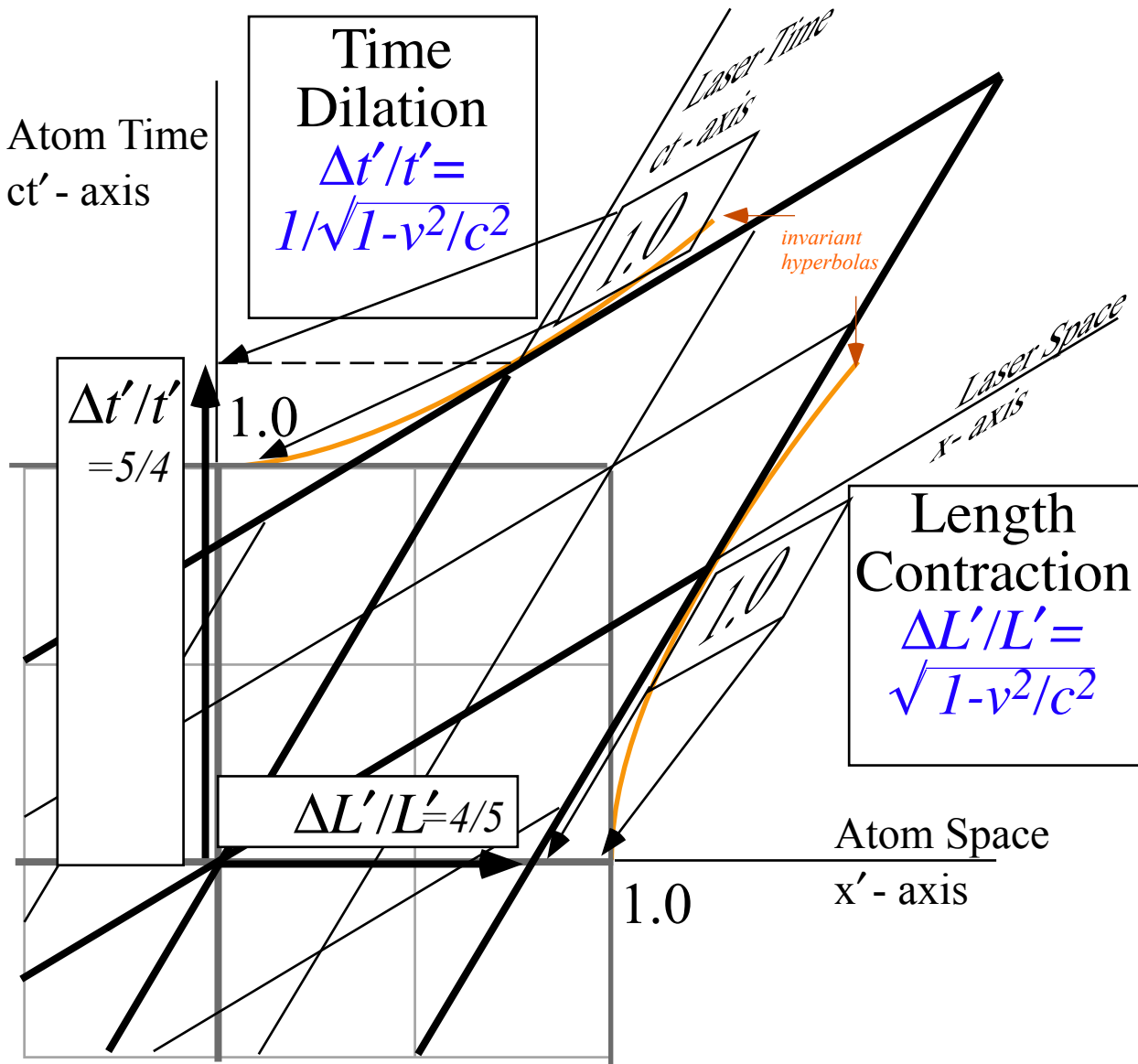


Fig. 3.6 Space-time grid intersections mark Lorentz contraction and Einstein time dilation.

## Chapter 4. Mechanics based on CW axioms

Each of the 2-CW structures or properties discussed so far are due to relative interference effects between pairs of 1-CW entities that, by themselves, lack key 2-CW properties such as a proper invariant frequency  $\omega$ , a rest frame, or any speed below the mortally unattainable velocity of  $c$ . To acquire “mortal” properties requires an interference encounter or *pairing* of 1-CW with another.

Now we see how 2-CW interference endows other “mortal” properties such as classical *mass* and relativistic mechanics of energy-momentum that characterize a *quantum matter wave*. Such endowment lies in P-hyperbola phase relations (3.10a) that in turn are due to CW axioms (1.1) and (1.2).

$$\begin{aligned} \omega_p &= B \cosh \rho & ck_p &= B \sinh \rho & \frac{u}{c} &= \tanh \rho \\ &\approx B + \frac{1}{2} B \rho^2 \text{ (for } u \ll c) & &\approx B \rho \text{ (for } u \ll c) & &\approx \rho \text{ (for } u \ll c) \end{aligned} \quad (4.1a) \quad (4.1b) \quad (4.1c)$$

Hyperbola in Fig. 3.4 has bottom  $B=\omega$  and **P**-vector components  $(\omega_p, ck_p)$  with tangent slope  $u/c$  at **P**. At low group velocity ( $u \ll c$ ) the rapidity  $\rho$  approaches  $u/c$ . Then  $\omega_p$  and  $k_p$  are simple functions of  $u$ .

$$\omega_p \approx B + \frac{1}{2} [B/c^2] u^2 \dots \quad (4.2a) \quad k_p \approx [B/c^2] u \dots \quad (4.2b)$$

The  $\omega_p$  and  $k_p$  fit Newtonian-energy  $E$  and Galilean-momentum  $p$ . Is that a coincidence? Perhaps, not!

$$E = \text{const.} + \frac{1}{2} Mu^2 \quad (4.3a) \quad p \approx Mu \quad (4.3b)$$

Wave  $\omega$  and  $k$  results (4.2), scaled by a *single* factor  $s=Mc^2/B$ , match classical  $E$  and  $p$  definitions (4.3).

$$E = s\omega_p \approx sB + \frac{1}{2} [sB/c^2] u^2 \dots \quad (4.4a) \quad p = sk_p \approx [sB/c^2] u \dots \quad (4.4b)$$

In Newton's mechanics, only energy *difference*  $\Delta E$  counts, so he might ignore the term  $E=\text{const.}$  (4.3a). But, in (4.4a) that  $\text{const.}=sB$  is the proper phase *carrier-frequency* value  $B=\omega$  at hyperbola bottom  $B$  in Fig. 3.4b. That is scaled by  $s=Mc^2/B$  to  $sB=s\omega$  in Fig. 4.1. It is *Einstein rest energy* and not ignorable!

$$\text{const.} = sB = Mc^2 = s\omega \quad (4.4c)$$

$\omega$ -mass-energy equivalence is a huge idea due to Einstein (1905) and Planck (1900).  $k$ -vector-momentum equivalence by DeBroglie came later (1920). CW results (4.1) give both directly and *exactly*.

$$E = s\omega_p = Mc^2 \cosh \rho = \frac{Mc^2}{\sqrt{1-u^2/c^2}} \quad (4.5a) \quad p = sk_p = Mc \sinh \rho = \frac{Mu}{\sqrt{1-u^2/c^2}} \quad (4.5b)$$

Scale factor  $s$  in Planck<sup>ix</sup>  $E=s\omega$  or DeBroglie<sup>x</sup>  $p=sk$  laws is found experimentally. The lowest observed  $s$ -value is Planck angular constant  $\hbar=1.05 \cdot 10^{-34} J \cdot s$ . That is Planck's axiom  $E=\hbar\omega_N=\hbar N\nu$  for  $N=1$ . Integer  $N$  is Planck's optical quantum number later called *photon-number*. At first, Planck regretted his 1900 axiom  $E=\hbar N\nu$ . It seems inconsistent with  $\omega^2$ -dependence of classical oscillator energy  $E=A^2\omega^2$ . In 1905, Einstein resolved this. A key idea is *quantized amplitude*  $A_N=\sqrt{\hbar N/\nu}$ . (Even amplitude is wavy!)

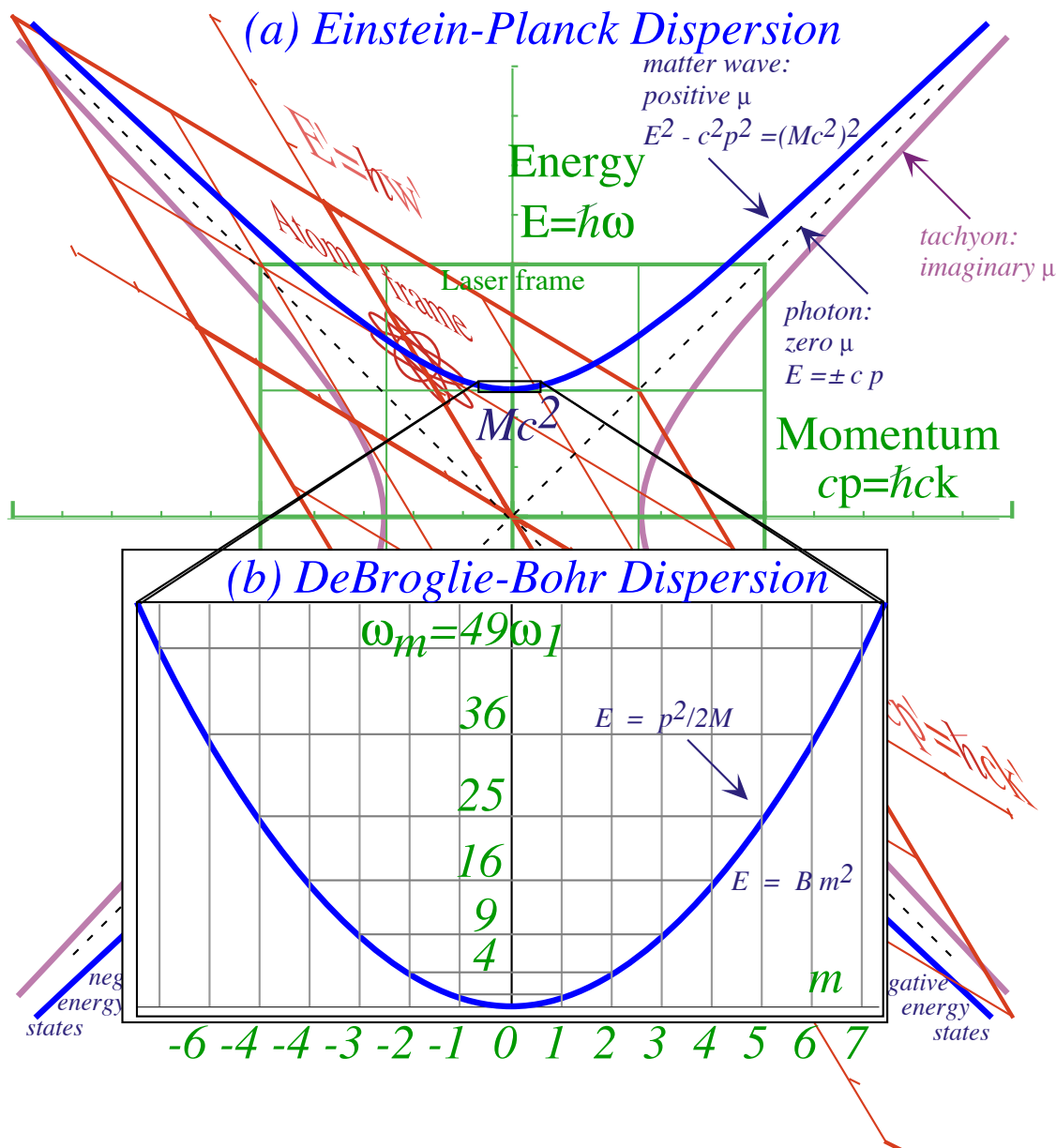


Fig. 4.1 Energy vs. momentum dispersion functions including mass  $M$ , photon, and tachyon.  
 (a) Relativistic (Einstein-Planck-deBroglie) case:  $(Mc^2)^2 = E^2 - (cp)^2 = 1$  or  $\mu^2 = \omega^2 - (ck)^2 = 1/\hbar^2$ .  
 (b) Non-relativistic (Bohr-Schrodinger-deBroglie) case:  $E = -(1/2M)p^2$  or  $\omega = \hbar k^2 / 2M$

Quantized cavity modes and “fuzzy” hyperbolas

Cavity boundary conditions “1<sup>st</sup>-quantize” classical wave mode variables  $(\omega_n, k_n)$  so as to have discrete numbers  $n=1,2,3,\dots$  of half-wave anti-nodes that fit in a cavity of length- $\ell$  as shown at the top of Fig. 4.2.

$$k_n = \pi / \lambda_n = n \cdot \pi / \ell \quad (4.6a)$$

$$\omega_n = c k_n = c n \cdot \pi / \ell \quad (4.6b)$$

Planck’s axiom “2<sup>nd</sup>-quantizes” each fundamental mode frequency  $\omega_n$  to have discrete quantum numbers  $N_n=0,1,2,3,\dots$  of photons. Each level  $E_N(n) = \hbar N_n \omega_n$  labels a hyperbola in Fig. 4.2 whose number  $n$  of anti-nodes and  $N$  of photons is *invariant*. This lends *object-permanence* to cavity “light particles” or photons.

As discussed later in Ch. 6, laser waves are *coherent state* combinations of  $N$ -photon states that have *semi-classical* properties that include well-defined wave phase. One “fuzzy” hyperbola of uncertain  $N$  and mass-energy

replaces the ladders in Fig. 4.2. This is a kind of 2<sup>nd</sup> Occam-razor cut after the 1<sup>st</sup> cut of PW into CW. As discussed in Ch. 6, it resolves CW into coherent combinations of “2<sup>nd</sup>-quantized” photons.

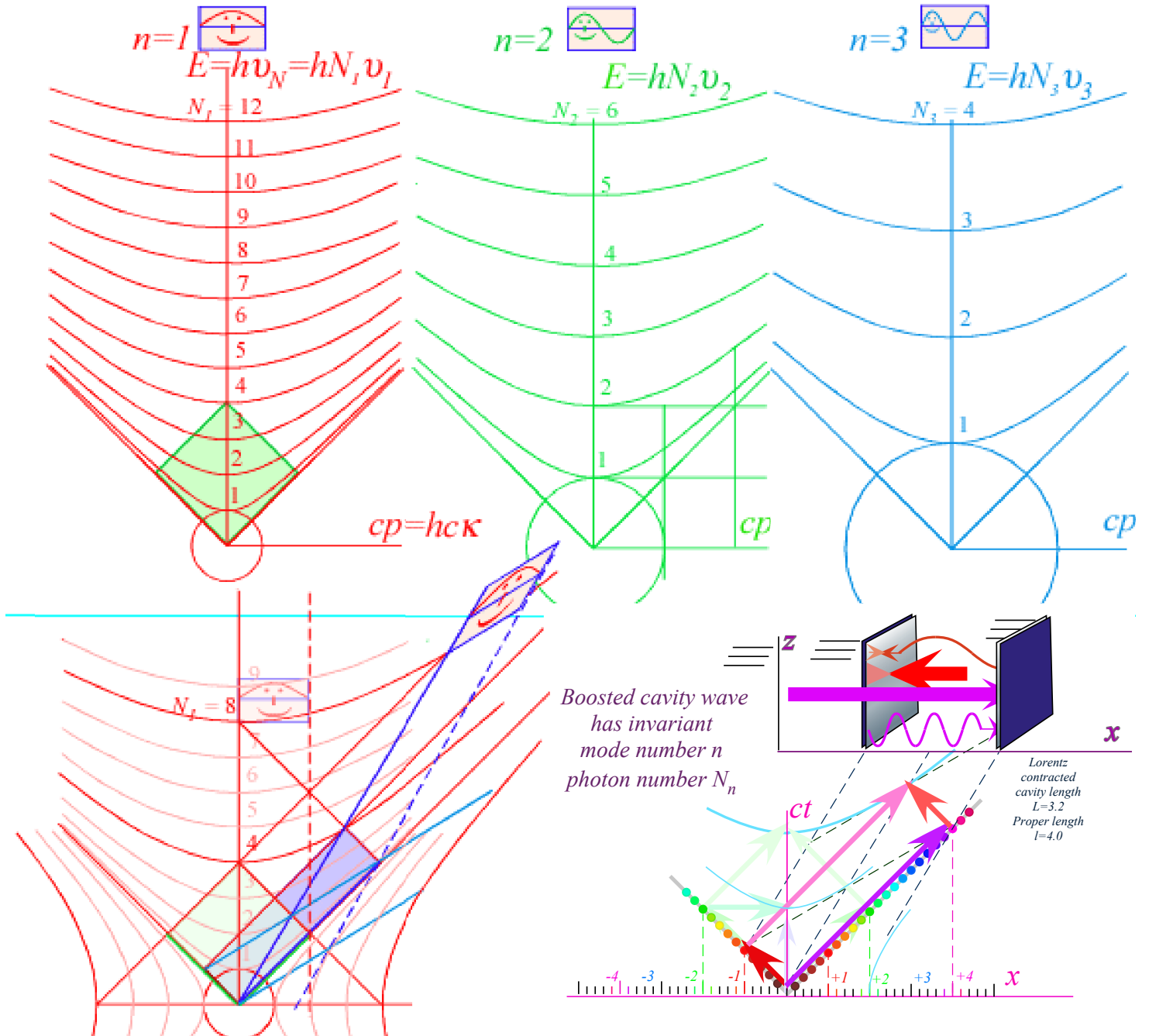


Fig. 4.2 Optical cavity energy hyperbolas for mode number  $n=1-3$  and photon number  $N=0, 1, 2, \dots$

*Alternative definitions of wave mass*

If mass or rest energy is due to proper phase frequency  $\omega$ , then a quantum matter wave has mass without invoking hidden Newtonian “stuff.” With Occam logical economy, 2-CW light led to *exact* mass-energy-momentum  $(\omega, k)$  relations (4.5) and not just low-speed classical ones (4.3). Now we see how 2-CW results expose some salient definitions of mass or matter that a classical theory might overlook.

First, the Einstein-Planck wave frequency-energy-mass equivalence relation (4.4c) ascribes *rest mass*  $M_{rest}$  to a scaled proper carrier frequency  $s\omega / c^2$ . The scale factor  $s$  is Planck’s  $s = \hbar N$  for  $N$  quanta.

$$M_{rest} = E / c^2 = \hbar N \omega / c^2 \tag{4.7}$$

For rest electron mass  $m_e = 9.1 \cdot 10^{-31} \text{kg}$  or  $M_p = 1.67 \cdot 10^{-27} \text{kg}$  of a proton, the proper frequency times  $N=2$  is called *zwitterbevegung* (“trembling motion”) and is as mysterious as it is huge. (Electron rest frequency  $\omega_e = m_e c^2 / \hbar = 7.76 \cdot 10^{20} (\text{rad})s^{-1}$  is the Dirac ( $e^+e^-$ )-pair production<sup>xi</sup> threshold as discussed in Ch. 8.)

Second, we define *momentum-mass*  $M_{mom}$  by ratio  $p/u$  of momentum (4.5b) to velocity  $u$ . (Galileo’s  $p=M_{mom}u$ ) Now  $M_{mom}$  varies as  $\cosh \rho \rightarrow e^\rho / 2$  at high rapidity  $\rho$  but approaches invariant  $M_{rest}$  as  $\rho \rightarrow 0$ .

$$\begin{aligned} \frac{p}{u} \equiv M_{mom} &= \frac{M_{rest}c}{u} \sinh \rho = M_{rest} \cosh \rho \xrightarrow{u \rightarrow c} M_{rest} e^\rho / 2 \\ &= M_{rest} / \sqrt{1 - u^2 / c^2} \xrightarrow{u \ll c} M_{rest} \end{aligned} \tag{4.8}$$

Frame velocity  $u$  is wave group velocity and the Euclid mean construction of Fig. 3.3a shows  $u$  is the slope of the tangent to dispersion function  $\omega(k)$ . A derivative of energy (4.5a) verifies this once again.

$$V_{group} = \frac{d\omega}{dk} = \frac{dE}{dp} = \frac{c^2 p}{E} = u \tag{4.9}$$

Third, we define *effective-mass*  $M_{eff}$  as ratio  $\dot{p} / \dot{u} = F/a = dp/du$  of momentum-*change* to acceleration. (Newton’s  $F=M_{eff}a$ )  $M_{eff}$  varies as  $\cosh^3 \rho \rightarrow e^{3\rho} / 2$  at high rapidity  $\rho$  but also approaches  $M_{rest}$  as  $\rho \rightarrow 0$ .

$$\begin{aligned} \frac{F}{a} \equiv M_{eff} &\equiv \frac{dp}{du} = \frac{\hbar dk}{dV_{group}} = \hbar \left/ \frac{d}{dk} \frac{d\omega}{dk} \right. = \hbar \left/ \frac{d^2\omega}{dk^2} \right. \\ &= M_{rest} / \left(1 - u^2 / c^2\right)^{3/2} \xrightarrow{u \ll c} M_{rest} \end{aligned} \tag{4.10}$$

Effective mass is  $\hbar$  divided by the curvature of dispersion function  $\omega(k)$ , a general quantum wave mechanical result. Geometry of a dispersion hyperbola  $\omega = Bc \cosh \rho$  is such that its bottom ( $u=0$ ) radius of curvature (*RoC*) is the rest frequency  $B = M_{rest}c^2 / \hbar$ , and this grows exponentially toward  $\infty$  as velocity  $u$  approaches  $c$ . The 1-CW dispersion ( $\omega = \pm ck$ ) is flat so its *RoC* is infinite everywhere and so is photon effective mass  $M_{eff}(\gamma) = \infty$ . This is consistent with the (*All colors go c*)-axiom (1.1). The other extreme is photon rest mass  $M_{rest}(\gamma) = 0$ . Between these extremes, photon momentum-mass depends on CW color  $\omega$ .

$$M_{rest}(\gamma) = 0 \tag{4.11a} \quad M_{mom}(\gamma) = p/c = \hbar k/c = \hbar \omega / c^2 \tag{4.11b} \quad M_{eff}(\gamma) = \infty \tag{4.11c}$$

For Newton this would confirm light’s “fits” to be crazy to the point of unbounded schizophrenia. A 2-CW 600THz cavity has zero total momentum  $p$ , but each photon adds a tiny mass  $M_\gamma$  to it.

$$M_\gamma = \hbar \omega / c^2 = \omega (1.2 \cdot 10^{-51}) \text{kg} \cdot \text{s} = 4.5 \cdot 10^{-36} \text{kg} \quad (\text{for: } \omega = 2\pi \cdot 600 \text{THz})$$

In contrast, a 1-CW state has no rest mass, but 1-photon momentum (4.5b) is a non-zero value  $p_\gamma = M_\gamma c$ .

$$p_\gamma = \hbar k = \hbar \omega / c = \omega (4.5 \cdot 10^{-43}) \text{kg} \cdot \text{m} = 1.7 \cdot 10^{-27} \text{kg} \cdot \text{m} \cdot \text{s}^{-1} \quad (\text{for: } \omega = 2\pi \cdot 600 \text{THz})$$

This  $p = Mc$  resembles Galilean relation  $p = Mu$  in (4.3b) and is perhaps another case of Galileo’s revenge!

*Absolute vs. relative phases: Method in madness*

Probably Newton would find a CW theory to be quite mad. Claiming that heavy hard matter owes its properties to rapid hidden “carrier” phase oscillations would not elicit a Newtonian invitation to the Royal

Society but rather to a lunatic asylum. Even though CW results (4.2) give Newtonian axioms (4.3) at low speeds, the result would seem to fail at high speeds where exact results (4.5) sag below Newton's. Also, having an enormous constant  $Mc^2$  be part of energy would, in 1670, seem insanely meaningless.

But, in 1905<sup>xii</sup> Einstein relations appear with both  $Mc^2$  and energy sag. Now Einstein's classical training left him leery of hidden quantum wave phases with dicey interpretations of intensity  $\Psi^*\Psi$  as *probability*. Also, he may have asked why observable results depend on a square  $\Psi^*\Psi=|\Psi|^2$  that kills that overall phase frequency, seemingly losing the one quantity that represents (or *is*) the total mass-energy.

Square  $|\Psi|^2$  of a 2-CW  $\Psi=e^{ia}+e^{ib}$  loses phase factor  $e^{i(a+b)/2}$  leaving group functions  $\cos^2(\frac{a-b}{2})$  of *differences*  $\omega_1 - \omega_3$  or  $k_1 - k_3$  of 1<sup>st</sup> or 3<sup>rd</sup> base frequencies or  $k$ -vectors. Group beat frequency  $\Delta\omega = \omega_1 - \omega_3$  is zero in the rest frame of Fig. 2.1c where it is a stationary wave. In Fig. 2.2c or any other frame,  $|\Psi|^2$  is not stationary but is observed to have velocity  $V_{group} \neq 0$ . Fourier sums of  $m=3$  or more terms  $\Psi = a_1 e^{i(k_1 x - \omega_1 t)} + a_2 e^{i(k_2 x - \omega_2 t)} + a_3 e^{i(k_3 x - \omega_3 t)} + \dots$  may have multiple beats in  $\Psi^* \Psi$  as in Fig. 2.2d.

$$P = |\Psi|^2 = \Psi^* \Psi = \sum a_i^* a_j e^{i(\Delta k_{ij} x - \Delta \omega_{ij} t)} \tag{4.12}$$

With  $m(m-1)/2$  observable *difference*  $\Delta\omega_{ij} = \omega_i - \omega_j$  or *beat* notes,  $P$  cannot rest in any frame. Differences or derivatives are observable while absolute  $\Psi$ -frequency stays hidden *until two quantum objects interfere*. Then new beats arise from differences between the two absolute frequencies and others. A new absolute phase ( $|\Psi|^2$  does not have this.) is the sum of all. But, we can only observe beats of relative frequency! That may be a quantum version of Einstein's popularized saw, "It's *all* relative." Phase velocity escapes with its Galilean arithmetic intact in Fig. 3.1, but here it finally surrenders its absolutes to relativism.

Total phase gives total energy  $E$  or momentum  $p$ , but *differentials* are what one feels through work  $\Delta E$  or impulse  $\Delta p$ . Invariant quantities like  $\varpi$  and  $M_{rest}$  depend on *total* phase but intensity (4.12) has only differentials  $\Delta k_{ij}$  or *relative* beats  $\Delta\omega_{ij}$ . Among frame-dependent relative quantities are group velocity  $u$  (4.9),  $M_{mom}$  (4.8), and  $M_{eff}$  (4.10), but rest mass  $M_{rest}$  (4.4c) is a frame-invariant absolute quantity. Also note that  $M_{mom}$  and  $M_{eff}$  approach  $M_{rest}$  at zero velocity. Now  $|\Psi|^2$  may register an  $\varpi$  beat with a DC (*static*  $\omega_0=0$ ) wave, but lack of resonance confines ( $\omega_0=0$ )-carrier waves to beat only locally.

Phase frequency  $\omega_p$  in a quantum wave  $e^{ip} \cos g = e^{-i(k_p x - \omega_p t)} \cos(k_g x - \omega_g t)$  is fast and silent like a carrier frequency of radio wave. Group frequency  $\omega_g$  is like the audible signal, much slower and heard in resonant beats  $\omega_a - \omega_b$  involving carrier and receiver. Atomic "carrier" frequencies  $\omega_p = M_p c^2 / \hbar$  due to rest mass are enormous as are those of atomic measuring devices that play the role of "receivers" in quantum experiments. Measurement involves resonant contact of an atom and devices that horse-trade beats at truly huge frequencies.

One way to avoid huge  $Mc^2/\hbar$ -related phase frequencies is to ignore them and approximate the relativistic equation  $E = Mc^2 \cosh \rho$  of (4.5a) by the Newtonian approximation (4.4a) that deletes the big rest-energy constant  $sB = Mc^2$ . The exact energy (4.5a) that obeys CW axioms (1.1) is rewritten in terms of momentum (4.5b) below to give a Bohr-Schrodinger (BS) approximation (4.14) with  $Mc^2$  deleted.

$$E = \frac{Mc^2}{\sqrt{1 - u^2/c^2}} = Mc^2 \cosh \rho = Mc^2 \sqrt{1 + \sinh^2 \rho} = \sqrt{(Mc^2)^2 + (cp)^2} \tag{4.13}$$

$$E = \left[ (Mc^2)^2 + (cp)^2 \right]^{1/2} \approx Mc^2 + \frac{1}{2M} p^2 \xrightarrow{\text{BS-approx}} \frac{1}{2M} p^2 \quad (4.14)$$

If only frequency difference affect observation based on  $|\Psi|^2$  (4.12), the BS claim is that energy origin may be shifted from  $(E=Mc^2, cp=0)$  to  $(E=0, cp=0)$ . (*Frequency is relative!*) Hyperbola (4.13) in Fig. 4.1a, for  $u$  way less than  $c$ , approaches the BS parabola (4.14) in Fig. 4.1b. That is the only  $E(p)$  Newton knew.

Group velocity  $u=V_{group}=\frac{d\omega}{dk}$  of (4.9) is a relative or differential quantity so origin shifting does not affect it. However, phase velocity  $\frac{\omega}{k}=V_{phase}$  is greatly reduced by deleting  $Mc^2$  from  $E=\hbar\omega$ . It slows from  $V_{phase}=c^2/u$  that is always faster than light to a sedate sub-luminal speed of  $V_{group}/2$ . Having  $V_{phase}$  go slower than  $V_{group}$  is an unusual situation but one that has achieved tacit approval for BS matter waves.<sup>xiii</sup> The example used in Fig. 1.6 of Ch. 1 is a 2-CW BS matter wave exhibiting this low  $V_{phase}$ .

Standard Schrodinger quantum mechanics, so named in spite of Schrodinger's protests<sup>xiv</sup>, uses Newtonian kinetic energy (4.14) or (4.3) with potential  $\phi$  (as the *const.*-term) to give a BS Hamiltonian.

$$H=p^2/2M + \phi \quad \text{or:} \quad \hbar\omega = \hbar^2 k^2/2M + \langle\phi\rangle_k \quad (4.15)$$

The CW approach to relativity and quantum exposes some problems with such approximations.

First, a non-constant potential  $\phi$  must have a vector potential  $\mathbf{A}$  so that  $(\phi, c\mathbf{A})$  transform like  $(\omega, c\mathbf{k})$  in (2.10a) or  $(ct, \mathbf{x})$  in (2.10b) or as  $(E, c\mathbf{p})$  with scaling laws  $\mathbf{p}=\hbar\mathbf{k}$  and  $E=\hbar\omega$ . Transformation demands equal powers for frequency (energy) and wavevector (momentum) such as the following.

$$(E-\phi)^2 = (\mathbf{p}-c\mathbf{A})^2/2M + Mc^2 \quad \text{or:} \quad (\hbar\omega - \langle\phi\rangle_k)^2 = (\hbar\mathbf{k}-c\mathbf{A})^2/2M + Mc^2 \quad (4.16)$$

Also, varying potentials perturb the vacuum so single-CW's may no longer obey axioms (1.1-2).

Dirac's elegant solution obtains  $\pm$ pairs of hyperbolas (4.13) or (4.16) from avoided-crossing eigenvalues of  $4 \times 4$  Hamiltonian matrix equations with negative frequency hyperbolas. The negative- $\omega$  hyperbolas in Fig. 4.1 are (conveniently) hidden by the BS approximate dispersion parabola.

Dirac's ideas require three-dimensional wavevectors and momenta. But first, fundamental Lagrangian-Hamiltonian geometric relations of quantum phase and frequency relate relativistic classical and quantum mechanics in the following Ch. 5. These relations expose more of the logic of phase-based Evenson axiom (1.1), Doppler  $T$ -symmetry axiom (1.2), and Euclid frequency means in Fig. 3.3.

## Chapter 5. Classical vs. quantum mechanics

The CW-spectral view of relativity and quantum theory demonstrates that wave phase and in particular, optical phase, is an essential part of quantum theory. If so, classical derivation of quantum mechanics might seem about as viable as Aristotelian derivation of Newtonian mechanics.

However, the 19<sup>th</sup> century mechanics of Hamilton, Jacobi, and Poincare developed the concept of *action*  $S$  defined variously by area  $\oint pdq$  in phase-space or a Lagrangian time integral  $\int Ldt$ . The latter action definition begins with the Legendre transformation of Lagrangian  $L$  and Hamiltonian  $H$  functions.

$$L = p \cdot \dot{x} - H \quad (5.1a)$$

$L$  is an explicit function of  $x$  and velocity  $u = \dot{x}$  while the  $H$  is explicit only in  $x$  and momentum  $p$ .

$$0 = \frac{\partial L}{\partial p} \quad (5.1b) \quad p = \frac{\partial L}{\partial \dot{x}} \quad (5.1c) \quad 0 = \frac{\partial H}{\partial \dot{x}} \quad (5.1d) \quad \dot{x} = \frac{\partial H}{\partial p} \quad (5.1e)$$

Multiplying by  $dt$  gives the differential *Poincare invariant*  $dS$  and its *action integral*  $S = \int Ldt$ .

$$dS = L dt = p \cdot dx - H dt \quad (5.2a) \quad S = \int L dt = \int p \cdot dx - \int H dt \quad (5.2b)$$

Planck-DeBroglie scaling laws  $p = \hbar k$  and  $E = \hbar \omega$  (4.5) identify action  $S$  as scaled quantum phase  $\hbar \Phi$ .

$$\hbar d\Phi = L dt = \hbar k \cdot dx - \hbar \omega dt \quad (5.3a) \quad \Phi = \int k \cdot dx - \int \omega dt \quad (5.3b)$$

If action  $dS$  or phase  $d\Phi$  is integrable, then *Hamilton-Jacobi equations* or  $(k, \omega)$  equivalents hold.

$$\frac{\partial S}{\partial x} = p \quad (5.4a) \quad \frac{\partial S}{\partial t} = -H \quad (5.4b) \quad \frac{\partial \Phi}{\partial x} = k \quad (5.4c) \quad \frac{\partial \Phi}{\partial t} = -\omega \quad (5.4d)$$

Phase-based relations (5.4c-d) define angular frequency  $\omega$  and wave number  $k$ . The definition (3.8) of wave group velocity is a wave version of Hamilton's velocity equation (5.1e).

$$\dot{x} = \frac{\partial H}{\partial p} \quad \text{equivalent to: } u = V_{\text{group}} = \frac{\partial \omega}{\partial k}$$

The coordinate Hamilton derivative equation relates to wave diffraction by dispersion anisotropy.

$$\dot{p} = -\frac{\partial H}{\partial x} \quad \text{equivalent to: } \dot{k} = -\frac{\partial \omega}{\partial x}$$

Classical HJ-action theory was intended to analyze families of trajectories (PW or particle paths), but Dirac and Feynman showed its relevance to matter-wave mechanics (CW phase paths) by proposing an approximate semi-classical wavefunction based on the Lagrangian action as phase.

$$\Psi \approx e^{i\Phi} = e^{iS/\hbar} = e^{i\int Ldt/\hbar} \quad (5.5)$$

The approximation symbol ( $\approx$ ) indicates that only phase but not amplitude is assumed to vary here. An  $x$ -derivative (5.4a) of semi-classical wave (5.5) has the  $\mathbf{p}$ -operator form in standard BS quantum theory.

$$\frac{\partial}{\partial x} \Psi \approx \frac{i}{\hbar} \frac{\partial S}{\partial x} e^{iS/\hbar} = \frac{i}{\hbar} p \Psi \quad (5.6a) \quad \frac{\hbar}{i} \frac{\partial}{\partial x} \Psi = p \Psi \quad (5.6b)$$

The time derivative is similarly related to the Hamiltonian operator. The HJ-equation (5.4b) makes this appear to be a BS Hamiltonian time equation.

$$\frac{\partial}{\partial t} \Psi \approx \frac{i}{\hbar} \frac{\partial S}{\partial t} e^{iS/\hbar} = -\frac{i}{\hbar} H \Psi \quad (5.7a)$$

$$i\hbar \frac{\partial}{\partial t} \Psi = H \Psi \quad (5.7b)$$

However, these approximations like the BS approximations of (4.14) ignore relativity and lack economy of logic shed by light waves. The Poincare phase invariant of a matter-wave needs re-examination.

### Contact transformation geometry of a relativistic Lagrangian

A matter-wave has a rest frame where  $x'=0=k'$  and its phase  $\Phi = kx - \omega t$  reduces to  $-\mu\tau$ , a product of its proper frequency  $\mu = N\omega$  (or  $Mc^2/\hbar$ ) with proper time  $t' = \tau$ . Invariant differential  $d\Phi$  is reduced, as well, using the Einstein-Planck rest-mass energy-frequency equivalence relation (4.4c) to rewrite it.

$$d\Phi = kdx - \omega dt = -\mu d\tau = -(Mc^2/\hbar) d\tau. \quad (5.8)$$

$\tau$ -Invariance (2.21) or time dilation in (2.10b) gives proper  $d\tau$  in terms of velocity  $u = \frac{dx}{dt}$  and lab  $dt$ .

$$d\tau = dt \sqrt{1 - u^2/c^2} = dt \operatorname{sech} \rho \quad (5.9)$$

Combining definitions for action  $dS = Ldt$  (5.2) and phase  $dS = \hbar d\Phi$  (5.3) gives the Lagrangian  $L$ .

$$L = -\hbar\mu\tau = -Mc^2\sqrt{1 - u^2/c^2} = -Mc^2 \operatorname{sech} \rho \quad (5.10)$$

Fig. 5.1 plots this free-matter Lagrangian  $L$  next to its Hamiltonian  $H$  using units for which  $c=1=M$ .

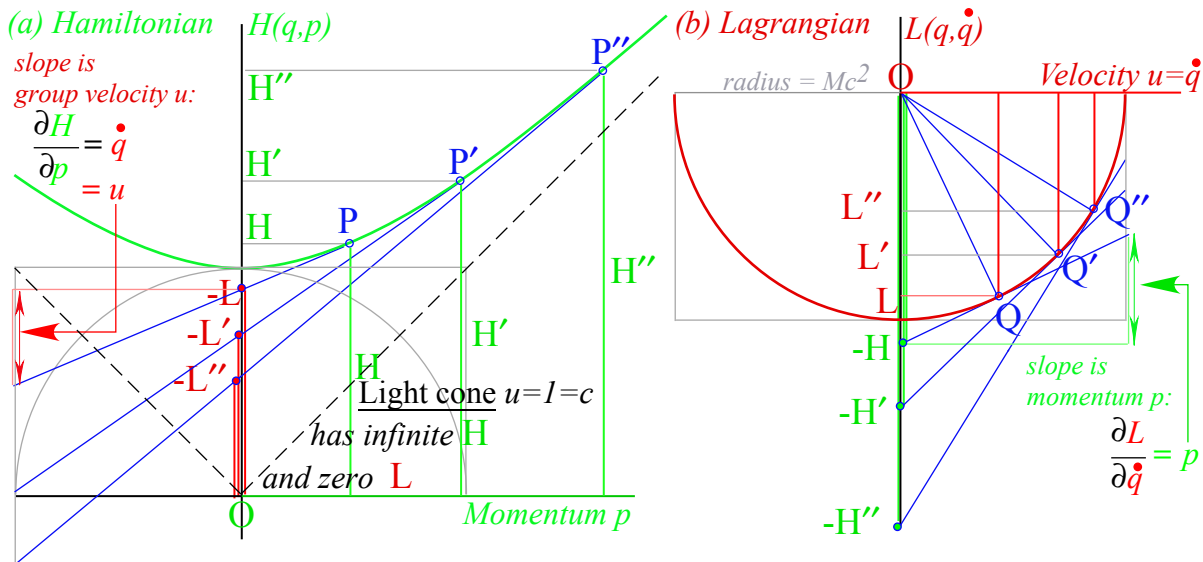


Fig. 5.1. Geometry of contact transformation between relativistic (a) Hamiltonian (b) Lagrangian

**Relativistic matter Lagrangian** (5.10) is a circle (Fig. 5.1b).  $L$ -values  $L, L',$  and  $L''$  in Fig. 5.1 are contact Legendre transforms of  $H$ -values  $H, H',$  and  $H''$  of Hamiltonian hyperbola in Fig. 5.1a. Abscissa  $p$  and ordinate  $H$  of a point  $P$  in plot (a) gives negative intercept  $-H$  and slope  $p$  of tangent  $HQ$  contacting the transform point  $Q$  in plot (b) and *vice-versa*. (Contact geometry is really wave-action-energy mechanics.)

If  $p = Mu$ , Lagrange kinetic energy  $L = \frac{1}{2} Mu^2$  is Hamilton  $H = p^2 / 2M$ . Then circle  $L$  and hyperbola  $H$  both approximate a Newtonian parabola at low speed  $u \ll c$ . But, as  $u \rightarrow c$  the  $L$ -circle rises above the parabola and the  $H$ -hyperbola sags below it and instead approaches contacting  $c$ -asymptote in Fig. 5.1.

Action integral  $S = \int L dt$  is to be *minimized*. Feynman's interpretation of  $S$  minimization is depicted in Fig. 5.2. A mass flies so that its "clock"  $\tau$  is *maximized*. (Proper frequency  $\mu = Mc^2 / \hbar$  is constant for fixed rest mass, and so minimizing  $-\mu\tau$  means maximizing  $+\tau$ .) An interference of Huygen wavelets favors stationary and extreme phase. This favors the fastest possible clock as is sketched in Fig. 5.3.

Feynman described families of classical paths or rays fanning out from each space-time point on a wavefront of constant phase  $\Phi$  or action  $S$ . Then, according to an application of Huygen's principle to matter wave, new wavefronts are continuously built in Fig. 5.3 through interference from "the best" of all the wavelets emanating from a multitude of source points on each preceding wavefront. Thus classical momentum  $\mathbf{p} = \nabla S$  by (5.4a) for the "best" ray ends up normal to each wavefront.

The "best" are so-called *stationary-phase* rays that are extremes in phase and thereby satisfy *Hamilton's Least-Action Principle* requiring that  $\int L dt$  is minimum for "true" classical trajectories. This in turn enforces Poincare' invariance by eliminating, by de-phasing, any "false" or non-classical paths because they do not have an invariant (and thereby stationary) phase. "Bad rays" cancel each other in a cacophonous mish-mash of mismatched phases. Each Huygen wavelet is tangent to the next wavefront being produced. That contact point is precisely on the ray or true classical trajectory path of minimum action and on the resulting "best" wavefront. Time evolution from any wavefront to another is thus a contact transformation between the two wavefronts described by the geometry of Huygens Principle.

Thus a Newtonian clockwork-world appears to be the perennial cosmic gambling-house winner in a kind of wave dynamical lottery on an underlying wave fabric. Einstein's God may not play dice, but some persistently wavelike entities seem to be gaming at enormous  $Mc^2/\hbar$ -rates down in the cellar!

It is ironic that Evenson and other metrologists have made the greatest advances of precision in human history, not with metal bars or ironclad classical mechanics, but by using the most ethereal and dicey stuff in the universe, light waves. This motivates a view of classical matter or particle mechanics that is more simply and elegantly done by its relation to light and its built-in relativity, resonance, and quantization that occurs when waves are subject to boundary conditions or otherwise confined. While Newton was complaining about "fits" of light, that crazy stuff was just trying to tell him something!

Derivation of quantum phenomena using a classical particle paradigm seems silly now. If particles are made by waves, optical or otherwise, rather than *vice versa* as Newton believed, the case is closed. Also, CW trumps PW as CW symmetry axioms (1.1-2) derive classical results (4.4) while giving exact relations (4.5) for relativity and quantum theory tossed into the bargain. Such Occam economy is found lacking on a PW path from Newton to Einstein and Planck.

Thus basic CW sum-and-difference phase relations seem to underlie the physics of Poincare contact geometry. This in turn is based on circular and hyperbolic geometry described next.

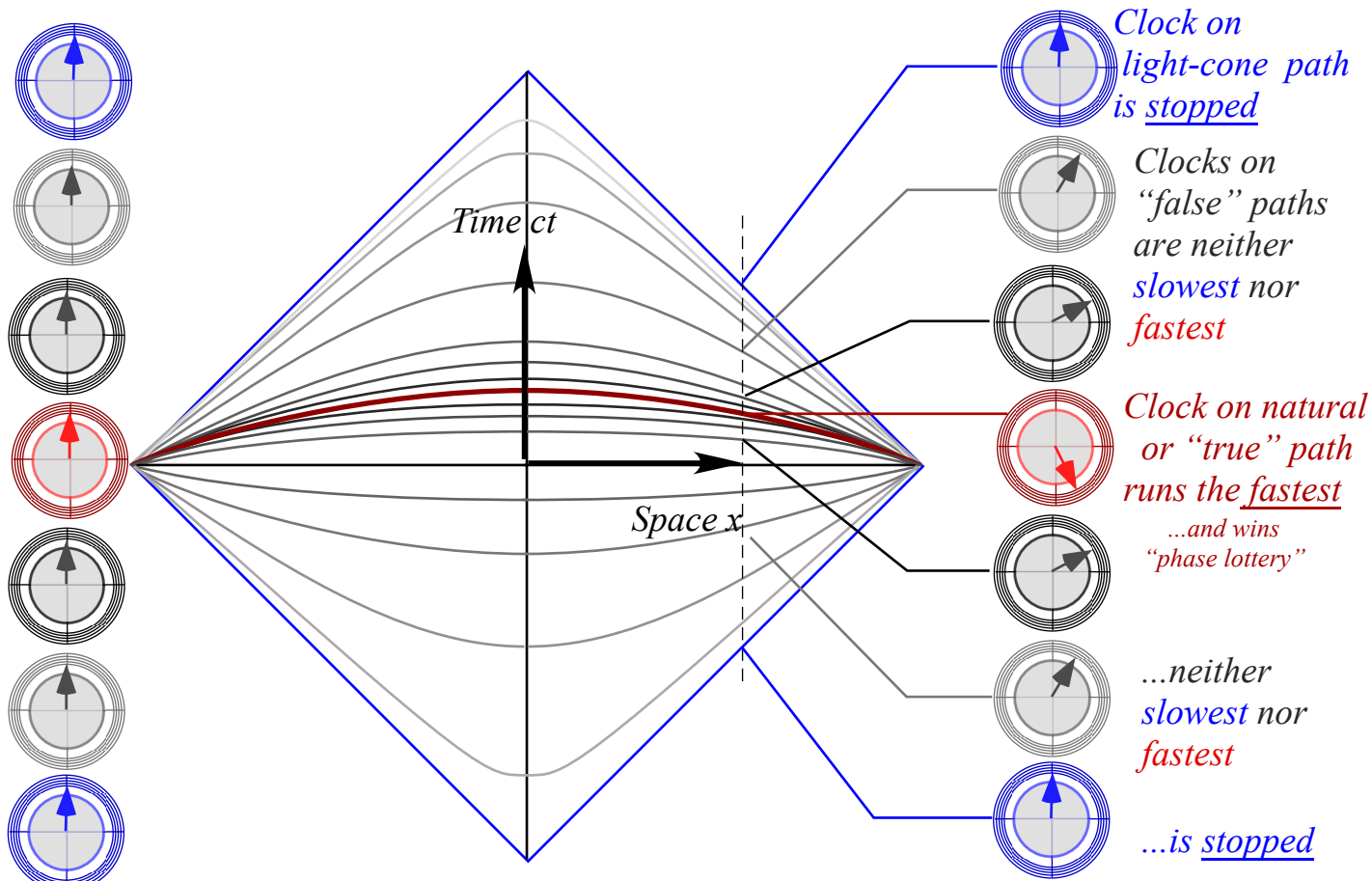


Fig. 5.2 "True" paths carry extreme phase and fastest clocks. Light-cone has only stopped clocks.

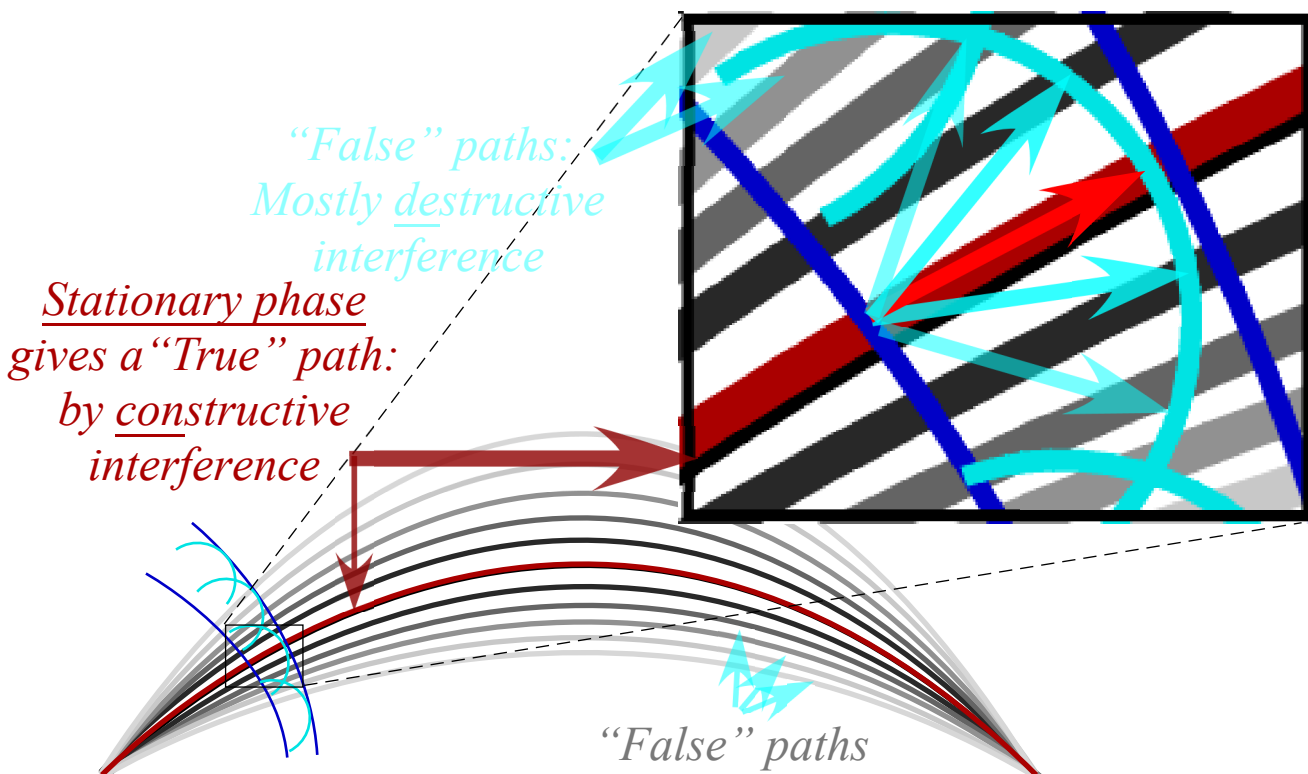


Fig. 5.3 Quantum waves interfere constructively on "True" path but mostly cancel elsewhere.

## Geometry of circular and hyperbolic functions

Geometry of half-sum and half-difference phase  $\mathbf{P}=(\mathbf{R}+\mathbf{L})/2$  and group  $\mathbf{G}=(\mathbf{R}-\mathbf{L})/2$  vectors is based on trigonometric exponential identities that are crown jewels of 18<sup>th</sup> century mathematics and have Euclidian geometric origins shown in Fig. 5.4. Phase angle- $\phi$  identities apply to Fig. 5.4a.

$$\begin{aligned} e^{+i\phi} &= \cos\phi + i\sin\phi & \cos\phi &= (e^{+i\phi} + e^{-i\phi})/2 \\ e^{-i\phi} &= \cos\phi - i\sin\phi & i\sin\phi &= (e^{+i\phi} - e^{-i\phi})/2 \end{aligned} \quad (5.11a) \quad (5.11b)$$

Circular function  $\tan\phi$  is named for a tangent to a unit circle shown in Fig. 5.4(a). Its incline (sine) elevation is  $\sin\phi$ . The complimentary tangent or cotangent  $\cot\phi$  completes the tangent distance between axes where  $\phi$  is circle arc-length- $\phi$  or *subtended area*- $\phi$ . Hyperbolic functions use area  $\rho$  for “angle.”

$$\begin{aligned} e^{+\rho} &= \cosh\rho + \sinh\rho & \cosh\rho &= (e^{+\rho} + e^{-\rho})/2 \\ e^{-\rho} &= \cosh\rho - \sinh\rho & \sinh\rho &= (e^{+\rho} - e^{-\rho})/2 \end{aligned} \quad (5.12c) \quad (5.12d)$$

Fig. 5.4b shows how hyperbolic functions relate to circular ones in Fig. 5.4a. The circular sine equals the hyperbolic tangent ( $\sin\phi = \tanh\rho$ ) and *vice versa* ( $\tan\phi = \sinh\rho$ ). Each circular function has a segment that matches one for a hyperbolic function, for example ( $\cos\phi = \operatorname{sech}\rho$ ) matches ( $\sec\phi = \cosh\rho$ ). These relations recap the CW view of the Legendre contact transformation in Fig. 5.1 that underlies classical and quantum theory that is in the algebra and geometry for every bit of light-and-matter in and around us!

In Fig. 5.4, circular area  $\phi$  and hyperbolic area  $\rho$  have been chosen so that  $\tan\phi = 1.15 = \sinh\rho$  and  $\sin\phi = 0.75 = \tanh\rho$ , that is for  $u=3c/4$ . The tangent to the circle in Fig. 5.4a-b is like the one that contacts the Lagrangian circle in Fig. 5.1b to contact-transform it to the Hamiltonian hyperbola in Fig. 5.1a, and *vice versa* the hyperbolic tangent in Fig. 5.4b is like the one that transforms the Hamiltonian hyperbola in Fig. 5.1a to the Lagrangian circle in Fig. 5.1b.

The hyperbolic tangent  $u/c = \tanh\rho$  of (2.19) corresponds to frame rapidity  $\rho$  and group velocity  $u = V_{\text{group}} = \frac{d\omega}{dk}$  in (2.8), (4.9) and in Fig. 3.3a-b. The circular tangent angle  $\phi$  or inclination  $\sin\phi$  belongs to Lagrangian velocity function (5.10) in Fig. 5.1b. (The horizontal axis of the latter in the vertical axis of Fig.11. This geometry is symmetric to axis-switching.) As  $u$  and  $\rho$  approach  $c$  and  $\infty$ , respectively, the circular angle  $\phi$  approaches  $\pi/2$ .

This angle  $\phi$  is the *stellar velocity aberration angle*, that is, the polar angle that vertical starlight is seen by a horizontally moving astronomer to tip into her direction of motion. Aberration angle  $\phi$ , like rapidity  $\rho$ , is 1<sup>st</sup>-order in velocity  $u$  and both  $\rho$  and  $\phi$  equal  $u/c$  at low speeds. (See the discussion of Fig. 5.6 near the end of this chapter. This deepens the development to include 4-vector space-time.)

Many of the twelve circular-hyperbolic trigonometric ratios in Fig. 5.1 belong to one or more physical or geometric effects shown in prior diagrams beginning with Euclid’s rectangle-in-circle mean construction of Fig. 3.3. Prior ratio constructions are overlapped in the form of Fig. 5.1 and results in Fig. 5.5a that might be described as a global ratio riot. This riot is simplified and labeled in zoom-in views of Fig. 5.5b-d and they are the basis of the following discussion of the role of tangent-contact geometry in CW analysis of Poincare contact transformation and relativistic quantum waves.

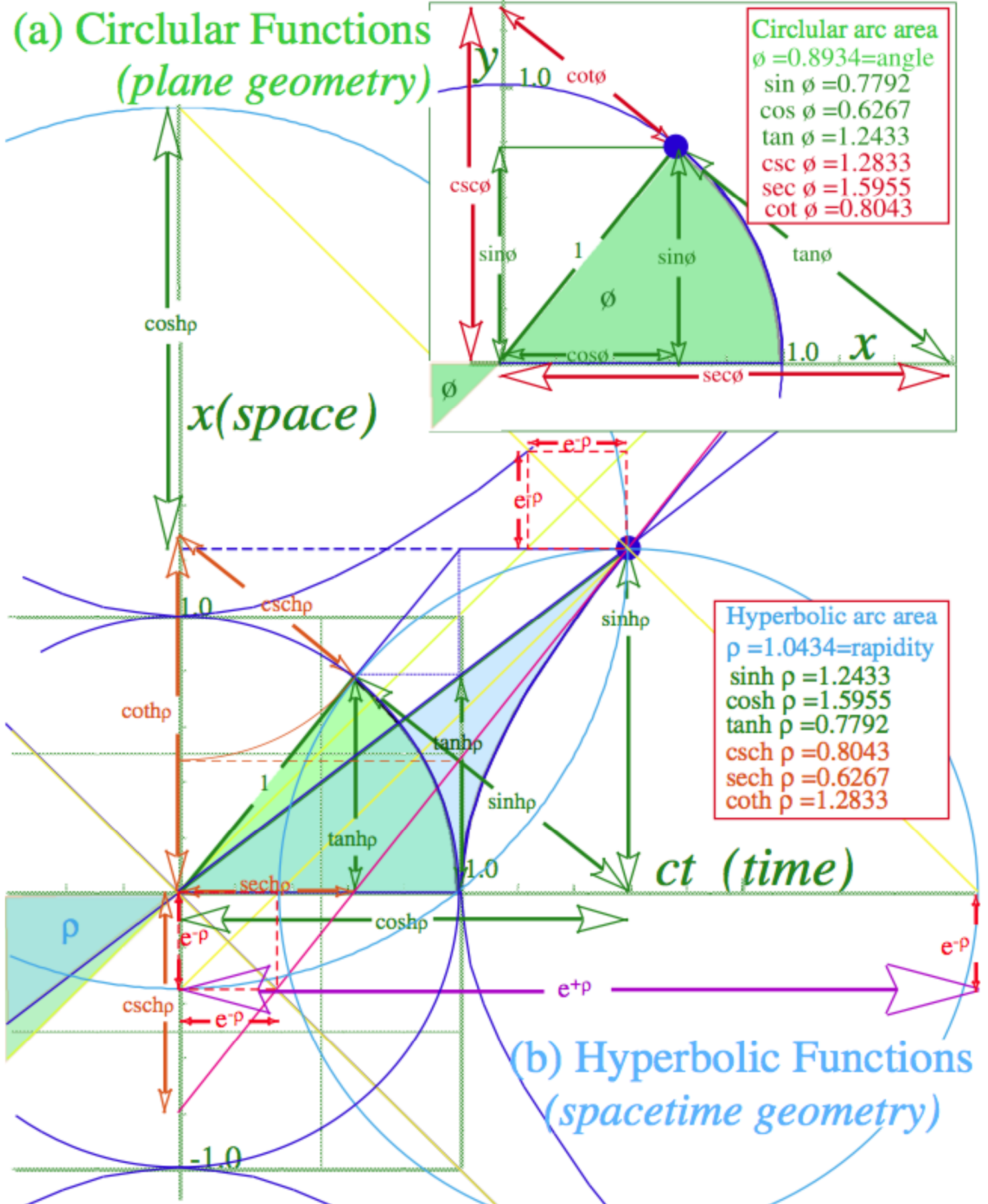


Fig. 5.4 Trigonometric geometry (a) Unit circular area  $\phi=0.86$  and (b) Unit hyperbolic area  $\rho=0.99$ .

*Hyper-circular contacts*

Beginning with the Euclidian mean diagram of Fig. 3.3, three mean frequencies arise from an interfering pair of left-moving “red” and right-moving “blue” beams of frequency  $\omega_L$  and  $\omega_R$ . First is a half-sum phase frequency  $\omega_p = (\omega_R + \omega_L)/2$  (arithmetic mean) that defines the circle radius in Fig. 3.3. Second is a half-difference group beat frequency  $\omega_g = (\omega_R - \omega_L)/2$  (difference mean) that is radial distance of circle center to origin. Third is a root-product proper frequency  $\omega = (\omega_R \cdot \omega_L)^{1/2}$  (geometric mean) that is the base radius or bottom of a  $\omega(k)$  hyperbola of rest energy  $B = \hbar \omega = Mc^2$  above origin in Fig. 3.3.

Phase and group frequencies are defined as ratios or shifts of the geometric mean frequency  $\omega$ , and this begins with the Doppler shift definition of the red  $\omega_L = e^{-\rho} \omega$  and blue  $\omega_R = e^{+\rho} \omega$  CW components. Ratio values  $\omega_p = \omega \cosh \rho$  and  $\omega_g = \omega \sinh \rho$  define each point on a  $\omega$ -hyperbola dispersion curve in Fig. 5.5.

Fig. 5.5 is based on circles with three different radii, one for each mean frequency. The base circle-*b* drawn centered at origin has radius  $B = \hbar \omega = Mc^2$  of the Lagrangian circle in Fig. 5.1b. A smaller circle-*g* has group radius  $\hbar \omega_g = B \sinh \rho$ . A larger circle-*p* has phase radius  $\hbar \omega_p = B \cosh \rho$  of the Euclidean circle in Fig. 3.3 and is drawn with dashed lines in Fig. 5.5. (Base value *B* is scaled for energy here.)

Circle-*p* of larger radius  $\hbar \omega_p = B \cosh \rho$  is centered at  $cp = \hbar \omega_g = B \sinh \rho$ , a horizontal distance equal to the radius of the smaller circle-*g*, while the latter is centered at  $E = \hbar \omega_p = B \cosh \rho$ , a vertical distance equal to the radius of the larger circle-*p*. Tangents that contact circles or hyperbolas define many of the physical quantities labeled in the zoom-in view of Fig. 5.5b. Intersections and chords shared by two of the circles also provide the key quantities as seen in Fig. 5.5a.

So far the CW development has emphasized the Doppler ratio as a starting point beginning with Fig. 2.2 and culminating with the Euclidean means of Fig. 3.3. However, most developments of relativity start with velocity *u*, and that geometric approach is excerpted in a simplified construction of Fig. 5.5c where  $u/c = 45/53$  and Fig. 5.5d where  $u/c = 3/5$ . (Fig. 5.5a-b and most other figures use  $u/c = 3/5$ .) Once the velocity *u/c* line intersects the basic *b*-circle and its horizontal tangent of unit-energy ( $B = 1 = Mc^2$ ), it only takes three more lines to derive Lagrangian  $-L = B \operatorname{sech} \rho$ , then momentum  $cp = B \sinh \rho$ , and finally the Hamiltonian  $H = B \cosh \rho$ . Then a compass is used to check accuracy with the phase *p*-circle by making sure it goes from  $(cp, H)$  to the  $(0, B)$ -point on top of the *b*-circle. The *p*-circle goes on to intersect the negative *cp*-axis at the Doppler red shift  $rB = B e^{+\rho}$ . Finally, the group *g*-circle in Fig. 5.5a-b has a chord intersection with the *p*-circle that is the hyperbolic contact tangent, and it grazes the  $\phi$ -angle normal to the Lagrangian circle tangent in Fig. 5.5b. This helps to clarify geometry of *H-L* contact transformations of Fig. 5.1 for per-space-time  $(\omega, ck)$  and  $(\Phi, u/c)$  that also apply to space-time.

If Fig. 5.5 is in space-time, the segment  $-L = B \operatorname{sech} \rho$  is Lorentz contraction  $\ell = B \sqrt{1 - u^2 / c^2}$ . The  $H = B \cosh \rho$  and  $cp = B \sinh \rho$  segments are, respectively Einstein time dilation  $d = B / \sqrt{1 - u^2 / c^2}$  and simultaneity  $a = ud/c$  coefficients. Node-to-node or peak-to-peak gaps contract by  $\ell = 4/5$  in Fig. 2.2d-e. As speed reduces in Fig. 5.5c-d from  $u/c = 45/53$  to  $u/c = 3/5$  or to lower values, the Lagrangian velocity angle  $\phi$  and Hamiltonian rapidity  $\rho$  approach the velocity ratio *u/c*. Galilean velocity addition rules resume. In the opposite ultra-relativistic regime,  $\phi$  approaches  $\pi/2$ ,  $\rho$  approaches  $\infty$ , and *u/c* nears unit slope or  $45^\circ$  in Fig. 5.5c. But, Galilean-like rules (3.6) apply to rapidity  $\rho$  at all speeds (so far).



### Transverse vs. longitudinal Doppler: Stellar aberration

A novel description of relativity by L. C. Epstein<sup>xv</sup> in *Relativity Visualized* introduces a "cosmic speedometer" consisting of a telescope tube tipped to catch falling light pulses from a distant overhead star. A stationary telescope points straight up the  $x$ -axis at the apparent position  $S$  of the star. (Fig. 5.6a) But, with velocity  $\mathbf{u}=u_z\mathbf{e}_z$  across to the star beam  $x$ -axis, the telescope has to tip to catch the starlight, so the apparent position  $S'$  tips toward  $\mathbf{u}$ . (Fig. 5.6b).

The telescope tips by a *stellar aberration angle*  $\sigma$  ( $\phi$  in (5.11a) or Fig. 5.4a.). The sine of angle  $\sigma$  is velocity ratio  $\beta = u_z/c$  which is the hyper-tangent of relativistic rapidity  $\nu_z$  ( $\rho$  in (5.12a) or Fig. 5.4b.)

$$\beta = u_z/c = \sin \sigma = \tanh \nu_z \tag{5.13}$$

Proper time  $\tau$  and frequency  $\omega$  invariance (3.10) forces 4-vector components normal to velocity  $\mathbf{u}$  of a boost to be unchanged. That is, a boost along  $z$  of  $(ct, z)$  to  $(ct', z')$  (or  $(\omega, ck_z)$  to  $(\omega', ck_{z'})$ ) must preserve both  $(x, y) = (x', y')$  and  $(ck_x, ck_y) = (ck_{x'}, ck_{y'})$  just as a rotation in the  $xy$ -plane of  $(x, y)$  to  $(x', y')$  leaves unaffected the components  $(ct, z) = (ct', z')$  and  $(\omega, ck_z) = (\omega', ck_{z'})$  transverse to the rotation.

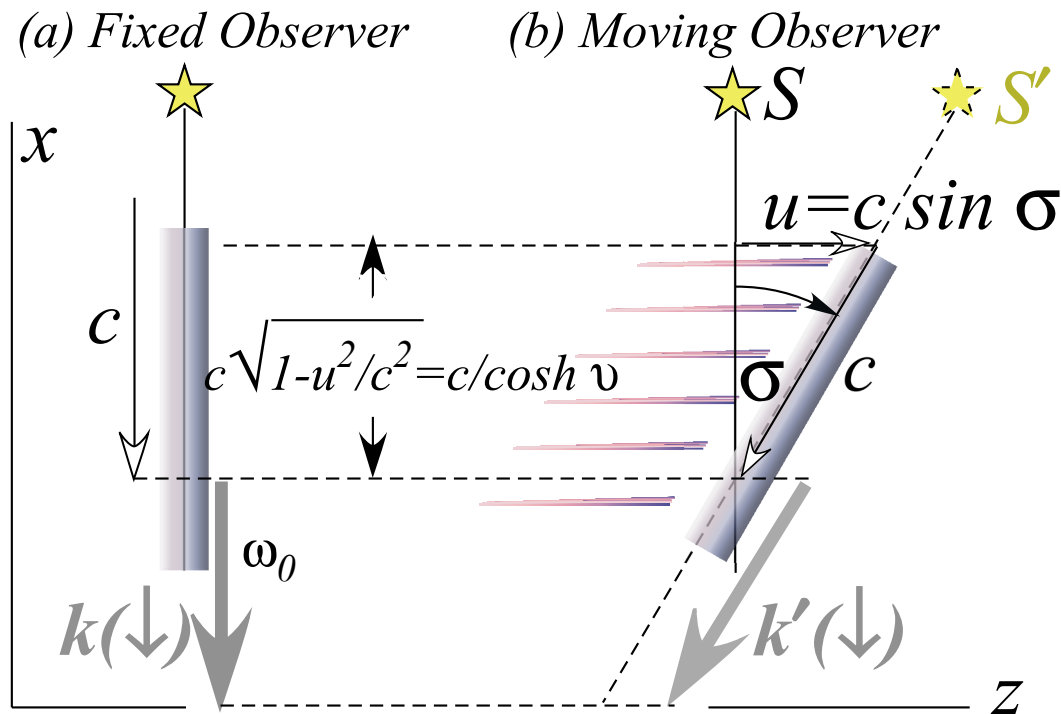


Fig. 5.6 Epstein's cosmic speedometer with aberration angle  $\sigma$  and transverse Doppler shift  $\cosh \nu$ .

Invariant (3.10) demands light-speed conservation as sketched in Fig. 5.6b. Starlight speed down the  $\sigma$ -tipped telescope is  $c$ , so the  $x$ -component of starlight velocity reduces from  $c$  to

$$c_x' = c \cos \sigma = c \sqrt{1 - u_z^2/c^2} = c / \cosh \nu_z. \tag{5.14}$$

Transformation (5.17a) below assures that  $x$ -or- $y$ -components of  $\mathbf{k}_\downarrow$  are unchanged by  $u_z$ -boost.

$$(ck_x, ck_y) = (ck_{x'}, ck_{y'}) \tag{5.15}$$

So the length of  $\mathbf{k}_\downarrow$  increases by a factor  $\cosh \nu$  as shown in Fig. 5.7 as does the frequency  $\omega'_\downarrow$ .

$$c|k'_\downarrow| = c|k_\downarrow| \cosh \nu_z = \omega_0 \cosh \nu_z = \omega_0 \sqrt{1 - u^2/c^2} \tag{5.16}$$

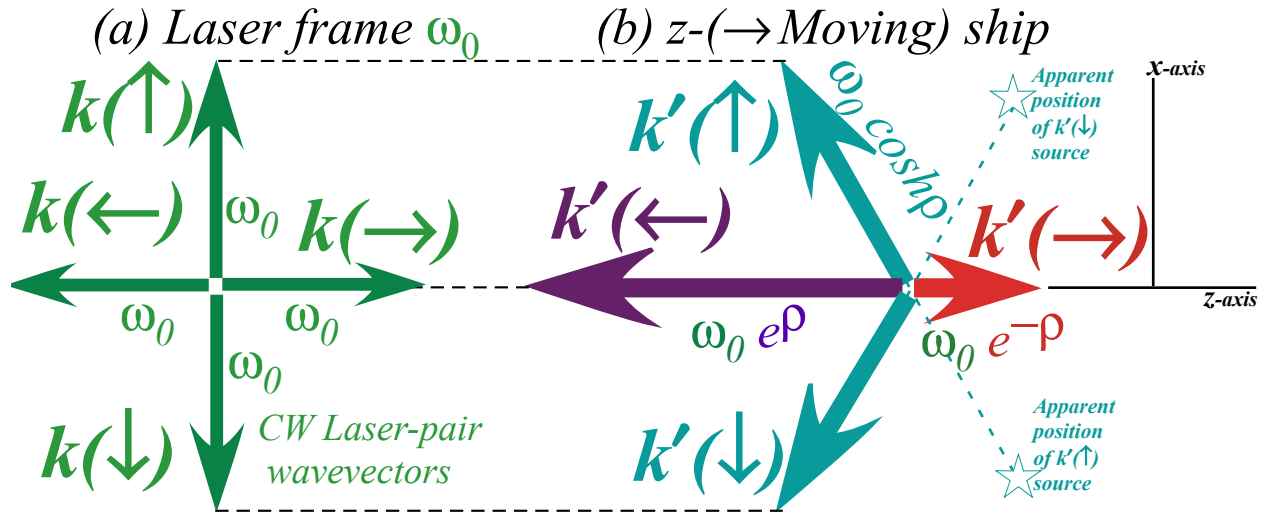


Fig. 5.7 CW version of cosmic speedometer showing transverse and longitudinal  $k$ -vectors.

If the observer crosses a star ray at very large velocity, that is, lets  $u_z$  approach  $c$ , then the star angle  $\sigma$  approaches  $90^\circ$  and the frequency increases until the observer sees an X-ray or  $\gamma$ -ray star coming almost head on! The  $\cosh v_z$  factor is a *transverse Doppler shift*. For large  $v_z$ , it approaches  $e^{v_z}$ , which is the ordinary *longitudinal Doppler shift* upon which the CW relativity derivations of Ch. 2 are based. Relations (5.13-16) are summarized in a 4-vector transformation:  $\omega_0$  has a *transverse Doppler shift* to  $\omega_0 \cosh v_z$ , so  $ck_z=0$  becomes  $ck_z' = -\omega_0 \sinh v_z$ , but the  $x$ -component is unchanged:  $ck_x' = \omega_0 = ck_x$ .

$$\begin{pmatrix} \omega'_\downarrow \\ ck'_{x\downarrow} \\ ck'_{y\downarrow} \\ ck'_{z\downarrow} \end{pmatrix} = \begin{pmatrix} \cosh v_z & \cdot & \cdot & -\sinh v_z \\ \cdot & 1 & \cdot & \cdot \\ \cdot & \cdot & 1 & \cdot \\ -\sinh v_z & \cdot & \cdot & \cosh v_z \end{pmatrix} \begin{pmatrix} \omega_\downarrow \\ ck_{x\downarrow} \\ ck_{y\downarrow} \\ ck_{z\downarrow} \end{pmatrix} = \begin{pmatrix} \cosh v_z & \cdot & \cdot & -\sinh v_z \\ \cdot & 1 & \cdot & \cdot \\ \cdot & \cdot & 1 & \cdot \\ -\sinh v_z & \cdot & \cdot & \cosh v_z \end{pmatrix} \begin{pmatrix} \omega_0 \\ -\omega_0 \\ 0 \\ 0 \end{pmatrix} = \omega_0 \begin{pmatrix} \cosh v_z \\ -1 \\ 0 \\ \sinh v_z \end{pmatrix} \quad (5.17a)$$

If starlight had been  $\mathbf{k}_\leftarrow$  or  $\mathbf{k}_\rightarrow$  waves going along  $\mathbf{u}$  and  $z$ -axis, the usual longitudinal Doppler blue shifts  $e^{+v_z}$  or red shifts  $e^{-v_z}$  would appear on both the  $k$ -vector and the frequency, as stated by the following.

$$\begin{pmatrix} \omega'_\rightarrow \\ ck'_{x\rightarrow} \\ ck'_{y\rightarrow} \\ ck'_{z\rightarrow} \end{pmatrix} = \begin{pmatrix} \cosh v_z & \cdot & \cdot & -\sinh v_z \\ \cdot & 1 & \cdot & \cdot \\ \cdot & \cdot & 1 & \cdot \\ -\sinh v_z & \cdot & \cdot & \cosh v_z \end{pmatrix} \begin{pmatrix} \omega_0 \\ 0 \\ 0 \\ \pm\omega_0 \end{pmatrix} = \omega_0 \begin{pmatrix} \cosh v_z \mp \sinh v_z \\ 0 \\ 0 \\ -\sinh v_z \pm \cosh v_z \end{pmatrix} = \omega_0 \begin{pmatrix} e^{\mp v_z} \\ 0 \\ 0 \\ \pm e^{\mp v_z} \end{pmatrix} \quad (5.17b)$$

The Epstein speedometer tracks light pulses and particles in space and time. Instead of space- $x$  and time- $ct$  coordinates of a Minkowski graph, he plots space coordinate- $x$  against *proper* time- $c\tau$ . This view has all things, light  $\gamma$  and particle  $P$  included, moving at the speed of light as shown in Fig. 5.8. Light never ages, so its “speedometer” is tipped to the maximum so it lies along the  $x$ -axis.

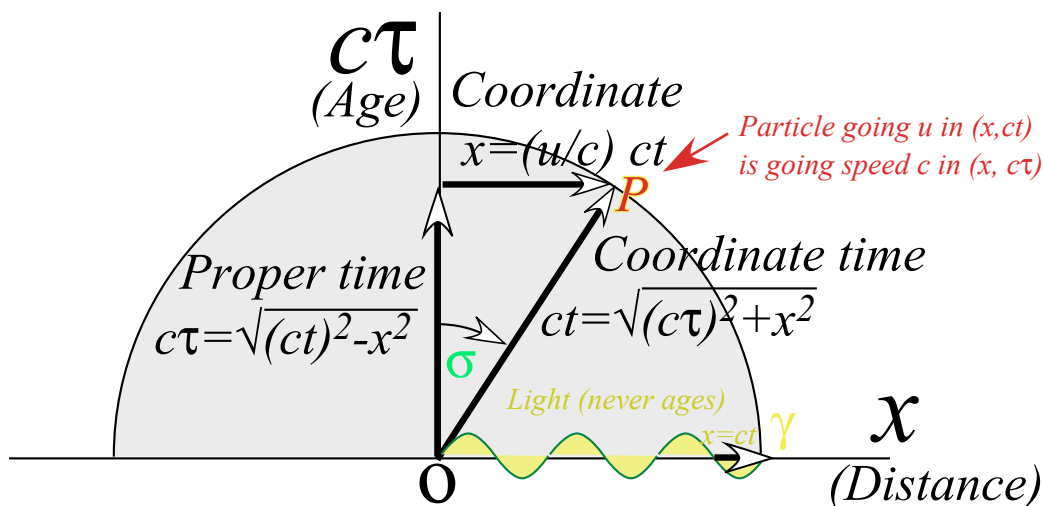


Fig. 5.8 Space-proper-time plot makes all objects move at speed  $c$  along their cosmic speedometer.

One cute feature of the Epstein space-proper-time view is its take of the Lorentz-Fitzgerald contraction of a proper length  $L$  to  $L' = L\sqrt{1-u^2/c^2}$ . (Recall discussion around (2.11).) As shown in Fig. 5.9 below,  $L'$  is simply the projection onto the  $x$ -axis of a length  $L$  tipped by  $\sigma$ .

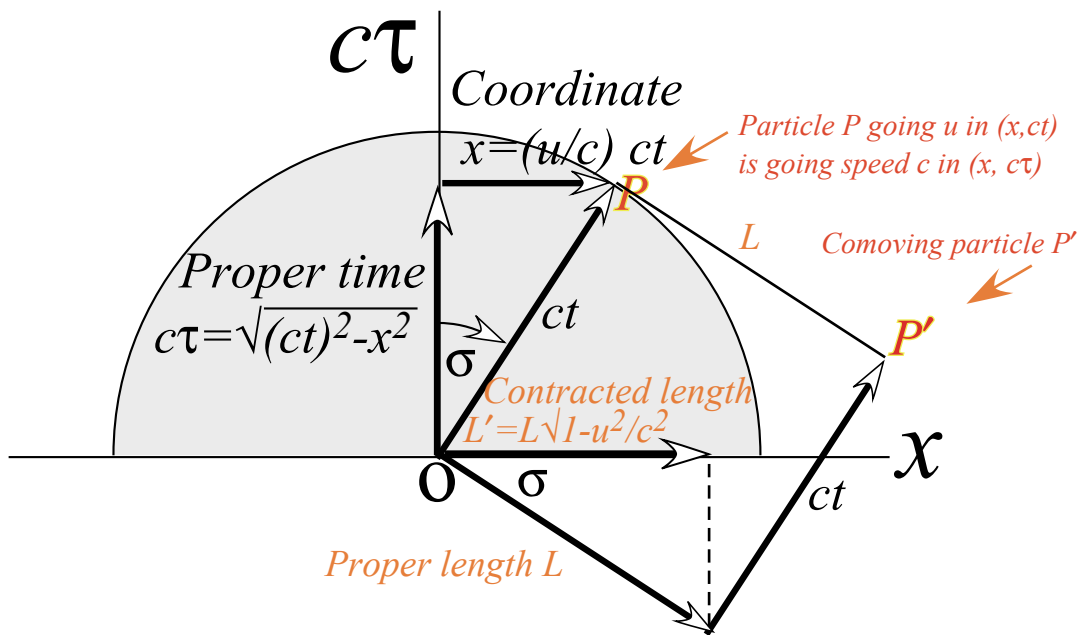


Fig. 5.9 Space-proper-time plot of Lorentz contraction as geometric projection of rotated line  $L$ .

The problem with the  $(x, c\tau)$  view is that a space-time event is not plotted as a single point for all observers. Since the time parameter  $\tau$  is an invariant, the  $(x, c\tau)$  graph it is not a metric space.

*Graphical wave 4-vector transformation*

Geometric constructions combining Fig. 5.6 and Fig. 5.7 help to quantitatively visualize 4-wavevector transformations. One is shown in Fig. 5.10. The  $c$ -dial of the “speedometer” is first set to the desired  $\mathbf{u}$ -speed which determines angle  $\sigma$ . The top of the  $c$ -dial (which may also represent a transverse  $c\mathbf{k}\uparrow$ -vector in units of Lab

frequency  $\omega_0$ ) is projected parallel to the velocity axis until it intersects the  $c$ -dial vertical axis. A transformed  $c\mathbf{k}'_{\uparrow}$ -vector of length  $\omega'_{\uparrow} = \omega_0 \cosh v$  results, similar to  $c\mathbf{k}'_{\downarrow}$  in (5.17a). Both  $c\mathbf{k}'_{\uparrow}$  and  $c\mathbf{k}'_{\downarrow}$  have a projection on the velocity axis of  $\omega_0 \sinh v$  while maintaining their transverse components  $\omega_0$  and  $-\omega_0$ , respectively, in order to stay on the light cone.

A dashed circle of radius  $\cosh v$  is drawn concentric to the  $c$ -dial and determines the longitudinal vectors  $c\mathbf{k}'_{\rightarrow}$  and  $c\mathbf{k}'_{\leftarrow}$  of Doppler shifted length and frequency  $\omega_0 e^{-v}$  and  $\omega_0 e^v$ , respectively, as required by transformation (5.17b). This construction is part of Fig. 5.4 and Fig. 5.5.

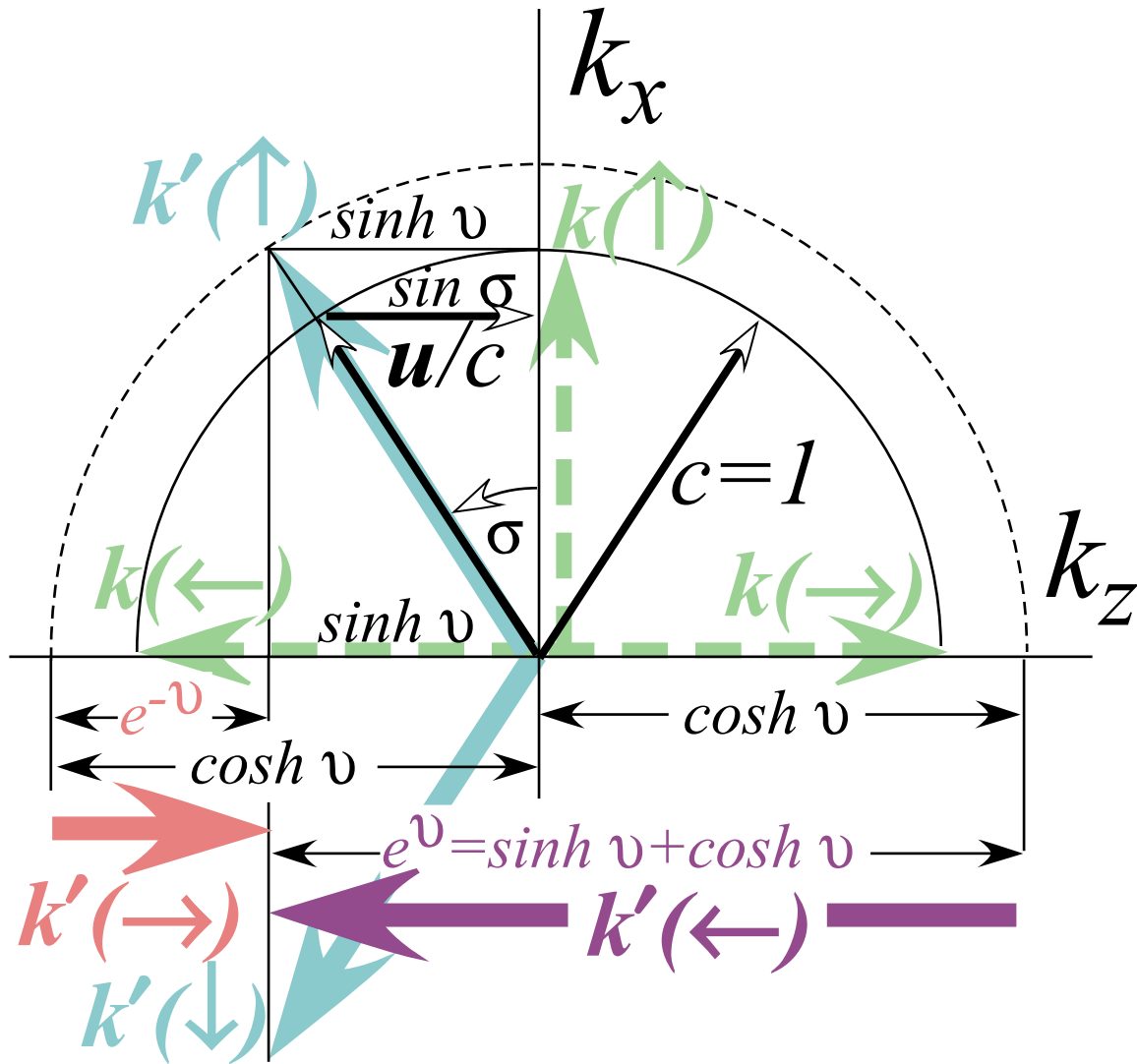


Fig. 5.10 CW cosmic speedometer. Geometry of Lorentz boost of counter-propagating waves.

*Symmetry and conservation principles*

In Newtonian theory the first law or axiom is momentum conservation. Physical axioms, by definition, have only experimental proof. Logical proof is impossible unless a theory like Newton’s becomes sub-summed by a more general theory with finer axioms. Proof of an axiom then undermines it so it becomes a theorem or *result* of more basic axioms. (Or else an axiom might be *disproved* or reduced to an approximate result subject to certain conditions.)

The logic of axioms yielding results or *theorems* in mathematical science probably goes back two thousand years to the time of Euclid’s *Elements*. Also, axiomatic approaches to philosophy and natural science show up in writings as early as that of Occam or even Aristotle, but it is not until the European Renaissance that experiments began to be precise enough to support mathematical models. By the European Enlightenment period, mathematical logic of physical science had become more effective and productive than any preceding philosophy due in no small part to increasingly precise evidence.

As stated by introduction, current time and frequency measurements have achieved almost unimaginable precision. In celebration of this, two continuous wave (CW) axioms (1.1-2) have been used to undermine Newtonian axioms for mass, energy, and momentum. They then became approximate results (4.4) and give rise to exact equivalents of Newtonian concepts in Einstein and Planck relativity and quantum theory in (4.5). It is a non-trivial example of undermining axioms by Occam razor-cutting.

The undermining of Newton’s first axiom (momentum conservation) by the shaved CW axioms is a good example to expose the logic involved. CW logic leads to the DeBroglie scaling law (4.5b) that equates momentum **p** to wavevector **k** scaled in  $\hbar$  units. A rough statement of how CW axioms undermine or “prove” **p**-conservation axioms is that **k**-conservation is required by wave coherence and so  $\mathbf{p}=\hbar\mathbf{k}$  must be conserved, as well. However, that oversimplifies a deeper nature of what is really *symmetry* logic.

A strength (and also, weakness) of CW axioms (1.1-2) is that they are *symmetry* principles due to the Lorentz-Poincare isotropy of space-time that invokes invariance to translation  $\mathbf{T}(\delta, \tau)$  in the vacuum. Operator **T** has plane wave eigenfunctions  $\psi_{k,\omega} = Ae^{i(kx-\omega t)}$  with roots-of-unity eigenvalues  $e^{i(k\delta-\omega\tau)}$ .

$$\mathbf{T}|\psi_{k,\omega}\rangle = e^{i(k\delta-\omega\tau)}|\psi_{k,\omega}\rangle \quad (5.18a) \qquad \langle\psi_{k,\omega}|\mathbf{T}^\dagger = \langle\psi_{k,\omega}|e^{-i(k\delta-\omega\tau)} \quad (5.18b)$$

This also applies to 2-part or “2-particle” states  $\Psi_{K\Omega} = \psi_{k_1,\omega_1}\psi_{k_2,\omega_2}$  where exponents add  $(k,\omega)$ -values of each constituent to  $K=k_1+k_2$  and  $\Omega=\omega_1+\omega_2$ , and  $\mathbf{T}(\delta, \tau)$ -eigenvalues also have the form  $e^{i(K\delta-\Omega\tau)}$  of (5.1). Matrix

$$\langle\Psi'_{K'\Omega'}|\mathbf{U}|\Psi_{K\Omega}\rangle \text{ of } \mathbf{T}\text{-symmetric evolution } \mathbf{U} \text{ is zero unless } K' = k'_1 + k'_2 = K \text{ and } \Omega' = \omega'_1 + \omega'_2 = \Omega .$$

$$\langle\Psi'_{K'\Omega'}|\mathbf{U}|\Psi_{K\Omega}\rangle = \langle\Psi'_{K'\Omega'}|\mathbf{T}^\dagger(\delta, \tau)\mathbf{U}\mathbf{T}(\delta, \tau)|\Psi_{K\Omega}\rangle \quad (\text{if } \mathbf{U}\mathbf{T} = \mathbf{T}\mathbf{U} \text{ for all } \delta \text{ and } \tau) \quad (5.19)$$

$$= e^{-i(K'\delta-\Omega'\tau)}e^{i(K\delta-\Omega\tau)}\langle\Psi'_{K'\Omega'}|\mathbf{U}|\Psi_{K\Omega}\rangle = 0 \text{ unless: } K' = K \text{ and: } \Omega' = \Omega$$

**T**-symmetry requires total energy  $E = \hbar\Omega$  and total momentum  $P = \hbar K$  be *conserved* for archetypical CW states, but laboratory CW have momentum uncertainty  $\Delta\mathbf{k}=l/\Delta\mathbf{x}$  due to finite beam size  $\Delta\mathbf{x}$  and energy uncertainty due to time limits. So, Newton’s 1<sup>st</sup> law or axiom is verified but only as an ideal limit.

Symmetry is to physics what religion is to politics. Both are deep and grand in principle but roundly flaunted in practice. Both gain power quickly by overlooking details. In Ch.4 relativistic and quantum kinetic properties of a massive “thing” arise from those of an optical 2-CW function in one space dimension. This means

that mass shares *symmetry* with 2-CW light, not that mass *is* 2-CW light. Massive “things” do not vanish if a laser turns off, but our tiny optical mass  $\hbar N\omega/c^2$  is quickly gone!

Puzzling questions remain. Why do simple *wave* optics lead directly to general properties (4.5) of relativity and quantum mechanics of a massive *particle*? How does a cavity of counter-propagating green light *waves* act like it holds *particles* of mass  $M=\hbar\omega/c^2$ ?

A short answer to one question is that particles are waves, too, and so forced by Lorentz symmetry to use available hyperbolic invariants  $\omega^2 - (ck)^2 = (Mc^2/\hbar)^2$  for dispersion. To answer the second question entails further loss of classical innocence. In Ch. 6 Occam’s razor is again applied to cut semi-classical CW laser fields down to single field quanta  $\hbar\omega$  or *photons*. So the second short answer is that waves are particles, too, even for optical dispersion ( $\omega^2 - (ck)^2 = 0$ ).

By many accounts, quantum theory begins with Planck axiom  $E=\hbar N\omega$ . This is distinguished from the scaling law  $E=s\omega$  derived in (4.5a) since its scale factor  $s=\hbar N$  is not an obvious consequence of CW phase axioms (1.1-2) that lead to (4.5). CW logic involves additional axioms for Maxwell electromagnetic energy  $E$  and field amplitude quantization to render Planck’s axiom. This is discussed shortly.

*1<sup>st</sup> and 2<sup>nd</sup> Quantization: phase vs. amplitude*

Waves resonate at discrete wave numbers  $k_m = m\frac{2\pi}{L} = mk_1$  in a ring or cavity of length  $L$ . Then relations (4.5b) between  $k$  and momentum  $p$  force  $p$ -quantization  $p_m = \hbar k_m = mp_1$  so momentum quantum numbers<sup>xvi</sup>  $m=0, \pm 1, \pm 2, \dots$  count waves on ring  $L$  as in Bohr electron orbitals or for cavity modes in (4.6a).

Then Planck dispersion  $E_m = \hbar\omega(k_m)$  (4.5a) gives electron energy levels  $E_m = m^2 E_1$  for the BS approximation  $E_1 = p_1^2 / 2M$  or for cavity fundamental frequency levels (4.6b). Wave-fitting in  $x$ -space is called *1<sup>st</sup> quantization*. Related fitting in wave amplitude space is called *2<sup>nd</sup> quantization*.

Heisenberg<sup>xvii</sup> showed quanta  $p_m$  or  $E_m$  arise from eigenvalues (literally “own-values”) of matrix operators  $\mathbf{p}$  or  $\mathbf{H}$  whose eigenvectors (“own-vectors”)  $|p_m\rangle$  or  $|E_m\rangle$  may be superimposed.

$$|\Psi\rangle = \psi_1 |E_1\rangle + \psi_2 |E_2\rangle + \psi_3 |E_3\rangle + \dots \tag{5.20}$$

(Dirac’s bra-ket<sup>xviii</sup> notation came later.) Allowing things to be at (or in)  $m$  places (or states) allows mean values  $\bar{E} = \langle \Psi | \mathbf{H} | \Psi \rangle$  to range continuously from lowest quantum levels  $E_1$  to the highest  $E_m$ .

$$\bar{E} = \langle \Psi | \mathbf{H} | \Psi \rangle = |\psi_1|^2 E_1 + |\psi_2|^2 E_2 + |\psi_3|^2 E_3 + \dots \tag{5.21}$$

For classicists, the notion that each multiple-personality- $k$  has a probability  $|\psi_k|^2$  seems, if not crazy, then at least dicey in the sense of Einstein’s skeptical quote, “*God does not play dice...*”<sup>xix</sup>

But, superposition is an idea borrowed from classical waves. Resulting interference makes them ultra-sensitive to relative position and velocity, a *first* order sensitivity that leads elegantly to relativity transformation (2.10) and kinematic relations (4.5) by geometry of optical phase  $kx-\omega t$  of  $\psi = Ae^{i(kx-\omega t)}$ .

Amplitude “ $A$ ” of wave (1.6) or (1.9) is set arbitrarily since only real wave zeros were needed. It is ignored in (5.5). Without Maxwell and Planck rules, CW amplitude or wave *quantity* is undefined and un-quantized while wave quality (frequency and phase) may be well defined and quantized. Amplitudes need a similar treatment that is begun in Ch. 6.

## Chapter 6. Variation and quantization of optical amplitudes

What is deduced from wave phase alone? Wave *amplitude* has so far been skirted for Occam economy:

“*Pluralitas non est ponenda sine neccesitate*” (Assume no plurality without necessity.) CW phase axioms (1.1-2) give Lorentz-Doppler and Planck-DeBroglie symmetry relations yet 2-CW amplitudes (1.10) are not defined beyond assuming their 1-CW amplitudes match. Standing wave grid reference frames in Fig. 2.1 and Fig. 2.2 are just points where amplitude is *zero*, that is, loci of real wave function *roots*.

Discussion of non-zero amplitude variation begins with counter-propagating 2-CW dynamics involving two 1-CW amplitudes  $A_{\rightarrow}$  and  $A_{\leftarrow}$  that we now allow to be *unmatched*. ( $A_{\rightarrow} \neq A_{\leftarrow}$ )

$$A_{\rightarrow} e^{i(k_{\rightarrow}x - \omega_{\rightarrow}t)} + A_{\leftarrow} e^{i(k_{\leftarrow}x - \omega_{\leftarrow}t)} = e^{i(k_{\Sigma}x - \omega_{\Sigma}t)} [A_{\rightarrow} e^{i(k_{\Delta}x - \omega_{\Delta}t)} + A_{\leftarrow} e^{-i(k_{\Delta}x - \omega_{\Delta}t)}] \quad (6.1a)$$

Half-sum mean phase rates  $(k_{\Sigma}, \omega_{\Sigma})$  and half-difference means  $(k_{\Delta}, \omega_{\Delta})$  appear here as in (1.10).

$$k_{\Sigma} = (k_{\rightarrow} + k_{\leftarrow}) / 2 \quad (6.1b)$$

$$k_{\Delta} = (k_{\rightarrow} - k_{\leftarrow}) / 2 \quad (6.1c)$$

$$\omega_{\Sigma} = (\omega_{\rightarrow} + \omega_{\leftarrow}) / 2$$

$$\omega_{\Delta} = (\omega_{\rightarrow} - \omega_{\leftarrow}) / 2$$

Also important is amplitude mean  $A_{\Sigma} = (A_{\rightarrow} + A_{\leftarrow}) / 2$  and half-difference  $A_{\Delta} = (A_{\rightarrow} - A_{\leftarrow}) / 2$ . Wave motion depends on standing-wave-ratio *SWR* or the inverse standing-wave-quotient *SWQ*.

$$SWR = \frac{(A_{\rightarrow} - A_{\leftarrow})}{(A_{\rightarrow} + A_{\leftarrow})} \quad (6.2a)$$

$$SWQ = \frac{(A_{\rightarrow} + A_{\leftarrow})}{(A_{\rightarrow} - A_{\leftarrow})} \quad (6.2a)$$

Recall mean frequency ratios for group velocity (2.3b) or its inverse that is phase velocity (2.3a).

$$V_{group} = \frac{\omega_{\Delta}}{k_{\Delta}} = c \frac{(\omega_{\rightarrow} - \omega_{\leftarrow})}{(\omega_{\rightarrow} + \omega_{\leftarrow})} \quad (6.3a)$$

$$V_{phase} = \frac{\omega_{\Sigma}}{k_{\Sigma}} = c \frac{(\omega_{\rightarrow} + \omega_{\leftarrow})}{(\omega_{\rightarrow} - \omega_{\leftarrow})} \quad (6.3b)$$

A 2-state amplitude continuum is bounded by a pure right-moving 1-CW ( $A_{\rightarrow} = 1, A_{\leftarrow} = 0$ ) of  $SWR=1$  and a pure left-moving 1-CW ( $A_{\rightarrow} = 0, A_{\leftarrow} = 1$ ) of  $SWR=-1$ . A 2-CW standing-wave ( $A_{\rightarrow} = \frac{1}{\sqrt{2}} = A_{\leftarrow}$ ) has  $SWR=0$ .

Wave paths for various *SWR* values are drawn in Fig. 6.1 for 600THz 2-CW pairs and in Fig. 6.2 for Doppler shifted 300THz and 1200THz 2-CW pairs at the same *SWR* values. The *SWQ* is the ratio of the envelope peak (interference maximum) to the envelope valley (interference minimum), and *vice versa* for  $SWR=1/SWQ$ . Single frequency 2-CW paths of nonzero-*SWR* in Fig. 6.1 do a galloping motion. Each wave speeds up to peak speed  $c/SWR=c \cdot SWQ$  as it first shrinks to squeeze through its envelope minima and then slows to resting speed  $c \cdot SWR$  as it expands to its maximum amplitude. Only at zero-*SWR* do 2-CW zero-paths appear to travel at a constant group speed (6.3a) and phase speed (6.3b) as in Fig. 6.1c or 6.2c. (For 1-CW paths or unit  $SWR=\pm 1$  there is just one speed  $\pm c$  by axiom (1.1).)

The real and imaginary parts take turns. One gallops while the other rests and *vice versa* and this occurs twice each optical period. If frequency ratio (6.3) and amplitude ratio (6.2) have opposite signs as in Fig. 6.1c ( $\pm 0$  or  $\pm \infty$ ) and in Fig. 6.2e ( $\pm 3/5$  or  $\pm 5/3$ ), wave zero paths will follow a right angle staircase. 1-frequency staircase ( $V_{group}=0=SWR$ ) in Fig. 6.1c is a Cartesian grid like Fig. 2.1c. 2-frequency waves ( $V_{group} \neq 0$ ) have Minkowski grids like Fig. 2.2c for  $SWR=0$  or quasi-Cartesian stair steps like Fig. 6.2e for  $V_{group} = -cSWR$ . To broadcast Cartesian grids to a *u*-frame one tunes both  $V_{group}$  and  $cSWR$  to *u*.

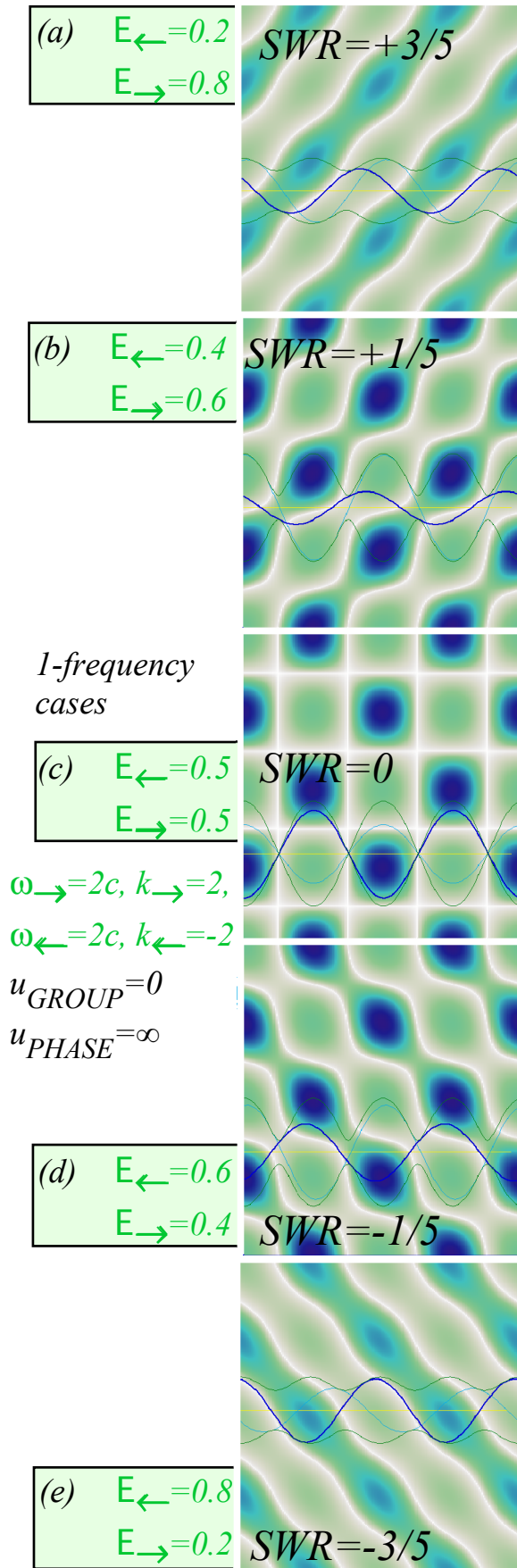


Fig. 6.1 Monochromatic (1-frequency) 2-CW wave space-time patterns.

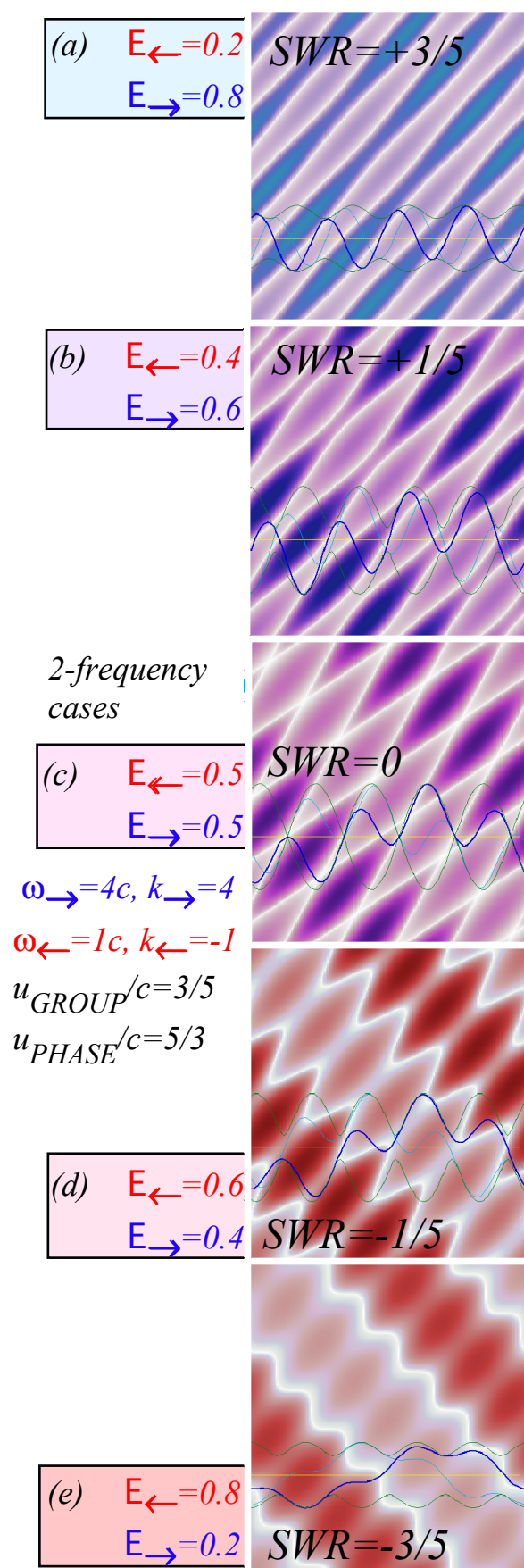


Fig. 6.2 Dichromatic (2-frequency) 2-CW wave space-time patterns.

Galloping is a fundamental interference property that may be clarified by analogy with elliptic orbits of isotropic 2D-harmonic oscillators and in particular with elliptic polarization of optical wave amplitudes. Fig. 6.3 relates polarization states and wave states of Fig. 6.1 beginning with left (right)-circular polarization that is analogous to a left (right)-moving wave in Fig. 6.3g (Fig. 6.3a). As sketched in Fig. 6.3(b-e), galloping waves are general cases analogous to general states of elliptic polarization or general 2DHO orbits obeying a Keplerian geometry shown in Fig. 6.3h. Standing waves correspond to plane-polarization. Polarization in the  $x$ -plane of Fig. 6.3d corresponds to a standing cosine wave and  $y$ -plane polarization (not shown) would correspond to a standing sine wave.

Isotropic oscillator orbits obey Kepler's law of constant orbital momentum. Orbit angular velocity slows down by a factor  $b/a$  at major axes or aphelions  $\pm a$  and then speeds up by a factor  $a/b$  at minor axes or perihelions  $\pm b$  just as a galloping wave, twice in each period, slows down to  $SWR \cdot c$  and speeds up to  $SWQ \cdot c$ . The galloping or eccentric motion of the eccentric anomaly angle  $\phi(t)$  in Fig. 6.3h is a projection of a uniformly rotating mean anomaly (phase angle  $\omega \cdot t$ ) of the isotropic oscillator, and this gives a Keplerian relation of the two angles seen in the figure.

$$\tan \phi(t) = \frac{b}{a} \tan \omega \cdot t \quad (6.4a)$$

The eccentric anomaly time derivative of  $\phi$  (angular velocity) gallops between  $\omega \cdot b/a$  and  $\omega \cdot a/b$ .

$$\dot{\phi} = \frac{d\phi}{dt} = \omega \cdot \frac{b \sec^2 \omega t}{a \sec^2 \phi} = \frac{\omega \cdot b/a}{\cos^2 \omega t + (b/a)^2 \cdot \sin^2 \omega t} = \begin{cases} \omega \cdot b/a & \text{for: } \omega t = 0, \pi, 2\pi, \dots \\ \omega \cdot a/b & \omega t = \pi/2, 3\pi/2, \dots \end{cases} \quad (6.4b)$$

The product of angular momentum  $r^2$  and  $\dot{\phi}$  is orbital momentum, a constant proportional to ellipse area.

$$r^2 \frac{d\phi}{dt} = \text{constant} = (a^2 \cos^2 \omega t + b^2 \cdot \sin^2 \omega t) \frac{d\phi}{dt} = \omega \cdot ab$$

Consider galloping wave zeros of a monochromatic wave (6.1a) having  $SWQ$  (6.2b).

$$\begin{aligned} 0 &= \text{Re } \Psi(x, t) = \text{Re} \left[ A_{\rightarrow} e^{i(k_0 x - \omega_0 t)} + A_{\leftarrow} e^{i(-k_0 x - \omega_0 t)} \right] \quad \text{where: } \omega_{\rightarrow} = \omega_0 = \omega_{\leftarrow} = ck_0 = -ck_{\leftarrow} \\ 0 &= A_{\rightarrow} [\cos k_0 x \cos \omega_0 t + \sin k_0 x \sin \omega_0 t] + A_{\leftarrow} [\cos k_0 x \cos \omega_0 t - \sin k_0 x \sin \omega_0 t] \\ (A_{\rightarrow} + A_{\leftarrow}) [\cos k_0 x \cos \omega_0 t] &= -(A_{\rightarrow} - A_{\leftarrow}) [\sin k_0 x \sin \omega_0 t] \end{aligned}$$

Space  $k_0 x$  varies with time  $\omega_0 t$  in the same way that eccentric anomaly varies in (6.4a).

$$\tan k_0 x = -SWQ \cdot \cot \omega_0 t = SWQ \cdot \tan \omega_0 \bar{t} \quad \text{where: } \omega_0 \bar{t} = \omega_0 t - \pi/2 \quad (6.5a)$$

Speed of galloping wave zeros is the time derivative of root location  $x$  in units of light velocity  $c$ .

$$\frac{dx}{dt} = c \cdot SWQ \frac{\sec^2 \omega_0 \bar{t}}{\sec^2 k_0 x} = \frac{c \cdot SWQ}{\cos^2 \omega_0 \bar{t} + SWQ^2 \cdot \sin^2 \omega_0 \bar{t}} = \begin{cases} c \cdot SWQ & \text{for: } \bar{t} = 0, \pi, 2\pi, \dots \\ c \cdot SWR & \bar{t} = \pi/2, 3\pi/2, \dots \end{cases} \quad (6.5b)$$

Single frequency 2-CW paths in Fig. 6.1 have a constant product of instantaneous wave velocity and wave amplitude analogous to the constant product of orbital velocity and radius. So vacuum optical amplitude and phase motion obey a funny version of Kepler and Galileo's rules. The extent to which 14<sup>th</sup> century geometric relations underlie basic wave physics may be surprising to some.

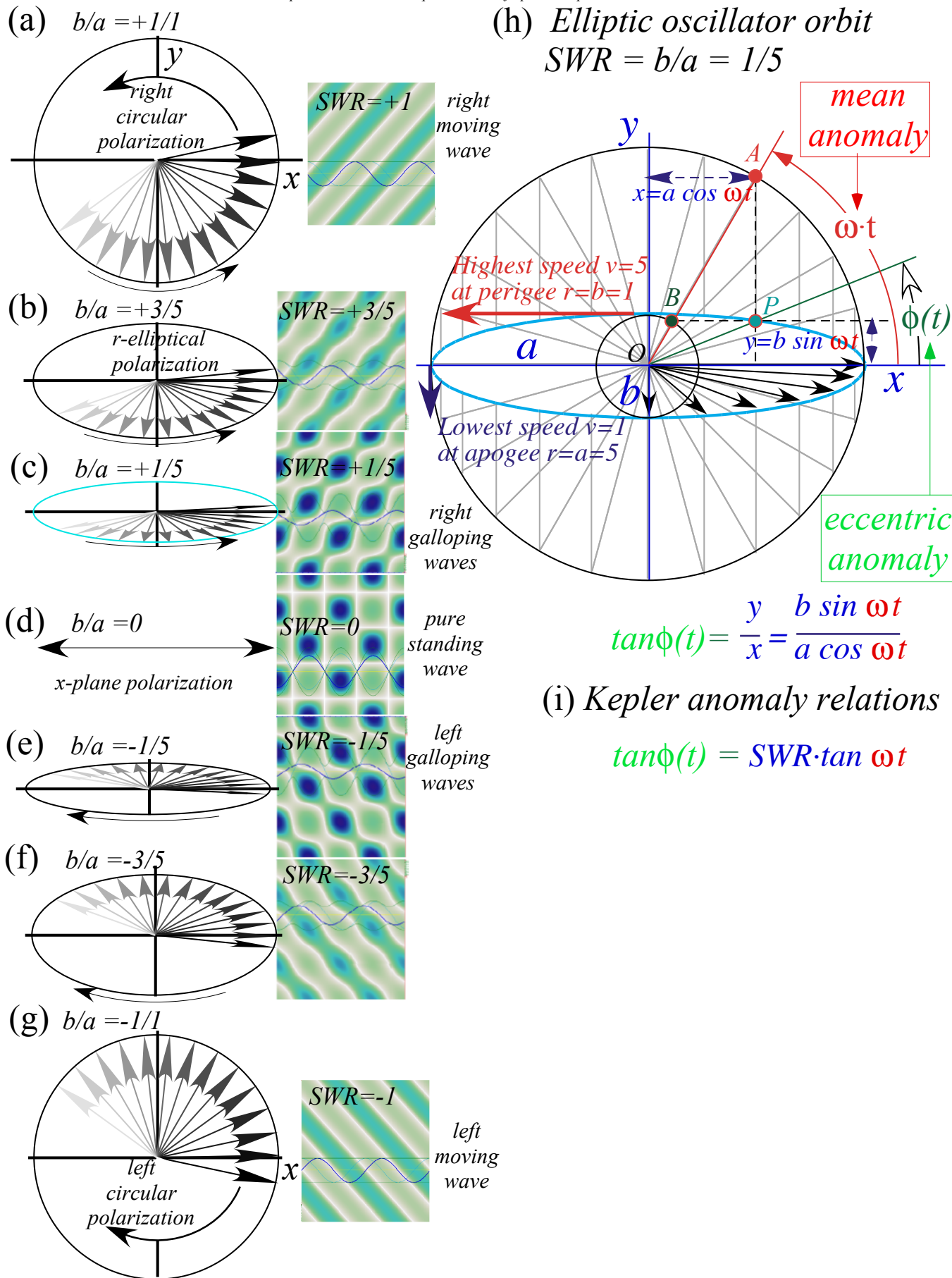


Fig. 6.3 (a-g) Elliptic polarization ellipses relate to galloping waves in Fig. 6.1. (h-i) Kepler anomalies.

## Maxwell amplitudes and energy

Classical Maxwell field amplitudes  $\mathbf{E} = -\dot{\mathbf{A}}$  and  $\mathbf{B} = \nabla \times \mathbf{A}$  are derivatives of vector potential  $\mathbf{A}$ . Maxwell energy  $U$  per volume  $V$  or total energy  $U \cdot V$  is a sum of amplitude squares  $\mathbf{E} \cdot \mathbf{E}$  and  $c^2 \mathbf{B} \cdot \mathbf{B}$ .

$$\langle U \rangle \cdot V = \left\langle \frac{\epsilon_0}{2} \mathbf{E} \cdot \mathbf{E} + \frac{1}{2\mu_0} \mathbf{B} \cdot \mathbf{B} \right\rangle \cdot V \quad \mu_0 \epsilon_0 = \frac{1}{c^2} \quad (6.7)$$

Fourier analysis of  $\mathbf{A}$  into amplitudes  $\mathbf{a}_k$  and  $\mathbf{a}_k^*$  leads to a harmonic oscillator sum over each plane CW mode frequency  $\omega_k = \pm c |\mathbf{k}_m|$ ,  $\mathbf{k}_m$ -vector allowed by a large-cavity, and polarization  $\alpha=x,y$  normal to  $\mathbf{k}_m$ .

$$\langle U \rangle \cdot V = 2\epsilon_0 V \sum \omega_k^2 \mathbf{a}_k^* \mathbf{a}_k \quad (6.8)$$

Harmonic oscillator frequency is independent of amplitude. This is consistent with CW phase axiom (1.1) and dispersion relations (3.5) derived from 2-CW superposition, but such a simple axiom seems unable to derive the Maxwell vector amplitude structure of 2-dimensional polarization normal to  $\mathbf{k}_m$  of each wave mode or even to establish that its wave variables  $\mathbf{A}$ ,  $\mathbf{B}$ ,  $\mathbf{E}$ , or  $\mathbf{k}_m$  are, in fact, 3D vectors.

The CW axiom (1.1) gives what is effectively a 2-dimensional harmonic oscillator (2DHO) with two complex amplitudes ( $a_L, a_R$ ) for the two longitudinal propagation directions, but each comes with two transverse polarization amplitudes ( $a_x, a_y$ ) that describe the second 2DHO in Maxwell light, namely polarization ellipsometry used in Fig. 6.3 as an analogy for propagation left-and-right along  $z$ .

### Quantized optical fields

Mode amplitude  $\mathbf{a}_k$  or  $\mathbf{a}_k^*$  in classical electromagnetic energy  $\sum \omega_k^2 \mathbf{a}_k^* \mathbf{a}_k$  are replaced by oscillator operators  $\mathbf{a}_k$  or  $\mathbf{a}_k^\dagger$  for a field Hamiltonian with explicit linear frequency dependence of Planck.

$$\mathbf{H} = \sum \hbar \omega_k (\mathbf{a}_k^\dagger \mathbf{a}_k) \Rightarrow \langle \mathbf{H} \rangle = \sum \hbar \omega_k N_k \quad (6.9)$$

The  $\mathbf{H}$ -eigenstates  $|N_1 N_2 \dots N_k\rangle$  for exactly quantized photon numbers  $\langle \mathbf{a}_k^\dagger \mathbf{a}_k \rangle = N_k$  fix a definite energy value  $\hbar \omega_k N_k$  for each mode- $k_m$  but has quite *uncertain* field phase. Average energy of one mode is

$$\langle U_k \rangle \cdot V = 2\epsilon_0 V \langle \mathbf{E}_k \cdot \mathbf{E}_k \rangle = \hbar \omega_k N_k \quad (6.10a)$$

where a 1-CW-1-photon E-field and vector potential  $A$ -amplitude is as follows.

$$\left\langle |\mathbf{E}_k| \right\rangle_{N_k=1} = \sqrt{\frac{\hbar \omega_k}{2\epsilon_0 V}} \quad (6.10b) \quad \left\langle |\mathbf{A}_k| \right\rangle_{N_k=1} = \sqrt{\frac{\hbar}{2\epsilon_0 \omega_k V}} \quad (6.10c)$$

Field quantization is called 2<sup>nd</sup>-quantization to distinguish 1<sup>st</sup>-quantization  $k_m$  *mode* numbers  $m$ , used for classical light, from “purely quantum” *photon* numbers  $n = N_{k_m}$  for wave amplitude. This may be a prejudice that waves (particles) are usual (unusual) for light but unusual (usual) for matter. Amplitudes involve relations (6.7) to (6.10) that are more complex than axioms (1.1-2) for wave phase. While Maxwell-Planck relations lack the simplicity of the latter, they do derive the linear dispersion (1.1) by Fourier transform of the Maxwell wave equations, and they show optical wave amplitude has an internal symmetry analogous to that of wave frequency. The following discussion of this analogy involves a Doppler shift of wave *amplitude* with invariance or covariance of photon number  $N_k$  and standing wave ratio (*SWR*) (6.5). Also, one begins to see how Born quantum probability formulas  $\langle n \rangle = \psi^* \psi$  arise and are consistent with Dirac amplitude covariance.

*Relativistic 1-CW covariance of Poynting flux*

Maxwell-Planck energy density  $U(\text{Joule}/\text{m}^3)$  in (6.10a) leads to a related Poynting flux  $\mathbf{S}[\text{Joule}/(\text{m}^2 \cdot \text{s})]$ .

$$\bar{\mathbf{S}} = \bar{\mathbf{E}} \times \bar{\mathbf{B}} = \langle U_k \rangle c \hat{\mathbf{k}} = 2\epsilon_0 c \langle \mathbf{E}_k \cdot \mathbf{E}_k \rangle \hat{\mathbf{k}} = \hbar \omega_k \bar{n}_k \hat{\mathbf{k}} \quad \text{where: } n_k = cN_k / V [m^{-2} \cdot s^{-1}] \quad (6.11)$$

Flux  $\mathbf{S}$  contains two frequency factors, the fundamental laser frequency  $\omega_k$  and the photon count rate  $n_k$  per  $[(m^2 \cdot s)]$ . Frequency  $\omega_k$  is quantum *quality* of a laser beam and rate  $n_k$  is its quantum *quantity*. The product  $\hbar \omega_k \cdot n_k$  is Poynting *flux*. Rate  $n_k$  and frequency  $\omega_k$  both Doppler shift by an exponential  $e^{\pm\rho}$  of rapidity  $\rho$  in (2.16). So do 1-CW fields  $E_{\pm k}$  as may be shown by Lorentz transforming them directly.

$$E'_{+k} = e^{+\rho} E_{+k} \quad (6.12a) \qquad E'_{-k} = e^{-\rho} E_{-k} \quad (6.12b)$$

Thus both electric field polarization  $\mathbf{E}$ -amplitudes  $E_x$  and  $E_y$  of a 1-CW field undergo the same  $e^{\pm\rho}$  Doppler shift that the frequency  $\omega_k$  or wavevector  $k$  experience. If  $\mathbf{E}$  in (6.11) scaled by 1-photon factor (6.10) a probability wave  $\psi$  follows whose square  $\psi^* \psi$  is a volume photon count  $N/(m^3)$ .

$$\psi_k = \sqrt{\frac{2\epsilon_0 V}{\hbar \omega_k}} E_k \Rightarrow \langle \psi_k^* \psi_k \rangle = \langle N_k \rangle = \bar{N}_k = \bar{n}_k \frac{V}{c} \quad (6.13a)$$

Or, a flux probability wave  $\psi$  is defined so its square  $\psi^* \psi$  is an expected flux photon count  $n/(m^2 \cdot s)$ .

$$\psi_k = \sqrt{\frac{2\epsilon_0 c}{\hbar \omega_k}} E_k \Rightarrow \langle \psi_k^* \psi_k \rangle = \langle n_k \rangle = \bar{n}_k = \frac{c}{V} \bar{N}_k \quad (6.13b)$$

Due to the  $1/\sqrt{\omega_k}$  scaling of (6.13) the Doppler factor of  $\psi_{\pm k}$  drops an  $e^{\pm\rho/2}$  factor from  $E_k$  in (6.12).

$$L_z(\rho) |\psi\rangle = \begin{pmatrix} \psi'_{+k} \\ \psi'_{-k} \end{pmatrix} = \begin{pmatrix} e^{+\rho/2} & 0 \\ 0 & e^{-\rho/2} \end{pmatrix} \begin{pmatrix} \psi_{+k} \\ \psi_{-k} \end{pmatrix} = e^{\sigma_z \rho/2} |\psi\rangle \quad (6.14)$$

This is a starting point for the spinor form of Lorentz transformation for Dirac amplitudes.

*Relativistic 2-CW invariance of cavity quanta*

Mean photon number  $\bar{N}_k$  of a 2-CW cavity mode, unlike a 1-CW flux quantum  $n_k$ , is invariant to cavity speed. By analogy, 2-CW modes have variant group-phase velocity ( $V_{group}, V_{phase}$ ), energy-momentum ( $\hbar ck, \hbar \omega$ ), but invariant mean velocity  $c = \sqrt{V_{group} V_{phase}}$  and frequency  $\varpi = \sqrt{\omega_{+k} \omega_{-k}} = \sqrt{\omega^2 - c^2 k^2}$ .

$$\frac{V_{phase}}{c} = \frac{\omega_{+k} - \omega_{-k}}{\omega_{+k} + \omega_{-k}} \quad (6.15a) \qquad \frac{V_{group}}{c} = \frac{\omega_{+k} - \omega_{-k}}{\omega_{+k} + \omega_{-k}} \quad (6.15b)$$

Linear dispersion  $\omega_{\pm k} = \pm ck$  and (1.11) or (2.7) are used. Note the analogy to *SWR* relations (6.2).

$$SWR = \frac{E_{+k} - E_{-k}}{E_{+k} + E_{-k}} \quad (6.15c) \qquad SWQ = \frac{E_{+k} + E_{-k}}{E_{+k} - E_{-k}} \quad (6.15d)$$

Each ratio (6.15) is a wave velocity that Doppler-transforms like relativistic (non-Galilean) velocity.

$$SWR' = \frac{SWR + u/c}{1 + SWR \cdot u/c} \quad (6.16a) \qquad \frac{V'_m}{c} = \frac{V_m/c + u/c}{1 + (V_m/c) \cdot (u/c)} \quad (6.16b)$$

Velocity  $u_{AB}/c = \tanh \rho_{AB}$  is a hyperbolic sum since rapidity is a simple sum  $\rho_{AB} = \rho_A + \rho_B$  by (3.6).

$$\frac{u_{AB}}{c} = \tanh \rho_{AB} = \tanh(\rho_A + \rho_B) = \frac{\tanh \rho_A + \tanh \rho_B}{1 + \tanh \rho_A \tanh \rho_B} = \frac{u_A/c + u_B/c}{1 + u_A u_B / c^2} \quad (6.17)$$

The energy and momentum flux values are found for counter- $k$  2-CW beam functions  $\Psi_{\rightleftharpoons}$ .

$$\Psi_{k\rightleftharpoons} = \psi_{\rightarrow} e^{i(k_{\rightarrow}x - \omega_{\rightarrow}t)} + \psi_{\leftarrow} e^{i(k_{\leftarrow}x - \omega_{\leftarrow}t)}$$

Lab 1-CW flux number expectation values  $|\psi_k|^2 = \langle n_k \rangle$  give 2-CW flux expectations in lab.

$$\begin{aligned} \langle E \rangle &= \langle \hbar\omega \rangle = \hbar\omega_{\rightarrow} \langle n_{\rightarrow} \rangle + \hbar\omega_{\leftarrow} \langle n_{\leftarrow} \rangle = \hbar\omega_{\rightarrow} |\psi_{\rightarrow}|^2 + \hbar\omega_{\leftarrow} |\psi_{\leftarrow}|^2 \\ \langle cp \rangle &= \langle \hbar ck \rangle = \hbar ck_{\rightarrow} \langle n_{\rightarrow} \rangle + \hbar ck_{\leftarrow} \langle n_{\leftarrow} \rangle = \hbar\omega_{\rightarrow} |\psi_{\rightarrow}|^2 - \hbar\omega_{\leftarrow} |\psi_{\leftarrow}|^2 \end{aligned}$$

The relation (6.13b) of quantum field  $\psi_k$  and classical Maxwell  $E_k$ -field expectation is used.

$$\langle E \rangle = \hbar\omega_{\rightarrow} |\psi_{\rightarrow}|^2 + \hbar\omega_{\leftarrow} |\psi_{\leftarrow}|^2 = 2\varepsilon_0 c \left( |E_{\rightarrow}|^2 + |E_{\leftarrow}|^2 \right) \quad (6.18a)$$

$$\langle cp \rangle = \hbar\omega_{\rightarrow} |\psi_{\rightarrow}|^2 - \hbar\omega_{\leftarrow} |\psi_{\leftarrow}|^2 = 2\varepsilon_0 c \left( |E_{\rightarrow}|^2 - |E_{\leftarrow}|^2 \right) \quad (6.18b)$$

Values  $\langle cp \rangle$  and  $\langle E \rangle$  lie on an invariant hyperbola of constant geometric means  $\varpi \bar{N}$  or  $|\bar{\mathbf{E}}|^2$ .

$$\langle E \rangle^2 - \langle cp \rangle^2 = (2c\varepsilon_0)^2 \left[ \left( |E_{\rightarrow}|^2 + |E_{\leftarrow}|^2 \right)^2 - \left( |E_{\rightarrow}|^2 - |E_{\leftarrow}|^2 \right)^2 \right] = (2c\varepsilon_0)^2 \left[ 4|E_{\rightarrow}|^2 |E_{\leftarrow}|^2 \right]$$

$$\langle E \rangle^2 - \langle cp \rangle^2 = 4 \left( 2c\varepsilon_0 |E_{\rightarrow}|^2 \right) \left( 2c\varepsilon_0 |E_{\leftarrow}|^2 \right) = 4 (\hbar\omega_{\rightarrow} \langle n_{\rightarrow} \rangle) (\hbar\omega_{\leftarrow} \langle n_{\leftarrow} \rangle) \quad (6.19)$$

$$\sqrt{\langle E \rangle^2 - \langle cp \rangle^2} = 2c\varepsilon_0 |2\bar{\mathbf{E}}|^2 = (\hbar\bar{\omega})(2\bar{n}) \quad (6.20a)$$

The geometric mean frequency  $\varpi$ , mean quantum number  $\bar{n}$ , and mean field  $|\bar{\mathbf{E}}|$  are defined.

$$\varpi = \sqrt{\omega_{\rightarrow}\omega_{\leftarrow}} \quad (6.20b) \quad \bar{n} = \sqrt{n_{\rightarrow}n_{\leftarrow}} \quad (6.20c) \quad |\bar{\mathbf{E}}| = \sqrt{E_{\rightarrow}E_{\leftarrow}} \quad (6.20d)$$

Doppler relations imply Lorentz invariance for the mean number  $\bar{n}$  and for the mean frequency  $\varpi$  as well as their geometric mean  $\sqrt{\bar{n}\varpi}$  that is  $2c\varepsilon_0$  times the mean field  $|\bar{\mathbf{E}}|$  and applies to a general 2-CW beam function  $\Psi$ . A factor 2 on  $|2\bar{\mathbf{E}}|$  or  $2\bar{n}$  in (6.20a) is consistent with 1-photon 2-CW states having equal average number  $n_{\rightarrow} = \bar{n} = n_{\leftarrow} = \frac{1}{2}$  and total 1-photon Planck energy expectation  $E = \hbar\omega$ .

Ideal cavities balance field  $E_{\rightarrow} = \bar{\mathbf{E}} = E_{\leftarrow}$ , frequency  $\omega_{\rightarrow} = \varpi = \omega_{\leftarrow}$ , and number. But, a general beam with  $\omega_{\rightarrow} \neq \omega_{\leftarrow}$ ,  $n_{\rightarrow} \neq n_{\leftarrow}$ , and  $E_{\rightarrow} \neq E_{\leftarrow}$  has a center-of-momentum CoM-frame of zero flux where  $E_{\rightarrow}^{CoM} = E_{\leftarrow}^{CoM}$  by (6.18b), an isochromatic IsoC-frame with  $\omega_{\rightarrow}^{IsoC} = \omega_{\leftarrow}^{IsoC}$ , and an IsoN-frame with balanced photon count  $N_{\rightarrow}^{IsoN} = N_{\leftarrow}^{IsoN}$ . Frame speeds  $u^\alpha$  may be distinct as sketched in Fig. 6.4.

$$\frac{u^{CoM}}{c} = \frac{E_{\rightarrow} - E_{\leftarrow}}{E_{\rightarrow} + E_{\leftarrow}} \quad (6.21a) \quad \frac{u^{IsoC}}{c} = \frac{\omega_{\rightarrow} - \omega_{\leftarrow}}{\omega_{\rightarrow} + \omega_{\leftarrow}} = \frac{V^{Group}}{c} \quad (6.21b) \quad \frac{u^{IsoN}}{c} = \frac{n_{\rightarrow} - n_{\leftarrow}}{n_{\rightarrow} + n_{\leftarrow}} \quad (6.21c)$$

Flux invariant  $|\bar{\mathbf{E}}|$  is maximized by balanced amplitude  $E_{\rightarrow} = E_{\leftarrow}$  but is zero if  $E_{\rightarrow}$  or  $E_{\leftarrow}$  is zero.

Thus optical rest mass (6.20a) decreases continuously as a 2-CW beam is unbalanced toward 1-CW.

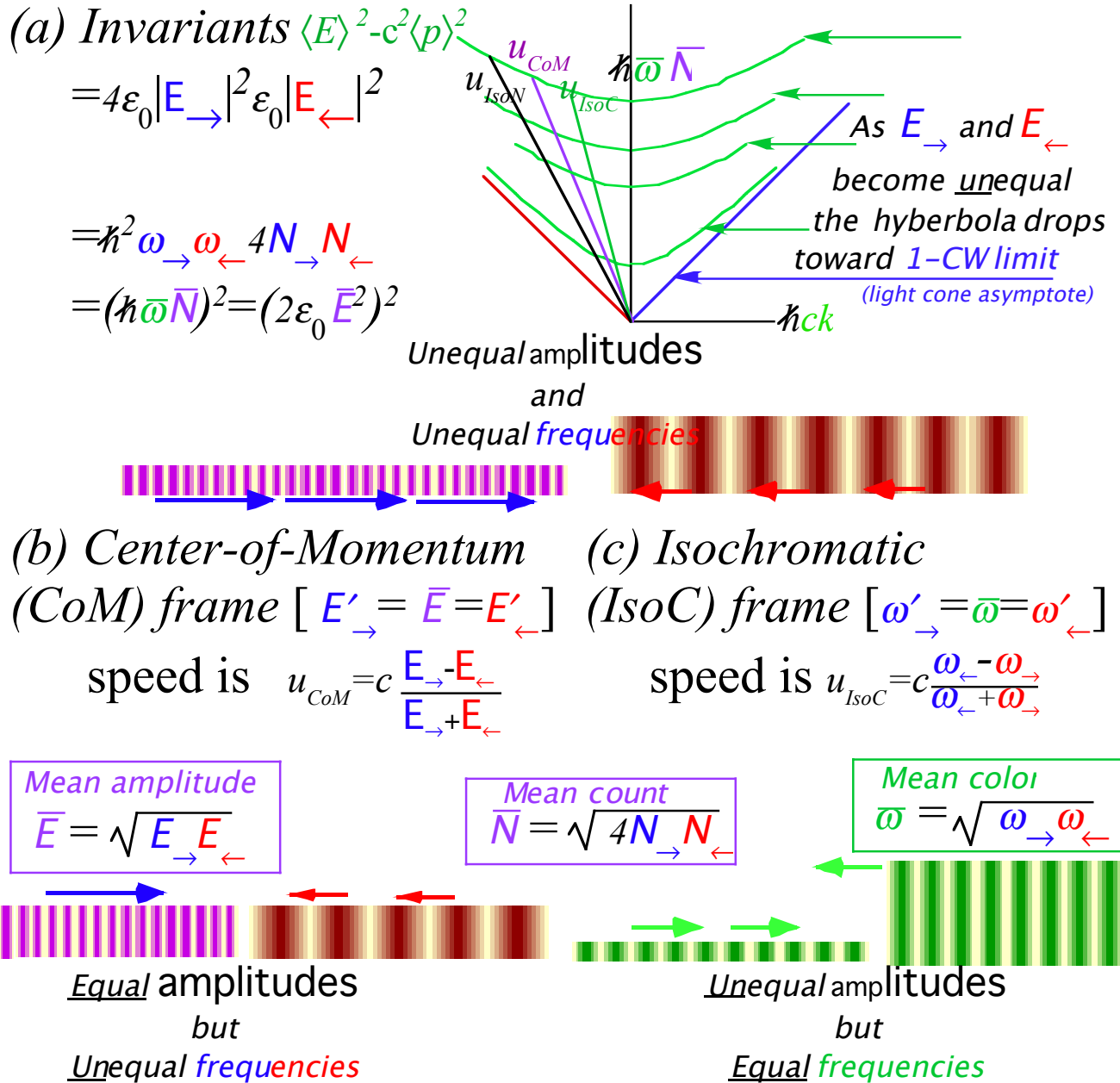


Fig. 6.4. Cavity 2-CW modes. (a) Invariant “mass” hyperbolas. (b) COM frame. (c) ISOC frame.

It is argued in Ch. 4 that mass is a coherent 2-CW interference effect that is not possible for a 1-CW beam. If we replace Planck energy relation  $\epsilon = Nh\nu$  by a Maslov form  $\epsilon = (N + \bar{\alpha})h\nu$  it has a tiny zero-point energy minimum  $\bar{\alpha}h\nu$ . Does a tiny mass  $\bar{\alpha}h\nu / c^2$  exist for 1-CW and even 0-CW beams in all frames in spite of the incoherence of such zero-point fluctuations? Such a presence in (6.20) may be ruled out if the speed-of-light axiom (1.1) is exact. There may still be much to learn about zero-point effects in QED and cosmology but this seems to indicate that their direct effects are effectively non-existent.

### N-Photon vs Coherent- $\alpha$ -states

Optical fields  $\mathbf{A}$  or  $\mathbf{E}$  have quantum expectation values of field operators based on mode amplitudes  $\mathbf{a}_k$  or  $\mathbf{a}_k^*$  in classical energy  $\sum \omega_k^2 \mathbf{a}_k^* \mathbf{a}_k$ . Each  $\mathbf{a}_k$  or  $\mathbf{a}_k^*$  is replaced by oscillator boson operator  $\mathbf{a}_k$  or  $\mathbf{a}_k^\dagger$  in a quantum field Hamiltonian  $\mathbf{H} = \sum \hbar \omega_k (\mathbf{a}_k^\dagger \mathbf{a}_k + \bar{\alpha})$  whose eigenstates  $|N_1 N_2 \dots N_k\rangle$  have exact quantized photon numbers  $\langle \mathbf{a}_k^\dagger \mathbf{a}_k \rangle = N_k$  for each mode- $k_m$ .

Each mode phase quanta  $m$  and amplitude quanta  $N_m$  are invariant constants that define another hyperbola with Einstein-Planck proper frequency  $\bar{\omega}_{N,m} = \hbar N_m \omega_m$  as sketched in Fig. 6.4a and Fig. 4.2. The problem is that absolute certainty of photon number  $N_m$  implies totally *uncertain* field phase just as absolutely certain  $k_m$  of 1-CW symmetry implies totally *uncertain* position in space and time.

Space-time position coordinates were defined by taking 1-CW combinations to make 2-CW coordinates of Fig. 2.1c or Fig. 2.2c. Ultimately an  $n$ -CW pulse-wave (PW) of Fig. 2.1d or Fig. 2.2d was localized with as low a space-time uncertainty  $\Delta\tau$  as desired but it acquires per-space uncertainty or bandwidth  $\Delta\nu$  according to Fourier-Heisenberg relation  $\Delta\nu \cdot \Delta\tau > 1$ .

So also must photon-number states be combined if amplitude and phase uncertainty are to be reduced to the point where wave space-time coordinates can emerge. Such combinations are known as coherent states or  $\alpha$ -states of harmonic oscillation. Sharper wave zeros require fuzzier hyperbolas.

#### Fuzzy hyperbolas vs. fuzzy coordinates

Model micro-laser states are *coherent* states  $|\alpha\rangle = \sum_N \psi_N |N\rangle$  made of single-mode eigenstates  $|N\rangle = (\mathbf{a}_1^\dagger)^N |0\rangle$  with amplitudes  $\psi_N = \alpha^N e^{-\alpha^2/2} / \sqrt{N!}$ . Variable  $\alpha = x + ip = |\alpha| e^{i\phi}$  is average mode phase, and  $(x = \text{Re } \alpha, p = \text{Im } \alpha)$ , rescaled by a quantum field factor  $f$ , are field averages  $(\langle A \rangle, \langle \dot{A} \rangle = -\langle E \rangle)$ .

$$\langle \alpha | A | \alpha \rangle = \langle A \rangle = (\alpha + \alpha^*) f = (\alpha + \alpha^*) \sqrt{\frac{\hbar}{2\epsilon_0 \omega V}} \tag{6.22}$$

Amplitude factor  $f$  makes Planck's  $\bar{E} = \hbar \omega \bar{N}$  equal Maxwell field energy  $\bar{E} = \bar{U} \cdot V$ .

$$\langle U \rangle V = 2\epsilon_0 \omega^2 V \langle A^2 \rangle = \hbar \omega |\alpha|^2 = \hbar \omega \bar{N} \tag{6.23}$$

A fundamental laser mode in a  $0.25\mu\text{m}$  cubic cavity (See  $\mathbf{E}$ -wave sketched in a strip of Fig. 2.2c.) has green light with  $\hbar\bar{\omega} = 4 \cdot 10^{-19}$  Joule or  $2.5\text{eV}$  per photon. The average photon number  $\bar{N} = |\alpha|^2 = 10^{10}$  models a laser with mean energy  $\bar{E} = \bar{U} \cdot V = \hbar\bar{\omega}\bar{N} = 4.0\text{ nanoJ}$  in a volume  $V = (\frac{1}{4}\mu\text{m})^3$ . Photon number uncertainty  $\Delta N = |\alpha| = 10^5$  varies inversely to phase uncertainty.

$$\Delta\Phi \cdot \Delta N = \pi \tag{6.24a} \qquad \Delta\Phi = \pi / \alpha \sim 3 \cdot 10^{-5} \tag{6.24b}$$

Amplitude expectation value  $\langle N | A | N \rangle$  is zero for  $|N\rangle$  states due to *incoherence* of phase, but number value  $\langle N | \mathbf{a}_k^\dagger \mathbf{a}_k | N \rangle = N$  is exact as is proper frequency  $\bar{\omega}N$  due to the phase factor  $(e^{-i\bar{\omega}t})^N$  of  $(\mathbf{a}_1^\dagger)^N$ .

A volume  $V$  with  $(N = 10^{10})$ -photons has energy  $E = \hbar\omega N$  or mass-equivalent  $M = E / c^2 = 10^{-25}$  kg on a hyperbola  $10^{10}$  quanta above the  $N=1$  hyperbola. A coherent-state  $|\alpha = 10^5\rangle$  has a mass  $M = 10^{-25}$  kg with uncertainty  $\Delta M = 10^{-30}$  kg so its *phase* uncertainty  $3 \cdot 10^{-5}$  is low enough to make an  $(x, ct)$ - grid (Fig. 6.6a) but a low- $\alpha$  state (Fig. 6.6c) has too few photon counts-per-grid to plot sharply. Photon-number eigenstate  $|N\rangle$  in Fig. 6.6d is a total wash even for high- $N$  since  $\Delta N = 0$  implies maximal phase uncertainty ( $\Delta\Phi = \infty \gg 2\pi$ ).

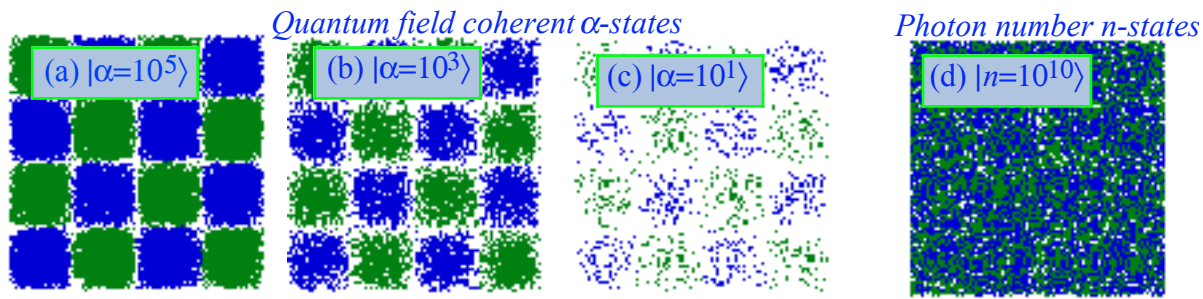


Fig. 6.6 Simulated spacetime photon counts for coherent (a-c) and photon-number states (d).

### Deeper symmetry aspects of pair creation

Discussion of relativity and quantum theory of wave amplitude requires further details. This includes Dirac's extraordinary theory that 2-CW light of certain frequencies in a vacuum may create "real" matter that does not vanish when the light is turned off. For example, we know that two  $0.51\text{MeV}$   $\gamma$ -ray photons of frequency  $\omega_e = m_e c^2 / \hbar$  may create an electron and positron "hole" that form positronium  $e + \bar{e}$  pairs. Also,  $0.94\text{GeV}$   $\gamma$ -rays with  $\omega_p = m_p c^2 / \hbar$  may create proton-anti-proton  $p + \bar{p}$  pairs, and so on.

Dirac creation processes raise questions, "What "cavity" traps  $0.51\text{MeV}$   $\gamma$ -pairs into stable  $e + \bar{e}$  pairs?" The discussion so far has only begun to define 2-CW symmetry properties by phase rates in per-spacetime  $(K, \Omega)$ -quantum variables. Conservation (5.2) of these kinetic  $(K, \Omega)$ -values implies that  $e + \bar{e}$  or  $p + \bar{p}$  pairs have the same  $(K, \Omega)$ -values as the 2-CW light that "creates" them.

However, space-time symmetry arguments by themselves seem unable to derive internal lepton or baryon structure that might show how light becomes "trapped." That question still lies beyond the scope of this discussion, and indeed, still largely beyond what is presently known. In fact, the current standard Weinberg-Salam model of high energy electroweak and strong quantum-chromo-dynamics (QCD) has abandoned the Dirac picture almost entirely. Pauli's apparent dislike for Dirac may have had an effect.

In its place there has arisen a large and controversial area known as super-symmetric-string-theory or "superstrings" that has generated over 10,000 publications in about 40 years and promised a "theory of everything" that would include quantum gravity. However, this flurry of mathematical activity has not yet yielded new experimental or physical insight nor has it provided a better way to study or teach existing areas of classical mechanics, relativity or quantum theory.

Two books give well written history of super-strings and related philosophy. One is by Lee Smolin and the other by Peter Woik. They show the presence at the highest academic levels of a rather pernicious group-think or make-believe that seems to have long given up the logical ideals of William of Occam.

L. Smolin, *Trouble in Physics: The rise of string theory and the fall of a science*, Houghton-Mifflin (New York 2006)  
 P. Woik, *Not even GNORW: The Failure of String Theory...*, Persius Basic Books (New York 2006).

## Chapter 7. Compton Effects and Optical Transitions

In Ch. 4-5 we found that space-time symmetry of a particle of mass  $M$  is like that of a 2-CW optical cavity wave of frequency  $\omega = Mc^2/\hbar$ . Here we relate 2-CW( $k, \omega$ ) “baseball diamond” Doppler shifts from Ch. 2-3 to light-matter collisions and scattering by molecules, atoms or nuclei. Doppler shifts are related to recoil shifts in 1-photon emission, 1-photon absorption, and 2-photon Compton scattering.

### 1-photon kinematics for emission and absorption of light

Photo-emission and photo-absorption allow you to see. In order to read this page, dye molecules in your eye absorb light emitted by atoms in a computer screen or lamp or other source such as the sun if you’re using daylight or moonlight. Without these processes we would all be blind.

There are several ways to describe and diagram emission and absorption by quantum levels. The first are Grotian level diagrams shown in Fig. 7.1a for a “quantum jump” between a molecular, atomic, or nuclear energy level- $E_m$  and a lower level- $E_\ell$ . Each “jump” involves light at *transition frequency*  $\omega_{m\ell}$  that is the *beat frequency*  $\Delta\omega_{m\ell} = \omega_m - \omega_\ell$  between Planck frequency  $\omega_m$  of level  $E_m$  and  $\omega_\ell$  of level  $E_\ell$ .

$$E_m = \hbar\omega_m \quad (7.1a) \qquad E_\ell = \hbar\omega_\ell \quad (7.1b)$$

Planck relation (4.5a) applies. We can only see beats or *relative differences*  $\Delta\omega_{m\ell}$  as noted *vis-à-vis* (4.12).

$$E_{m\ell} = \hbar \Delta\omega_{m\ell} = \hbar(\omega_m - \omega_\ell) = E_m - E_\ell \quad (7.1c)$$

Beat-frequency light is indicated by a wave emerging from a line connecting the energy level  $E_m$  to  $E_\ell$  in Fig. 7.1a. A wavy single arrow going out (or in) indicates output emission (or input absorption).

### The kicker: Recoil shifts

Optical transitions have, quite literally, a “kicker.” Due to Axiom-1 ( $\omega = \pm ck$ ), each 1-CW causing a frequency shift  $\Delta\omega_{m\ell} = \omega_m - \omega_\ell$  must come with a “kick” due to  $k$ -vector shift  $\Delta k_{m\ell} = (\omega_m - \omega_\ell)/c$ . The kick or *recoil* by visible light is usually ignorable since  $1/c$  is so tiny, but it is important for high-resolution spectra and for high-energy light such as  $\gamma$ -rays. Grotian diagrams in Fig. 7.1a tend to obscure or ignore recoil.

Feynman diagrams in Fig. 7.1b show atomic  $\mathbf{K}$ -vectors  $\mathbf{K} = (\omega, ck)$  being kicked into  $\mathbf{K}' = (\omega', ck')$  as atoms emit (or absorb) photons with vector  $\omega_{K'K} = \omega_{K'K}(\pm 1, 1)$ . Baseball geometry in Fig. 7.2a fits vectors  $\omega_{K'K}$  to connect low-level ( $\omega_\ell$ ) and mid-level ( $\omega_m$ ) hyperbolas and conserve total  $\mathbf{K}$ -vector consistent with translation symmetry conservation rules of (5.19). Fig. 7.2b shows head-to-tail vector sum triangles.

$$\mathbf{K}' = \mathbf{K} - \omega_{K'K} \quad [\text{emission}] \qquad \mathbf{K}' = \mathbf{K} + \omega_{K'K} \quad [\text{absorption}]$$

Vector  $\mathbf{M}' = (\omega, ck) = \omega_m(\cosh\rho, \sinh\rho)$  on  $\omega_m$ -hyperbola in Fig. 7.2a has recoil rapidity  $\rho$  and invariant  $\omega_m$  and rest energy  $E_m = \hbar\omega_m = M_m c^2$ . Vector  $\mathbf{L}'$  on lower  $\omega_\ell$ -hyperbola below  $\mathbf{M}'$  has the same  $\rho$  but lower  $E_\ell = \hbar\omega_\ell$ .  $\mathbf{K}$ -vector baseball diagram geometry follows directly from earlier Fig. 2.2 and Fig. 3.3.

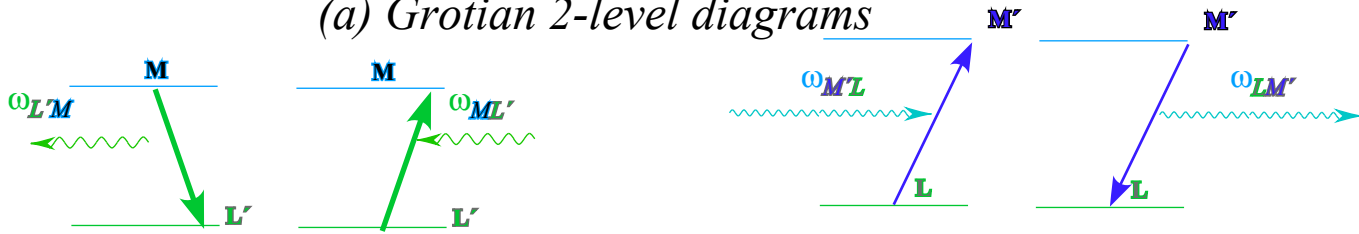
*This is not rocket science! (Or is it?)*

Some quantum texts call photons “light bullets” since they have a “kick.” Doppler redshift relation  $\omega_\ell = e^{-\rho} \omega_m$  (top of Fig. 7.2a) shows atoms are like *light-rockets*. Consider invariant rest-mass ratio  $M_m/M_\ell$ .

$$M_m/M_\ell = \omega_m/\omega_\ell = e^{+\rho} \quad (7.2a) \qquad c \cdot \rho = c \cdot \ln(M_m/M_\ell) \sim u \quad (7.2b)$$

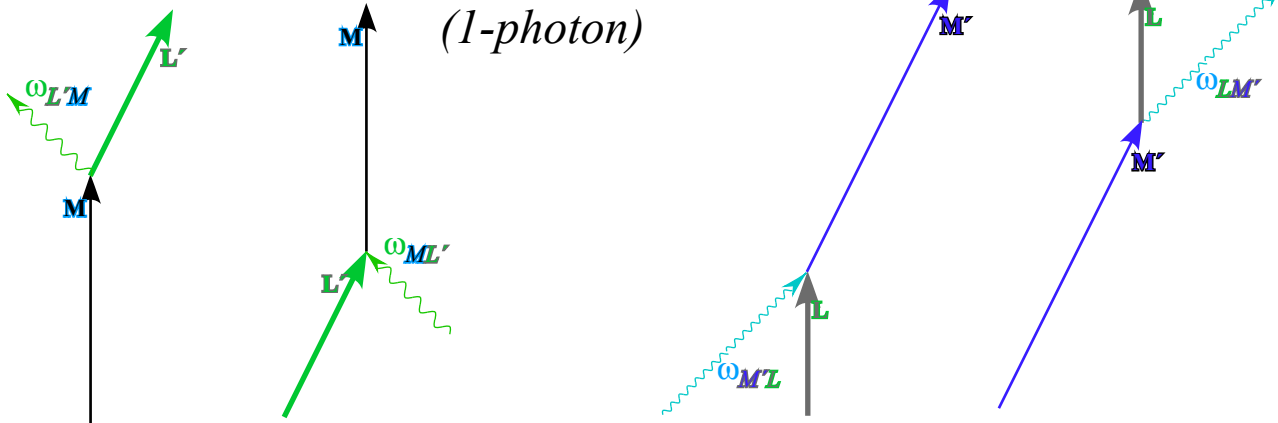
At low recoil ( $\rho \sim u/c \ll 1$ ) this is rocket equation (8.8b Unit 1) if “exhaust velocity” is light-speed  $c$ . By uncertainty relation  $\Delta v \cdot \Delta t \sim 1$  high quality emission (low  $\Delta v$ ) means long time  $\Delta t$  to “exhaust” light.

(a) Grotian 2-level diagrams



(b) Feynman ( $\omega, ck$ ) diagrams

(1-photon)



M-to-L' emission

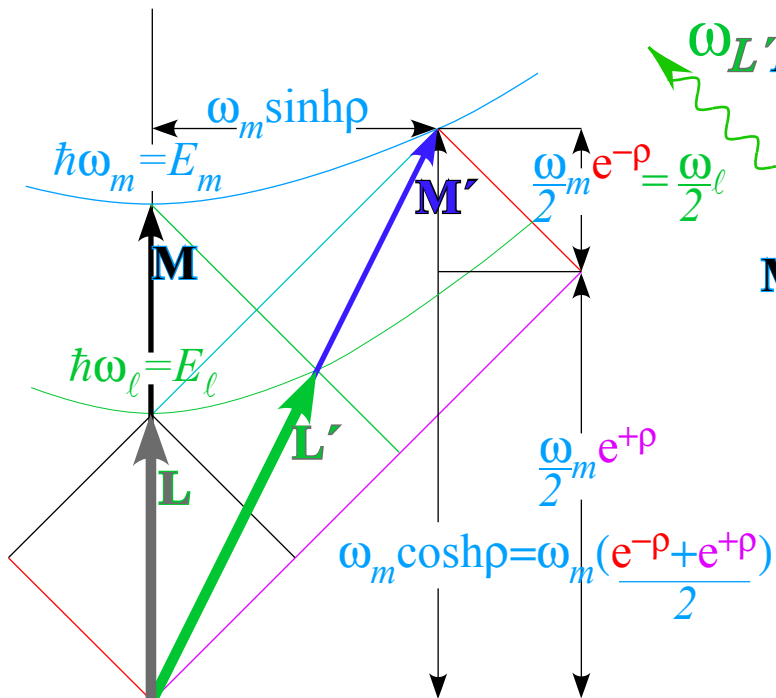
L'-to-M absorption

L-to-M' absorption

M'-to-L emission

Fig. 7.1 Quantum optical transitions represented by (a) Grotian and (b) Feynman diagrams.

(a) 2-Level ( $\omega, ck$ ) "baseball" diamonds



(b) ( $\omega, ck$ ) vector sum (energy-momentum conservation)

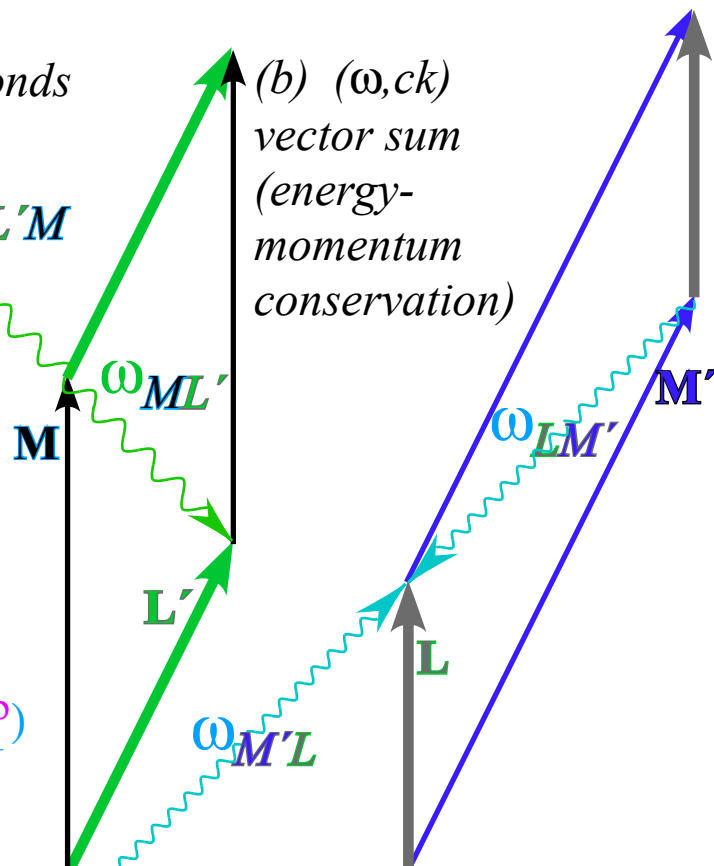


Fig. 7.2 Optical transitions displayed on (a) "Baseball diamond" and (b) Vector conservation sums.

A typical atomic transition (such as we use to read by) has a huge *spectral quality (q) factor*.

$$q = \omega_0 / 2\Gamma = (\text{angular resonant frequency}) / (\text{transition decay rate}) = \omega_0 \cdot \Delta t = \omega_0 / \Delta \nu$$

Atomic *q* factors, discussed after (10.49) in Ch. 10 of Unit 1, range from  $10^6$  to over  $10^8$ . The *q* qualifies a resonance by giving its amplification factor (over DC), its spectral purity, and its lifetime  $\Delta t$  in numbers of atomic beat periods or “heartbeats” it takes to complete a transition with 96% certainty. (Recall:  $e^{-\pi} = 4.321\%$ .)

High quality means a long “burn” to reduce an atomic mass energy from  $E_m = M_m c^2$  to  $E_\ell = M_\ell c^2$ , so maybe a rocket formula  $u \sim c \cdot \ln(M_m / M_\ell)$  makes sense. (Exact formula (7.2a) is  $\rho = \ln(M_m / M_\ell)$ .) Just saying quantum transitions are “jumps” misses a lot of physics. Getting there is (at least) half the fun!

*2-photon processes: Rayleigh-Thompson-Compton scattering*

Atomic 1-photon absorption shown in Fig. 7.1 is like an inelastic (“ka-runch”) SUV-VW collision in Fig. 1.1b or Fig. 2.1 of Unit 1. An atom (SUV) absorbs a photon (VW) to become more massive as it “jumps” from low level  $M_\ell$  to a higher mass  $M_m$ . While we just write off lost energy in SUV-VW crashes, the energy of atom plus light is conserved and time reversible. An SUV-VW cannot “uncrash” but atoms may emit light as well as absorb it. Atomic emission equation (7.2) is analogous to rocket propulsion.

An atomic 2-photon process of *Compton scattering* is sketched in Fig. 7.3a. It is like an *elastic* (“ka-bong”) SUV-VW collision in Fig. 2.2 of Unit 1. Atom- $M_\ell$  (SUV) briefly absorbs the  $\omega_{K'K}$ -photon (VW) but then just as quickly bounces it back as the atom recoils and returns to its initial  $M_\ell$ -level after emitting the photon. Fig. 2.2 of Unit 1 is in Center-of-Momentum COM frame as are the process diagrams in Fig. 7.3 where  $\Delta k$ -component of total- $\Delta \mathbf{K}$  is zero. So, non-resonant Compton processes are a quick 1-2-punch.

*Car 54 where are you?*

An atomic *2-photon absorption* process sketched in Fig. 7.3a is somewhat analogous to a 3-car pile-up. (See car crash in Fig. 8.5 of Unit 1.) However, wave time-energy uncertainty fuzzes auto-analogies. Pure  $(\omega, ck)$ -per-space-time pictures imply delocalization in classical space-time. CW  $(\omega, ck)$  represented in Fig. 7.1 thru Fig. 7.4 make CW space-time grids everywhere and forever. Nevertheless, scaled CW  $(\omega, ck)$  vectors overlap PW  $(x, ct)$ -paths as shown in Fig. 1.5 or Fig. 1.6 of Unit 1. Then Feynman  $(\omega, ck)$ -diagrams mimic  $(x, ct)$ -diagrams and  $\mathbf{K}$ -arrows can represent PW  $(x, ct)$ -collision paths resembling car crashes.

However, with low- $\Delta t$  PW paths comes fuzzy  $\mathbf{K}$ -conservation. Time interval  $\Delta t$  and space  $\Delta x$  is large for initial and final vectors in Fig. 7.3a but not so for mid lines  $\mathbf{M}$  or  $\mathbf{K}$ . Thus intermediate  $(\omega, ck)$  values must be fuzzy and include combinations of non-resonant values known as *virtual state sums*.

*Suspended 2-photon diamonds*

Photon lines in Fig. 7.3a arise from diamonds in Fig. 7.4 that resemble a  $\pm 45^\circ$  baseball diamond used in Fig. 2.1 to develop relativity. However, the general diamond example in Fig. 7.4b differs in that 1<sup>st</sup> and 3<sup>rd</sup> bases are not on the light-cone baselines but suspended by vectors  $\mathbf{L}$  and  $\mathbf{L}'$  like chopsticks pinch a piece of tofu. A new home plate lies at  $\mathbf{K}(\omega_k)$  above origin and 2<sup>nd</sup> base is at  $\mathbf{M}(\omega_m)$  above that. Pitcher’s-mound lies at  $\mathbf{L}(\omega_\ell)$  just below diamond center (as it does in regulation baseball). Half-sum-and-difference of *invariant*  $[\omega_k, \omega_\ell, \omega_m]$  define a diamond with “rocket ratios”  $\omega_m / \omega_\ell = \omega_\ell / \omega_k = e^\rho$  and geo-mean  $\omega_\ell = \sqrt{(\omega_m \cdot \omega_k)}$ .

$$\text{Diamond center: } \frac{1}{2} (\omega_m + \omega_k) = \omega_\ell \cosh \rho \quad (7.3a)$$

$$\text{Diamond radius: } \frac{1}{2} (\omega_m - \omega_k) = \omega_\ell \sinh \rho \quad (7.3b)$$

One exponential  $e^\rho$  ratio defines a whole geometric series of hyperbola levels with equal recoil rapidity  $\rho$ .

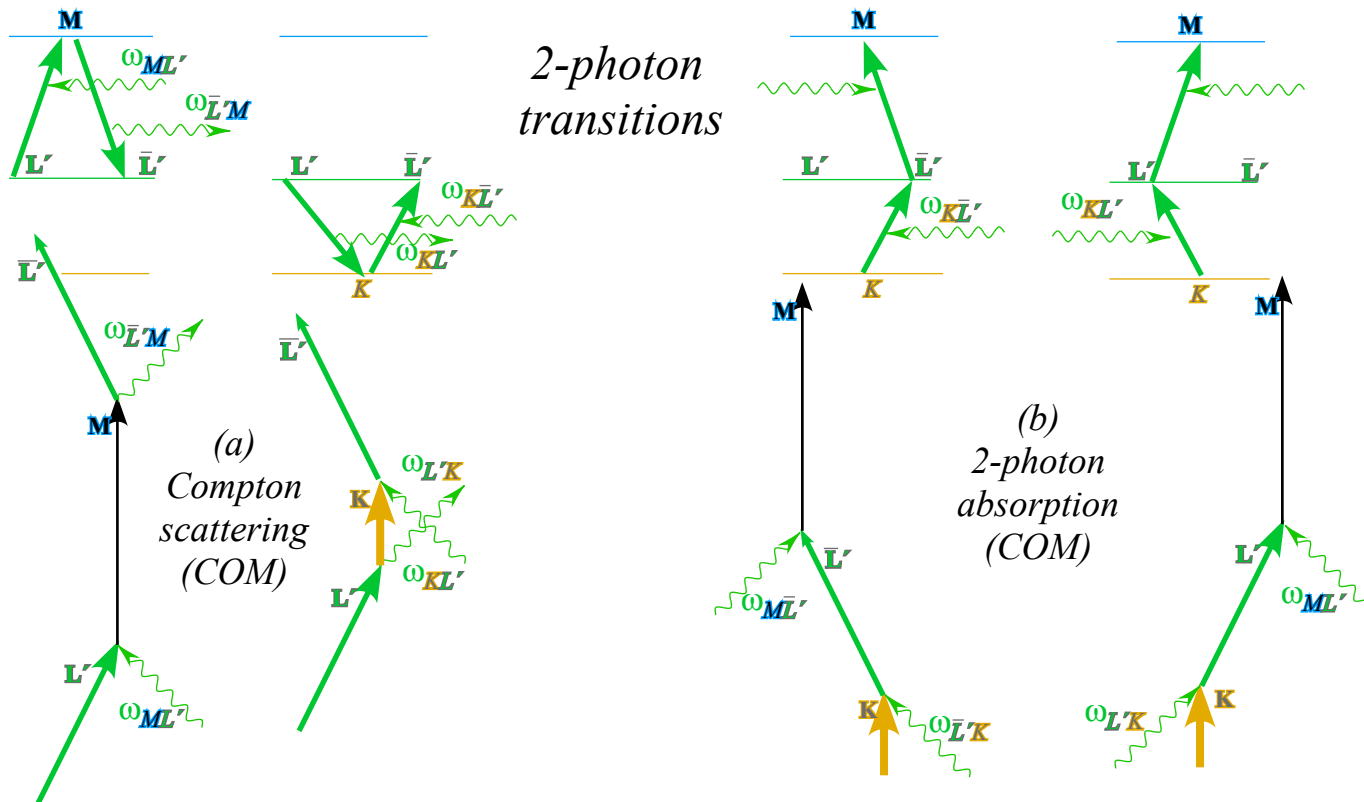
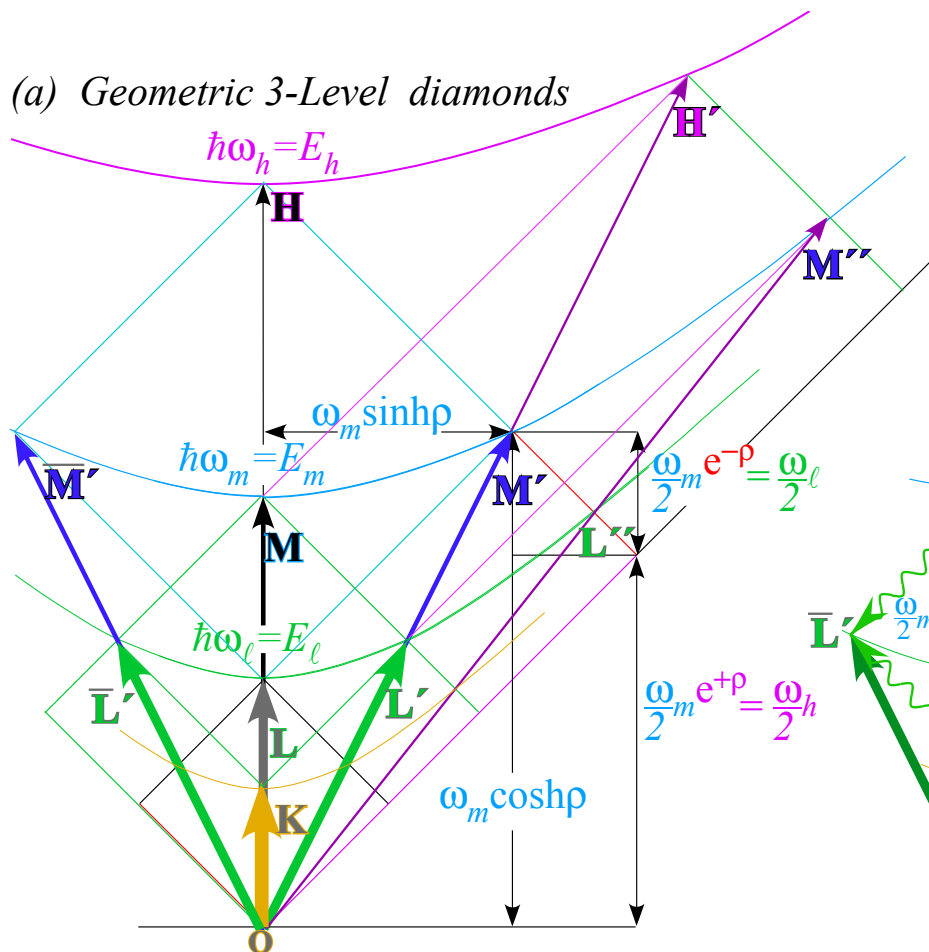


Fig. 7.3 Level and Feynman diagrams of 2-photon processes: (a) COM Compton, (b) COM absorption.

(a) Geometric 3-Level diamonds



(b)  $[\omega_k, \omega_l, \omega_m]$  photon diamond

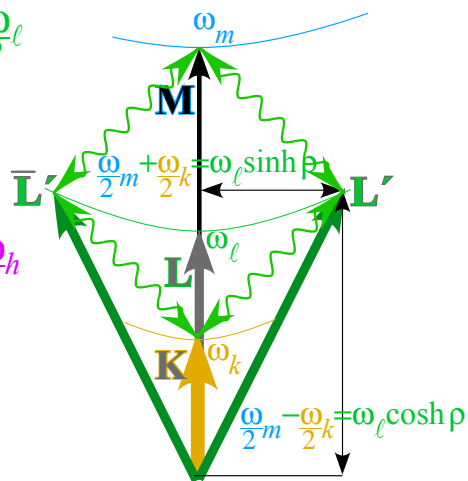


Fig. 7.4 3-level diamond connection map in  $(\omega, ck)$  per-spacetime. (b) COM example of “kite.”

We now look at recoil effects in frames other than COM. We imagine we can “cut-and-paste” or create-and-destroy photon frequencies in the 2-CW cavity baseball diamond model of mass kinetics.

*Feynman’s Father’s query*

Right after Richard Feynman graduated from MIT his father asked a question, “Where is a photon before an atom emits it?” The question caught the new graduate off guard and it appeared that maybe a pricey MIT education was not worth all the money that his father had paid.<sup>xx</sup> Let us give a quantitative answer for Feynman’s father’s query using 2-CW optical analog for an atom that emits some of its “inner light” following its baseball-diamond geometry in Fig. 7.2.

To apply baseball diamonds of Fig. 7.2 to an atom, we say it has the *symmetry* of 2-CW cavity state represented by 2<sup>nd</sup> base  $\mathbf{K}_2$  in the lower half Fig. 7.5a. A 1<sup>st</sup> base  $\mathbf{K}_1=(\omega, \omega)$  and 3<sup>rd</sup> base  $\mathbf{K}_3=(-\omega, \omega)$  sum to an atom’s 2<sup>nd</sup> base  $\mathbf{K}_2=(0, 2\omega)$  on a hyperbola of mass  $M_Q$  at Q.

$$M_Q = 2\hbar\omega / c^2$$

The pitcher’s mound P represents a 1-photon momentum-energy expectation value  $E_P$  at  $\mathbf{K}_p = (1/2)\mathbf{K}_2$

$$E_p = \hbar\omega / c^2$$

Point Q in Fig. 7.5a represents a 2-photon state of energy  $M_Q=2E_P$ .

In Fig. 7.5a an emitted photon  $\omega_{Qp'}$  is imagined being “cut” from 3<sup>rd</sup> base so  $\omega_3 = \omega$  shrinks by what we will call<sup>xxi</sup> a *father-Feynman factor ff* as 3<sup>rd</sup> base alone loses the outgoing  $\omega_{Qp'}$  photon energy.

$$\omega'_3 = ff\omega = \omega_3 - \omega_{Qp'} \quad (ff=1/4 \text{ in Fig. 7.5a.})$$

If 1<sup>st</sup> base stays at its old value ( $\omega'_1 = \omega = \omega_1$ ) the 2<sup>nd</sup> base moves from Q on its initial  $2\omega$ -hyperbola to P' on its final  $2\omega'$ -hyperbola. Its new proper frequency  $\omega'$  is a geometric mean of 3<sup>rd</sup> and 1<sup>st</sup> as in Fig. 3.3.

$$2\omega' = 2\sqrt{\omega'_3\omega'_1} = 2\sqrt{ff}\omega \tag{7.4a}$$

$$\omega'_3 = f\omega' = ff\omega \tag{7.4b}$$

$$\omega'_1 = f^{-1}\omega' = f^{-1}f\omega = \omega_1 \tag{7.4c}$$

The new 3<sup>rd</sup> base is a *Feynman<sup>xxii</sup>redshift f*  $\equiv \sqrt{ff}$  of the new mean  $\omega'$  and a *father-Feynman shift ff* of the old bases values  $\omega_3 = \omega = \omega'_1 = \omega_1$ . They are each an inverse-shift  $f^{-1}$  of the new mean  $\omega'$ . The *ff*-shift is a product of two *f*-shifts  $ff=f^2$ . This tricky notation is due to the Doppler derived group multiplication rule (3.5c) for an  $f = b_{3'2'}$  and an equal  $f = b_{2'1'}$  to give composite  $ff = b_{3'1'} = b_{3'2'}b_{2'1'} = f^2$ .

In Fig. 7.5a old 1<sup>st</sup> base and new 3<sup>rd</sup> base span a diamond of rapidity  $\rho$  like Fig. 3.3b where  $e^{-\rho} = \frac{1}{2}$ . That redshift  $\omega' / \omega = f = \frac{1}{2}$  in Fig. 7.5a-c is another example of “rocket” mass ratio introduced in (7.2).

$$e^{-\rho} = f \equiv \sqrt{ff} = \omega' / \omega = M_P / M_Q \tag{7.5}$$

**Photo-absorption and Compton effects**

The factor  $ff = \frac{1}{4}$ , chosen in Fig. 7.5a, cuts a fraction  $1 - ff = \frac{3}{4}$  off the 3<sup>rd</sup> base photon  $\omega_3 = \omega$  to emit  $\omega_{Qp'} = \frac{3}{4}\omega$  and reduces mass  $M_2$  by factor  $f = \sqrt{ff} = \frac{1}{2}$  to  $M_1$ . Doppler factor  $f^{-1}=2=e^\rho$  gives an atomic recoil boost of  $u = \frac{3}{5}c$ . (Recall Fig. 2.2 where  $b=2$  gives frame velocity  $u = \frac{3}{5}c$ .) Mass  $M_1$  gets that boost by absorbing  $\omega_{PQ'} = \frac{3}{2}\omega$  to jump from P up to Q' in Fig. 7.5b. Inverse  $\omega_{Qp'}$  cut falls from Q to P' in Fig. 7.5a. Paste  $\omega_{PQ'} = \frac{3}{2}\omega$  onto 1<sup>st</sup> baseline in Fig. 7.5b ups  $M_1$  to  $M_2$  on  $\omega'$ -axis P'Q' in Fig. 7.5c.

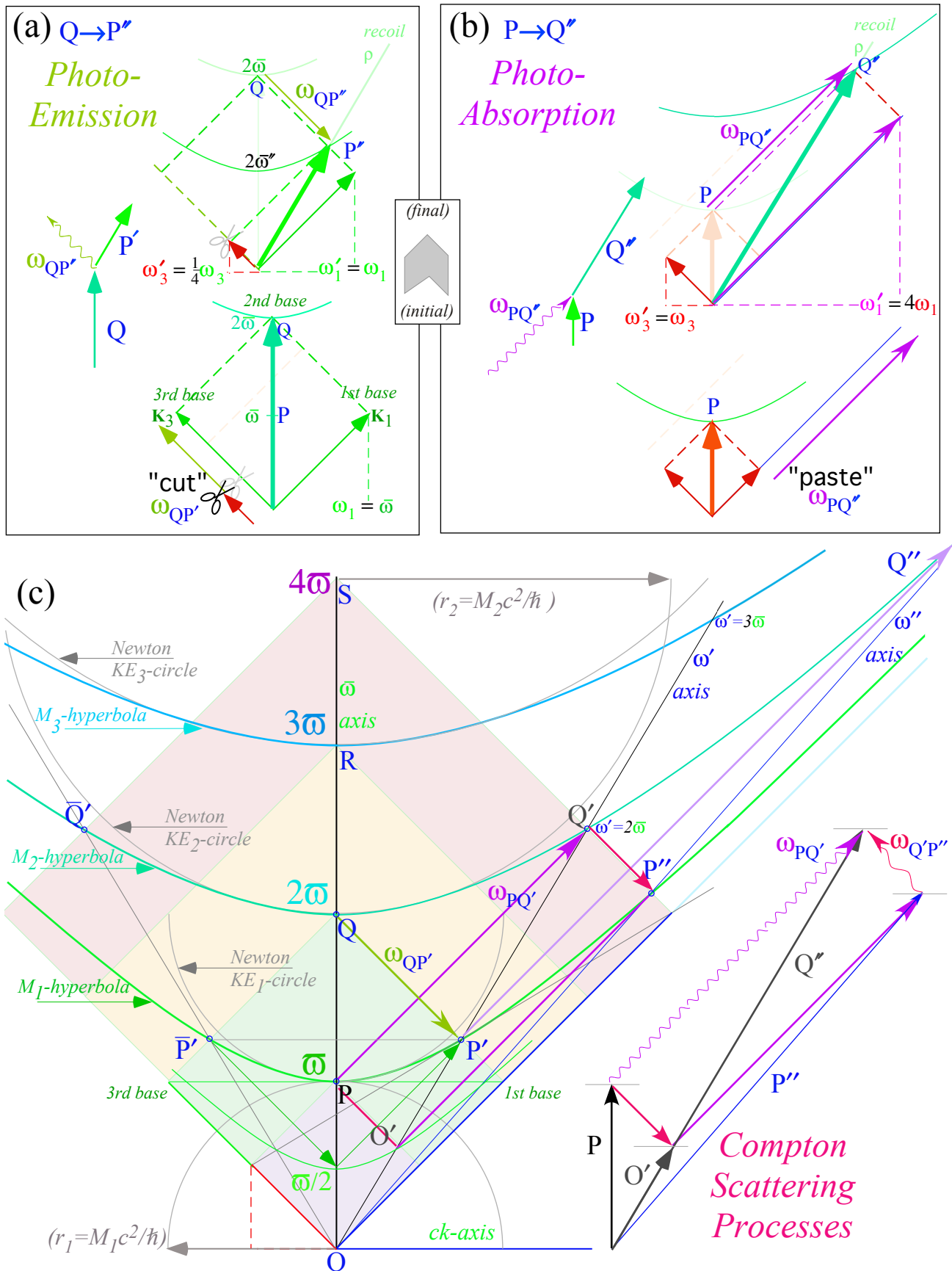


Fig. 7.5 Optical cavity model of (a) Emission, (b) Absorption, and (c) Compton scattering

Final  $\omega'$ -frame shift is  $b=e^\rho = 2$  of rapidity  $\rho = \ln 2$  for either process. Emission  $\omega_{Q'P''}$  is the final “cut” in a Compton “paste-and-cut”  $P \rightarrow Q' \rightarrow P''$  process with the Feynman diagram in Fig. 7.6c. Its segments form an  $OP'Q''O$  “kite” in Fig. 7.5c that is bent from a symmetric kite  $O\bar{P}'QP'O$  by the boost  $\rho = \ln 2$  of the main kite  $OQ$ -axis relative to either of its wings  $O\bar{P}'$  or  $OP'$ . Each kite is a suspended baseball diamond like Fig. 7.4b or a boosted  $\rho$ -warped version of one.

Both “paste-and-cut” ( $P \rightarrow Q' \rightarrow P''$ ) and reverse “cut-and-paste” ( $P \rightarrow O' \rightarrow P''$ ) processes in Fig. 7.6 entail total recoil boost  $2\rho = \ln 2^2$  from the lab  $\omega$  axis to an  $\omega''$  axis of the Compton scattered atom in Fig. 7.5c. The latter first “cuts” down to point  $O'$  on a  $\frac{\omega}{2}$ -hyperbola by emitting photon  $\omega_{PO'} = \frac{3}{8}\omega$  before absorbing the  $\omega_{O'P''} = \frac{3}{2}\omega = \omega_{PQ'}$  photon that comes first in the former sequence.

An inverse Compton process ( $Q \rightarrow P' \rightarrow Q''$ ) emits photon  $\omega_{QP'} = \frac{3}{4}\omega$  (as in Fig. 7.5a) then absorbs photon  $\omega_{P'Q''} = 3\omega$  that moves it from rapidity  $\rho$  on hyperbola  $\omega$  to rapidity  $2\rho$  on hyperbola  $2\omega$  at point  $Q''$  (upper right of Fig. 7.5c). Here a fixed mass  $M_2 = 2\hbar\omega$  emits  $\frac{3}{4}\omega$  to gain speed ( $\frac{u}{c} = \frac{3}{5}$ ) by reducing its mass to  $M_1 = \hbar\omega$  then recovers mass by absorbing  $3\omega$  to end up at an even faster speed ( $\frac{u}{c} = \frac{15}{17}$ ).

Photon  $\mathbf{K}$ -vectors for any Compton process between  $2:1$ -rest mass hyperbolas make a  $\rho$ -warped baseball diamond with  $\rho = \ln 2$  according to (7.5) as shown in Fig. 7.5c and Fig. 7.6a. Like a  $2:1$ -Doppler diamond in Fig. 3.3b, it has an aspect ratio that is twice its blue-shift  $b=e^\rho = 2$ , that is  $2e^\rho = 4$ .

A  $2:1$ -rest mass drop shows geometry more clearly than a realistic ratio  $10^{10}:10^{10}-1$  for an atomic transition that is about  $10^{-10}$  of rest mass. Atomic rest-energy level ratios  $E_m : E_h$  are close to unity and fortunately so for our health! Harmonic levels with integral  $m:h$  ratios used in Fig. 7.5 apply to optical-cavity models but  $m$  and  $h$  are small integers only for special spectra like Rydberg or rotor transitions.

### Compton-Doppler staircase

In going from higher hyperbola  $h\omega$  to middle  $m\omega$  the lab recoil shift is  $f_{hm} = e^{-\rho_{hm}} = \frac{m}{h}$  by (7.5), and its emitted frequency  $\omega_{hm}$  is the altitude of a kite triangle, like  $\bar{P}'QP'$  in Fig. 7.5c, given as follows.

$$\omega_{hm} = (1 - f_{hm}^2) \frac{h\omega}{2} = \frac{h^2 - m^2}{2h} \omega = m\omega \sinh \rho_{hm} \quad (7.6)$$

The example in Fig. 7.5a has  $\omega_{QP'} = \frac{3}{4}\omega = \omega_{2,1}$ . Doppler shifts of  $\omega_{2,1}$  by  $f_{2,1} = \frac{1}{2}$  form a geometric series  $(\dots, \frac{3}{32}, \frac{3}{16}, \frac{3}{8}, \frac{3}{4}, \frac{3}{2}, 3, 6, 12, \dots)\omega$  of steps on a Compton staircase  $PQ'P''Q'' \dots$  between  $(2:1)$ -levels  $2\omega$  and  $1\omega$  in Fig. 7.5c. For any rational level ratio  $e^{\rho_{hm}} = \frac{h}{m}$ , each dilation factor  $\gamma_{hm}$ , recoil  $\beta_{hm}$ , or ratio  $\omega_{hm} / \omega$  is a rational ratio, too, and the Pythagorean sum  $1 = \gamma_{hm}^{-2} + \beta_{hm}^2$  belongs to a rational triangle, e.g.,  $1 = \frac{3^2}{5^2} + \frac{4^2}{5^2}$ .

$$\beta_{hm} = \frac{u_{hm}}{c} = \tanh \rho_{hm} = \frac{h^2 - m^2}{h^2 + m^2} \quad (7.7a)$$

$$\gamma_{hm} = \cosh \rho_{hm} = \frac{h^2 + m^2}{2mh} \quad (7.7b) \qquad \sinh \rho_{hm} = \frac{h^2 - m^2}{2mh} \quad (7.7c)$$

Recoil trims emitted  $\omega_{hm}$  below  $\Delta = |h-m|\omega$  by a factor  $(h+m)/2h$  while absorption  $\omega_{mh}$  costs more than  $\Delta$  by a factor  $(h+m)/2m$ . Newtonian recoil  $KE_h \equiv M_h u^2 / 2$  is a circle of radius  $M_h c^2$  in Fig. 7.5, so even low- $u$  recoil costs a little. Photons, like money-changing tourists, get nicked coming and going.

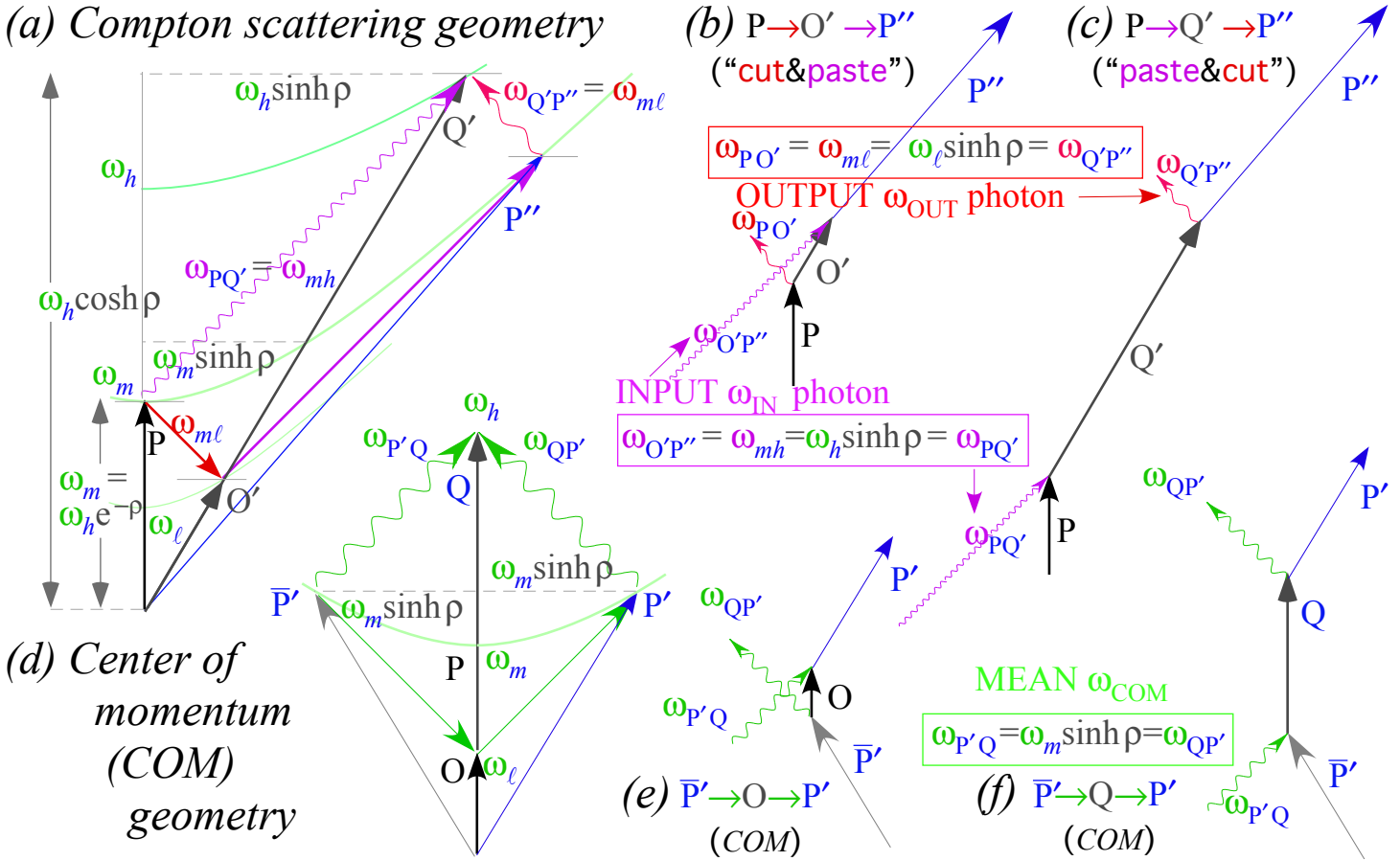


Fig. 7.6 Compton scattering. (a) Vector sums on mass hyperbolas of low  $\omega_\ell$ , medium  $\omega_m$ , and high  $\omega_h$ . (b-c) Feynman graphs. (d) Center of Momentum (COM) vector sums. (e-f) COM Feynman graphs.

An absorption ( $m < h$ ) frequency  $\omega_{mh} = \omega^{IN}$  is greater than emission  $\omega_{hm}$  by a factor  $f_{mh} = \frac{h}{m}$ . A Compton  $\omega^{OUT}$  due to  $\omega^{IN}$  is less than  $\omega_{hm}$  by the inverse factor  $f_{mh}^{-1} = f_{hm} = \frac{m}{h}$ . Hence a Compton output  $\omega^{OUT}$  is less than its input  $\omega^{IN}$  by the Doppler ratio-square  $ff = f_{hm}^2 = (\frac{m}{h})^2$  as shown before.

$$\omega^{IN} = \omega_{mh} = \frac{h}{m} \omega_{hm}, \quad \omega^{OUT} = \frac{m}{h} \omega_{hm} = (\frac{m}{h})^2 \omega^{IN} \quad (7.8)$$

Compton processes in Fig. 7.6 start on middle  $\omega_m = m\bar{\omega}$  hyperbola to do a 2-photon bounce off a lower  $\omega_\ell = \ell\bar{\omega}$  or a higher  $\omega_h = h\bar{\omega}$  hyperbola. An intermediate “bouncer” is said to be a *virtual* level if its  $\omega_\ell$  or  $\omega_h$  values are integration variables being summed. A process ( $m \rightarrow h \rightarrow m$ ) or ( $m \rightarrow \ell \rightarrow m$ ) is said to be a *resonant* Compton process if an  $h$ -state or  $\ell$ -state exists. Whether numbers  $m$ ,  $h$ , and  $\ell$  are integers in a cavity model or real values for an atomic model, the results (7.6), (7.7), and (7.8) apply in any case.

### Compton wavelength sum rule

Inverse frequencies  $\omega^{-1} = (kc)^{-1} = \lambda(2\pi c)^{-1} \equiv \tilde{\lambda} / c$  give the famous Compton wavelength sum rule.

$$(\omega^{OUT})^{-1} = (\omega^{IN})^{-1} + 2(m\bar{\omega})^{-1}, \text{ or: } \tilde{\lambda}^{OUT} = \tilde{\lambda}^{IN} + 2\tilde{\lambda}_c \text{ where: } \tilde{\lambda}_c = \frac{\hbar c}{m\bar{\omega}} = \frac{\hbar}{M_m c}. \quad (7.9)$$

Compton radius  $\tilde{\lambda}_c \equiv \lambda_c / 2\pi$  is a minimum cavity radius with a frequency equal to the “zwitterbevegung” of mass  $M_m$ . As input  $\tilde{\lambda}^{IN}$  reflects from an  $M_m$ -cavity it picks up diameter  $2\tilde{\lambda}_c$  to become  $\tilde{\lambda}^{OUT}$ . Size  $\tilde{\lambda}^{OUT}$  depends on mass  $M_m$  of level- $m$ , *not* on  $M_h$  or  $M_\ell$  of higher level- $h$  or lower level- $\ell$  that bounces level- $m$ .

Compton radius  $\lambda_c = \hbar/Mc$  is a curious inverse measure of mass size. Larger mass  $M$  has a *smaller*  $\lambda_c$  size that recoils less and reflects photons more elastically. Elastic mirror reflection is what we expect in classical wave optics where light is assumed to be as “light” as anything can be.

*Geometric transition series*

A geometric  $\omega f^p$  -series  $\omega(\dots f^{-2}, f^{-1}, 1, f^1, f^2 \dots)$  of *levels* also has a geometric series  $f^p |f^2 - 1|_{\frac{\omega}{2}}$  of *transitions*. This gives Compton “nets” such as the ( $f = 2$ )-net in Fig. 7.7a or a finer ( $f = \sqrt{2}$ )-net in Fig. 7.7b. Finer fractions ( $f \rightarrow 1$ ) give smaller jumps and acceleration that is more continuous and constant.

An acceleration of space-time frames by geometric or exponential frequency chirping is described in Chapter 8. Space-time grid in Fig. 8.2 has a geometric spacing like the Compton nets in Fig. 7.7 but with a (P,G)  $\rightleftharpoons$  (P,G) axis switch and is an optical version of Einstein’s famous thought experiment.

*Optical PW bounce and accordian-like CW shifts*

If the  $\omega$  vs  $ck$  net plots in Fig. 7.7 were instead space-time  $ct$  vs  $x$  plots one could imagine each vertically sloping line is a path of an object moving at constant rapidity  $\rho$  away from the stationary ( $\rho=0$ ) time  $ct$ -axis of the lab frame. Each hyperbola in Fig. 7.7a crosses a path at proper times  $\tau = \dots \tau, 2\tau, 4\tau, \dots$  that are local times on each object’s  $ct'$ -axis given  $e^\rho = f = 2$ . For general  $f = e^\rho$ , the times are  $\tau = \dots \tau, f\tau, f^2\tau, f^3\tau, \dots$

Imagine each  $\pm 45^\circ$  photon line is part of a PW light path reflecting back and forth between the lab  $ct$ -axis and the object  $ct'$ -axis. Let the lab and moving frame have reflecting mirrors to receive light of a certain frequency (for CW) or a band of frequencies (for PW) and reflect it back and forth between them.

If mirror-1 sends out wavelength  $\lambda_0$ , mirror-2 sees it as a Doppler red-shifted wavelength  $\lambda_1 = \lambda_0 e^\rho$  that it promptly returns to mirror-1 who sees another red-shift factor  $e^\rho$  tacked on to give  $\lambda_2 = \lambda_1 e^\rho = \lambda_0 e^{2\rho}$ . Locally observed reflection times  $\tau_k$  and reflected wavelengths  $\lambda_k$  both form geometric series  $\dots 1, f, f^2, f^3, \dots$

$$\tau_k = (\dots \tau, \tau_1, \tau_2, \tau_3, \dots) = (\dots \tau, f\tau, f^2\tau, f^3\tau, \dots) = \tau(\dots 1, f, f^2, f^3, \dots) \tag{7.10a}$$

$$\lambda_k = (\dots \lambda, \lambda_1, \lambda_2, \lambda_3, \dots) = (\dots \lambda, f\lambda, f^2\lambda, f^3\lambda, \dots) = \lambda(\dots 1, f, f^2, f^3, \dots) \tag{7.10b}$$

Resulting space-time zigzag paths in Fig. 7.8a have even “zig” reflections ( $k = \dots 0, 2, 4, \dots$ ) off the stationary lab mirror-1 and odd “zag” reflections ( $k = \dots 1, 3, 5, \dots$ ) off mirror-2. Fig. 7.8b has added counter-propagating odd-time “zag” and even-time “zig” reflections to frame rectangular diamond- $k$  whose 1<sup>st</sup> and 3<sup>rd</sup> bases lie at time  $\tau_k$  for lab mirror-1 and mirror-2. Its 2<sup>nd</sup> and home base lie on a line of rapidity half that of mirror-2 with red-shift  $e^{\rho/2} = \sqrt{f} = 2^{1/2}$  in Fig. 7.8b. Diamond- $k$  2<sup>nd</sup>-base is home base for diamond- $(k+1)$ .

The space-time analog of “rocket” relations (7.2) is  $\tau_{k+1}/\tau_k = e^{+\rho} = \tau_k/\tau_{k-1}$ . Reflection path-nets also have half-sum-and-difference relations analogous to (7.3) and geometric mean relations  $\tau_k = \sqrt{(\tau_{k+1} \tau_{k-1})}$ . This is used to slice reflection time intervals into units of  $2^{1/2}\tau_0$  or  $2^{1/4}\tau_0$  as is done in Fig. 7.8b, and this gives lines of rapidity  $\rho/4, 2\rho/4, 3\rho/4$ , and  $\rho$ , with red-shifts  $2^{1/4}, 2^{2/4}, 2^{3/4}$ , and 2, respectively.

Ideal light bounces in Fig. 7.8 and mass bounces in Fig. 6.7 of Unit 1 share some key properties. While they change energy without limit, both conserve *action* perfectly. For a light cavity made of mirror-1 and mirror-2, action is an integral number  $n$  of 1/2-waves that is shown for  $n=4$  in Fig. 7.8b where CW nodes move  $\rho/n$  faster than the one behind and  $\rho/n$  slower than one ahead. Adiabatic  $n$  invariance is the rule for quantum wave systems and applies to photon number  $N$ , too. But, rules are made to be broken!

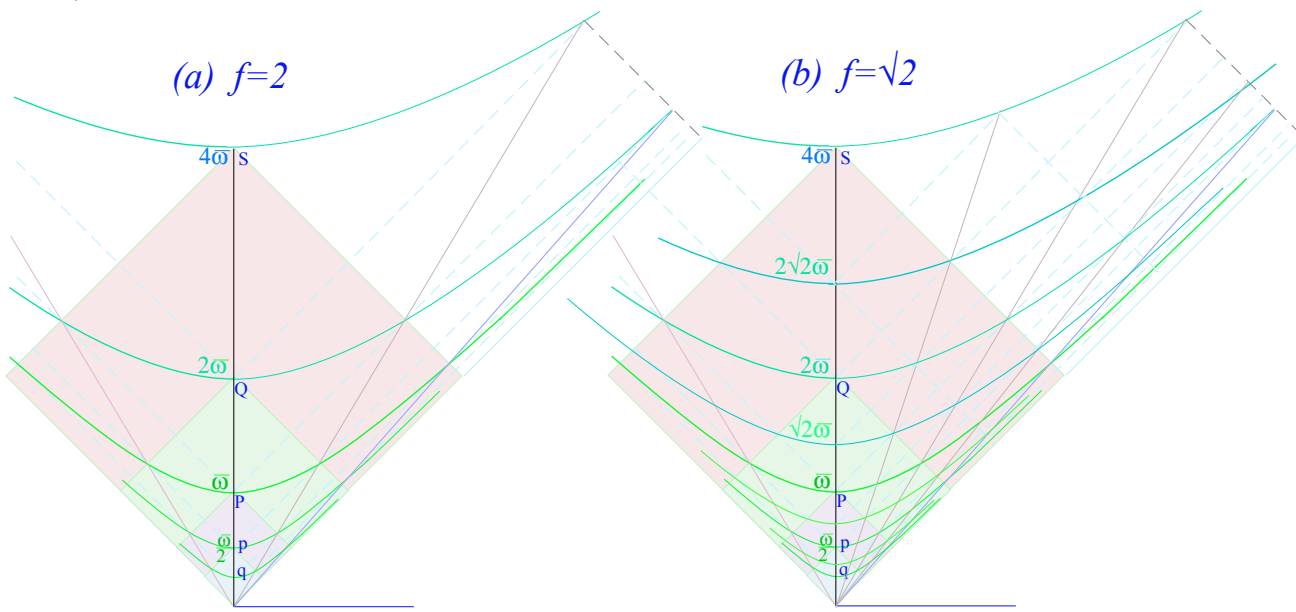


Fig. 7.7 Compton nets are congruent Compton staircases of transitions. (a)  $f=2:1$  (b)  $f=\sqrt{2}:1$

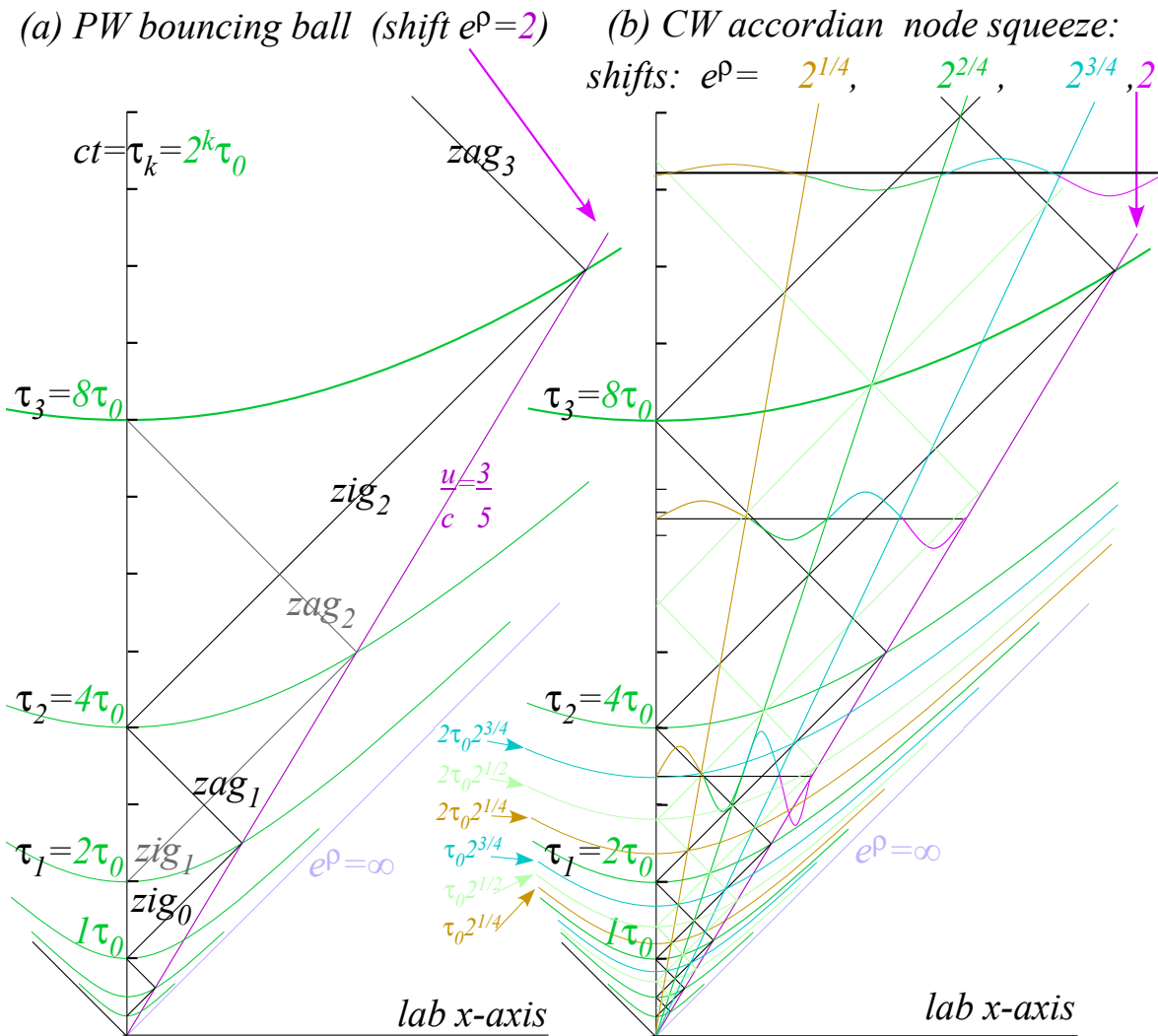


Fig. 7.8 Space-time nets (a) PW zigzag paths bounce. (b) CW nodes squeeze like an accordian.

## Chapter 8. Wave Frame Acceleration

Here we turn the hyperbola geometry of space-time Fig. 7.8 on its side to expose an accelerating wave frame made by CW, PW, or intermediate wave fields. This provides a coherent interference view of the Einstein elevator *gedanken* (thought) experiment. Like many such experiments of imagination, there are quite a few practical details left out. So it may be some time before we can actually *do* them!

### Chirping and Einstein elevators

A spacetime version of Compton nets are curved coordinates for accelerated Einstein elevators and this helps to visualize equivalence principles for general relativity.<sup>xxiii</sup> Plots in Fig. 8.1 and Fig. 8.2 show waves from chirping tunable lasers forming colorful renderings of hyper-net coordinates.

A previous Fig. 2.2c plotted an atom ( $x', ct'$ )-view of it running head-on at rapidity  $\rho$  into a green  $\varpi$ -beam that is blue ( $\varpi e^{+\rho}$ ) shifted while the receding laser appears red ( $\varpi e^{-\rho}$ ) shifted. The laser ( $x, ct$ )-grid then appears as a  $\rho$ -tipped Minkowski grid. If instead the lasers had been tuned to frequencies  $\varpi e^{-\rho}$  and  $\varpi e^{+\rho}$ , respectively, the ( $u=c \tanh \rho$ )-moving atom would see beams of green  $\varpi$ -light waves interfering to make a *square* ( $\rho=0$ ) *Cartesian* ( $x, ct$ )-grid like Fig. 2.1c. (Amplitude would also be tuned along with frequency if we wanted to squelch the wave galloping shown in Fig. 6.2 and Fig. 6.3.)

Varying tuning parameter  $\rho$  of the lasers changes local grid rapidity  $\rho$  at the beams' spacetime intersection as sketched in Fig. 8.1a-b. This produces a curved space-time coordinate system of paths with rapidity changing just so *both* beams end up always the *same* color on any given trajectory.

Each trajectory plotted in Fig. 8.2 has its own constant proper acceleration  $g$  and local color  $\varpi$ . A mass  $M$  following such a  $x(t)$ -path has a  $\mathbf{K}$  that follows its  $M$ -hyperbola in Fig. 7.7. The lasers each send waves that meet at each trajectory point  $x(t)$  and paint a local interference grid of varying rapidity  $\rho$  on a trajectory  $x(t)$  of varying velocity  $u(t)$  given by (6a) and sketched in Fig. 8.1a.

$$u = \frac{dx}{dt} = c \tanh \rho \tag{8.1}$$

Setting  $x'=0$  and  $t'=\tau$  in (2.21) relates proper time interval  $d\tau$  to lab  $dt$ . This gives  $x(t)$  by  $\tau$ -integrals.

$$\frac{dt}{d\tau} = \cosh \rho \tag{8.2a} \qquad \frac{dx}{d\tau} = \frac{dx}{dt} \frac{dt}{d\tau} = c \tanh \rho \cosh \rho = c \sinh \rho \tag{8.2b}$$

$$ct = c \int \cosh \rho \, d\tau \tag{8.2c} \qquad x = c \int \sinh \rho \, d\tau \tag{8.2d}$$

Path  $x(t)$  depends on  $\rho(\tau)$  variation in proper  $\tau$ . Linear rate  $u \sim g\tau$  or  $\rho = g\tau/c$  gives a hyperbolic path in Fig. 8.1b of fixed proper acceleration  $g$  and a family of concentric paths of different  $g$  in Fig. 8.2.

$$ct = c \int \cosh\left(\frac{g\tau}{c}\right) d\tau = \frac{c^2}{g} \sinh\left(\frac{g\tau}{c}\right) \tag{8.3a} \qquad x = c \int \sinh\left(\frac{g\tau}{c}\right) d\tau = \frac{c^2}{g} \cosh\left(\frac{g\tau}{c}\right) \tag{8.3b}$$

Paths closer to the left hand blue-chirping laser have a higher  $g$  than flatter ones nearer the red-chirping right hand source.  $\rho$ -skewed baseball diamonds of PW and CW paths in lower Fig. 8.2 are spaced geometrically along the  $x$ -axis of a spaceship at a moment when its lab-relative rapidity is  $\rho=0.2$ .

(a) *Varying Acceleration by Chirping*

*Only green  $\omega_0$ -light is seen on accelerated path*

(b) *Constant acceleration*

*Only green is seen along  $\omega_0$ -light invariant hyperbola*

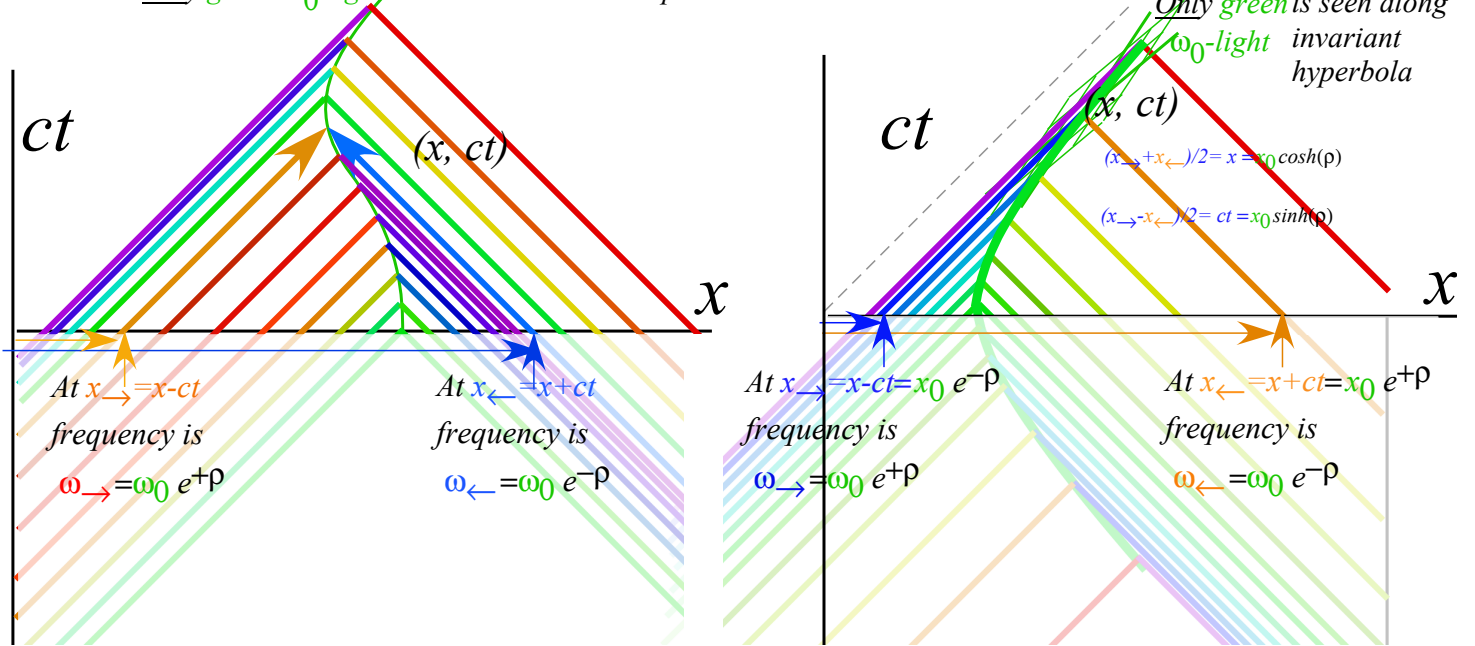


Fig. 8.1 Optical wave frames by red-and-blue-chirped lasers (a)Varying acceleration (b)Constant  $g$ .

Geometric  $e^{\pm\rho}$ -variation (8.3) of wave and coordinate spacing is due to a left-hand laser’s right-moving wave of frequency  $\omega_{\rightarrow} = \omega_0 e^{+\rho}$  on light cone  $x_{\rightarrow} = x - ct = x_0 e^{-\rho}$  and a right-hand laser’s left-moving wave of frequency  $\omega_{\leftarrow} = \omega_0 e^{-\rho}$  on light cone  $x_{\leftarrow} = x + ct = x_0 e^{+\rho}$ . Wave interference does the rest.

Initial ( $\rho=0$ ) position of hyperbola  $\omega_0$  is  $\ell_0 = x_0 = c^2/g_0$ . Each hyperbola has different but fixed location  $\ell$ , color  $\omega$ , and artificial gravity  $g$  that, by (8.3), are proper invariants of each path.

$$x^2 - (ct)^2 = \ell^2, \quad \text{where: } \ell = c^2/g \tag{8.4}$$

Frequency  $\omega$  and acceleration  $g$  vary inversely with the path’s proper location  $\ell$  relative to origin.

$$\omega \ell = \omega c^2/g = \omega_0 c^2/g_0 = \text{const.} \tag{8.5}$$

Rapidity  $\rho = g\tau/c$  in (8.3) has proper time be a product of hyperbolic radius  $\ell$  in (8.4) and “angle”  $\rho$ .

$$c\tau = \rho c^2/g = \ell \rho \tag{8.6}$$

This is analogous to a familiar circular arc length formula  $s = r \phi$ . Both have a singular center.

The less familiar hyperbolic center  $(x, ct) = (0, 0)$  here begins an elementary *event horizon*. The blue-chirp laser would need infinite frequency  $\omega_0 e^{+\rho}$  at origin where  $ct = e^{-\rho}$  goes to zero, so it gives up *before*  $t=0$ . After  $t=0$ , light from the laser to any path  $S$  or  $T$  given by (8.3) never arrives. Fig. 8.2 shows paths of a spaceship  $S$  and a “trailer”  $T$  trailing by invariant length  $\ell_{ST} = \ell(S) - \ell(T)$  on an  $x$ -axis of rapidity  $\rho$  through origin  $(x, ct) = (0, 0)$ .  $S$  and  $T$  always have the *same velocity* (8.1) relative to the lab, maintain proper interval  $\ell_{ST}$ , but trailer  $T$  *feels greater*  $g$ . Lower parts of a rigid rod accelerate more, and this gives the lab-observed Lorentz length-contraction indicated at the top of Fig. 8.2.

In a Newtonian paradigm, asymmetric acceleration seems paradoxical, but if waves make a coordinate frame, asymmetry is a consequence of the DeBroglie relation (4.5b) between  $k$ -vector and momentum. Accelerating frames require shortening wavelength and this crowds waves.

Wave properties also manifest the accelerated frames’ upstairs-downstairs disparity in proper time  $\tau$  (“later” upstairs by (8.6)) and shift in frequency  $\omega$  (lower or “red shifted” upstairs by (8.5)). Along nodal (white)



*Constant velocity gives constant acceleration*

This leads one to ask if chirped light might be used for atomic or molecular acceleration. Logarithmic dependence  $\rho = \ln b$  of rapidity on Doppler  $b$  favors ultra-precise *low* energy acceleration, more appropriate for nanotechnology than high-energy acceleration with its extreme bandwidth.

The flip symmetry between two sides of a light cone suggests optical cavities with a geometric chirp. If you flip the diamond sequence in lower Fig. 8.2 across the light cone to the sides of Fig. 8.2 you get spacetime light paths bouncing between mirrors moving relative to each other as analyzed in Fig. 7.8.

As mirrors close, trapped light blue-chirps exponentially as on the right side in Fig. 8.2. It red-chirps if the two mirrors separate as they do on the left side of Fig. 8.2 and in Fig. 7.8. Together, a desired  $e^{\pm i p}$  spectrum could in principle be made by translating one etalon cavity at constant velocity relative to another stationary cavity that is enclosed by the translating one. In this way, light generated by mirrors of constant *velocity* provides the spectrum needed to make an interference net of constant *acceleration*. Coherent acceleration like Fig. 8.2 (but slower) might be done with precision needed for laser metrology.

*Wave geometry vs. Newton*

Wave geometry ought to make us more skeptical of the coordinate boxes and manifolds that have been our paradigm for centuries. A common image is the Newton-Descartes empty-box at some absolute time existing whether or not it contains any “particles.” We first learn to picture spacetime coordinates as a giant metal frame of clocks like Fig. 9 in Taylor and Wheeler’s<sup>xxiv</sup> relativity text. That figure is more like a parody of common views of spacetime manifolds that remain with us to this day. Such a monstrosity of a framework is decidedly nonexistent and non-operational. Current metrology uses light waves.

A wave frame like Fig. 2.1, Fig. 2.2, or Fig. 8.2 is *physical* metrological coordinate system whose geometry and logic arises from the light that makes it. The things being coordinated (waves) have their own coordinates and dynamics built in. Einstein general theory of relativity trumped Newton’s box by showing how it is affected (curved) by any energy or mass it holds. Quantum theory seems to go a step further by indicating that this box and its contents should be viewed as one and the same thing.

*Pair creation and quantum frames.*

Dirac, before others, realized that per-spacetime has the symmetry of spacetime. Past and future (time-reversal) symmetry demands *negative* frequency as well as positive. In order to visualize Dirac’s pair-creation process we extend the playing field to back-to-back baseball-diamonds with *four* nets of invariant hyperbolas. Examples of pair-creation are sketched in Fig. 8.3 as seen from two different reference frames. Pair creation-destruction is a strange sort of Compton process in which the “photon diamond” of Fig. 7.4 is centered at the light baseline intersection with 2<sup>nd</sup> base at  $+mc^2$  and home base at  $-mc^2$  and 1<sup>st</sup> and 3<sup>rd</sup> bases on  $\pm G$ -hyperbolas.

The Feynman graph of Compton scattering in Fig. 7.6c-d is turned on its side in Fig. 8.3 so it may start and end on different branches of the  $m$ -hyperbola corresponding to mass  $\pm m$ . Two photons, whose energy sum equals the energy gap  $2mc^2$ , appear to bounce off intermediate hyperbolas in Fig. 8.3 that are conjugate hyperbolas defining group wavevectors  $\mathbf{K}_g$  in Fig. 2.1 or 2.2. Such dispersion is said to belong to *instanton* or *tachyon* waves of imaginary frequency  $\pm i\mu$  that entails a huge damping factor  $e^{-mc^2\tau/\hbar}$  that proscribes their direct observation. They are said to be in the virtual or intermediate realm.

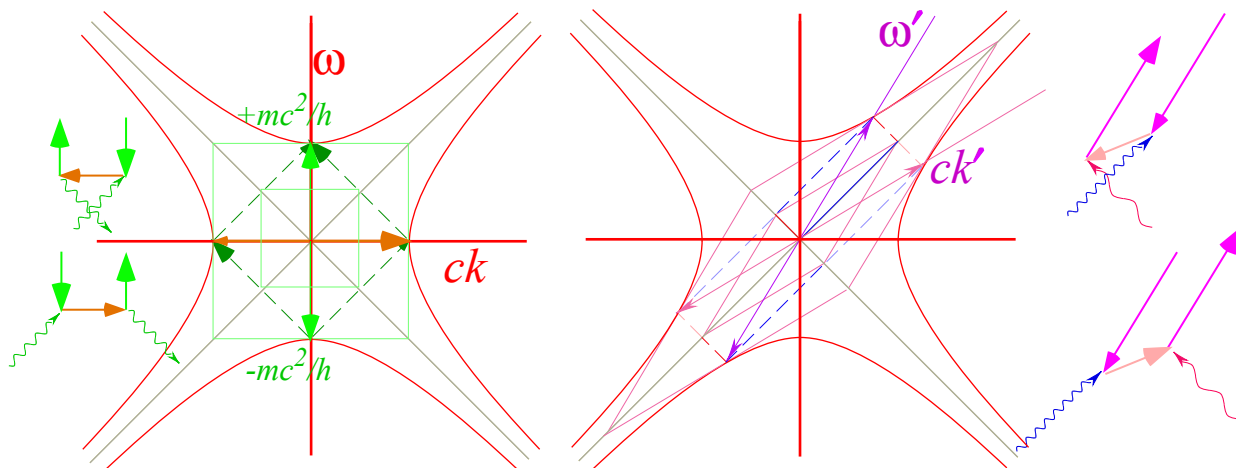


Fig. 8.3 Dirac matter-antimatter dispersion relations and pair-creation-destruction processes.

Dirac's is the first quantum theory to fully incorporate relativity. It introduces dual anti-worlds, in which all three mass definitions (3.6), (3.7), and (3.9) have negative values, but leaves many questions about their physical meaning. Analogies between the  $(2\gamma \rightarrow e + \bar{e})$  process in Fig. 8.3 and exciton formation in the band theory of solids, shed some light on the physics. However, the exciton process is a straight-up 1-photon process whose momentum is tiny compared to the energy jump, and it lacks the world-anti-world symmetry of the Dirac exciton in which both the electron and an anti-electron have the same group velocity but opposite momentum. The Dirac model has duality of reversed energy (frequency), momentum ( $\mathbf{k}$ -vector), space, and time that is quite extraordinary.

A number of implications of Dirac's theory have been mostly ignored. There is an unwillingness to abandon vestigial concepts associated with absolute classical frames, manifolds, or "boxes." However, quantum frames are like all things quantum mechanical and have an intrinsic *relativity* associated with their wavelike interference. Quantum frames, as they are used in molecular and nuclear physics, are known to have internal or body-relative parts in addition to the more commonly known external or laboratory-relative parts. This inside-and-out duality is a deep quantum mechanical result arising first in the theory of quantum rotors by Casimir, but it also underlies Lorentz-Poincare symmetry that includes locally rotating frames as well as translating ones.

Indeed, the quantum theory of angular momentum has a built-in duality that is as fundamental as the left-and-right or bra-and-ket duality of the conjugate parts of Dirac's elegant quantum notation  $\langle A|B \rangle$ . The Wigner  $D_{m,n}^J$ -functions are quantum rotor wavefunctions  $D_{m,n}^{J*}(\alpha\beta\gamma)$  that have their external laboratory  $m$ -quantum numbers on the left and their internal or body  $n$ -quantum numbers on the right. Their  $J$ -multiplicity is thus  $(2J+1)$ -squared and not simply the  $(2J+1)$  so familiar in elementary Schrodinger quantum theory of atomic angular momentum.

It took many years for classical physics to fully accept Einstein's translational relativity principles. Perhaps, if the wave nature of quantum physics had already been established, the relativistic axioms would have been seen as an immediate consequence of wave interference. Indeed, these two subjects are, perhaps, *too* closely related for that to have happened.

Now quantum theory demands a more general kind of relativity involving rotation and other accelerations that is a step beyond the special relativity of constant velocity. This brings up a quite controversial area first explored by Ernst Mach, the originator of *Mach's Principle*. Mach made the seemingly impossible proposal that centrifugal forces, the kind physicists assign the label *fictitious force*, are somehow due to their relativity to all matter in the universe.

Mach's idea may sound silly, but a kind of quantum Mach's Principle is needed to understand spectra and dynamics of quantum rotor  $D'_{m,n}$  waves even in the non-relativistic limit. We are unaware of any fully relativistic quantum treatment of such systems, and it is not clear what if anything would be the cosmological implication of such a grand relativistic quantum wave mechanics. Nevertheless, it seems that the dual 4-by-4 wave-anti-wave space of Dirac is one of the first to re-examine.

Physics is still at a stage where large-scale phenomena use Newton-Einstein particle-in-manifold theory while small-scale phenomena employ Planck-DeBroglie-Schrodinger wave field theory. However, both employ some form of space and time coordinates. In this they share an enigma whose existence is largely unquestioned. Supposed invariance to reference frame definition is taken to mean that underlying frames don't matter.

That leaves our fundamental metrology in a dysfunctional dysphoria of an ignored spouse, indispensable, but having only marginal identity. If Evenson and Einstein have taught us anything, it is that this has to be a mistake. Frames *do* matter! The results of Dirac and many others have shown they *make* matter and indeed *are* our matter.

## References

- Mark K. M. Evenson, J.S. Wells, F.R. Peterson, B.L. Danielson, G.W. Day, R.L. Barger and J.L. Hall, Phys. Rev. Letters 29, 1346(1972).
- Mark Guinness Book of Records (1973).
- Mark Glauber, Roy J., Hall, John L. and Hansch, Theodor W. *The Nobel Prize in Physics, 2005*. <http://nobelprize.org/>
- Mark J. L. Hall and T. Hensch, Opt. Lett. 9, 502-504 (1984).
- Mark N. Ashby, *Physics Today*, 55(5): 41 (May 2002).
- Mark J. L. Hall, Laser Spectroscopy VII, (T. W. Hansch and Y. R. Shen, Eds., Springer-Verlag, 1985), pp. 393-394.
- Mark William of Occam (1245-1326) "*Pluralitas non est ponenda sine neccesitate*" (Do not assume plurality without necessity.)
- Mark A. Cho, Science 306, 1461 (2004).
- Mark A. Einstein, Annalen der Physik 17,891(1905). (Translation by W. Perrett and G.B. Jeffery, *The Principle of Relativity*(with notes by A. Sommerfield) (Methuen, London 1923), (republished by Dover, London 1952).
- Mark W. G. Harter, J. Mol. Spectrosc. 210, 166(2001).
- Mark W. G. Harter, J. Evans, R. Vega, and S. Wilson, Am. J. Phys. 53, 671(1985).
- Mark W.G. Harter and T. C. Reimer, //www.uark.edu/ua/pirelli/html/poincare\_inv\_2.htm
- Mark D. E. Herschbach, (unpublished, 2005).
- Mark H. Minkowski, *Mathematisch-Physikalische Klasse*, vol. 1, 53 (1908).
- Mark H. A. Lorentz Koninklijke Akademie van Wetenschappen te Amsterdam. Section of Science. Proc. 6: 809-831 (1904).
- Mark Albert Einstein "*Zur Elektrodynamik bewegter Korper.*" Annalen der Physik 18,639 (1905); Annalen der Physik 17,891(1905). (Translation: Perrett and Jeffery, *The Principle of Relativity*, (Methuen, London 1923), (Dover, 1952).
- Mark Max Planck "*Zur Theorie des Gesetzes der Energieverteilung im Normal-spectrum.*" Deutsche Physikalische Gesellschaft. Verhandlungen 2: 237-245 (1900).
- Mark Louis de Broglie, Nature 112, 540 (1923); Annalen der Physik (10) 2 (1923).
- Mark P. A. M. Dirac, "Forms of Relativistic Dynamics" *Rev. Mod. Physics*, 21: 392 (1949).
- Mark Albert Einstein "*Über einen die Erzeugung und Verwandlung des Lichtes betreffenden heuristischen Gesichtspunkt.*" Annalen der Physik 17: 132-148 (1905). (Translation by A.B. Aarons and M.B. Peppard, Am. J. Phys. 33, 367(1965).)
- Mark E. Schrodinger, Annalen der Physik (4) 79 361 and 489 (1923); 80, 437 (1926); 81,109 (1926).
- Mark Schrodinger's protests about prevailing quantum mechanical interpretations are widely circulated. So far we have been unable to locate more solid references.
- Mark N. Bohr, *Zeitschrift fur Physik*, 9, 1-2, (1922).
- Mark W. Heisenberg, *The Physical Principles of the Quantum Theory*, (Dover, New York, 1930).
- Mark P.A.M. Dirac, *Lectures on quantum mechanics*, (New York, Belfer Graduate School of Science, Yeshiva University, 1964). Dirac's first text in 1931 used  $\alpha$  and  $\beta$  to denote bra-ket duality.
- Mark A. Einstein, "*I shall never believe that god plays dice with the universe*" Albert Einstein Archives, The Jewish National & University Library, The Hebrew University of Jerusalem ([www.albert-einstein.org](http://www.albert-einstein.org)), Einstein Archives Online, Volume 15, #294, Letter to Cornelius Lanczos, March 21, 1942, <http://www.alberteinstein.info/db/ViewDetails.do?DocumentID=30893>.
- Mark R. Feynman, *The Pleasure of Finding Things Out*, (Perseus Publishing, Cambridge, MA,1999) p. 8.
- Mark (unpublished) A huge energy shift is used for sake of geometric clarity. Atoms usually lose less than one part in  $10^9$  or  $10^{10}$  of their rest mass in optical emission. The atom in the example loses rest mass  $1/2 M_2c^2$  emitting a  $3/8 M_2c^2$  photon.
- Mark R. P. Feynman, R. Leighton, and M. Sands, *The Feynman Lectures* (Addison Wesley 1964) Our development owes a lot to Feynman's treatment cavity wave dispersion in Vol. II Ch. 24 and Vol. III Ch. 7.
- Mark W. Rindler, *Essential Relativity-Special, General, and Cosmological*, Springer (New York 1977) p. 18. See also ref. 8, p. 111.
- Mark E.F.Taylor and J.A. Wheeler, *Spacetime Physics* (W. H. Freeman San Francisco 1966) p. 18.

## Acknowledgements

The author would like to thank Ronald F. Fox and Eric J. Heller for careful reading and suggestions regarding early versions of this work and Daniel Kennefick for information from the Einstein Centennial bibliography project. Also, I appreciate many years of discussion with John E. Heighway about aspects of special and general relativity. Finally, I am grateful to Molly Longstreth and Usha Gupta for help with general bibliographic search.

## -- The Purest Light and a Resonance Hero – Ken Evenson (1932-2002) --

When travelers punch up their GPS coordinates they owe a debt of gratitude to an under sung hero who, alongside his colleagues and students, often toiled 18 hour days deep inside a laser laboratory lit only by the purest light in the universe.

Ken was an “Indiana Jones” of modern physics. While he may never have been called “Montana Ken,” such a name would describe a real life hero from Bozeman, Montana, whose extraordinary accomplishments in many ways surpass the fictional characters in cinematic thrillers like *Raiders of the Lost Arc*.

Indeed, there were some exciting real life moments shared by his wife Vera, one together with Ken in a canoe literally inches from the hundred-foot drop-off of Brazil’s largest waterfall. But, such outdoor exploits, of which Ken had many, pale in the light of an in-the-lab brilliance and courage that profoundly enriched the world.

Ken is one of few researchers and perhaps the only physicist to be twice listed in the *Guinness Book of Records*. The listings are not for jungle exploits but for his lab’s highest frequency measurement and for a speed of light determination that made  $c$  many times more precise due to his lab’s pioneering work with John Hall in laser resonance and metrology<sup>†</sup>.

The meter-kilogram-second (mks) system of units underwent a redefinition largely because of these efforts. Thereafter, the speed of light  $c$  was set to  $299,792,458\text{ms}^{-1}$ . The meter was defined in terms of  $c$ , instead of the other way around since his time precision had so far trumped that for distance. Without such resonance precision, the Global Positioning System (GPS), the first large-scale wave space-time coordinate system, would not be possible.

Ken’s courage and persistence at the Time and Frequency Division of the Boulder Laboratories in the National Bureau of Standards (now the National Institute of Standards and Technology or NIST) are legendary as are his railings against boneheaded administrators who seemed bent on thwarting his best efforts. Undaunted, Ken’s lab painstakingly exploited the resonance properties of metal-insulator diodes, and succeeded in literally counting the waves of near-infrared radiation and eventually visible light itself.

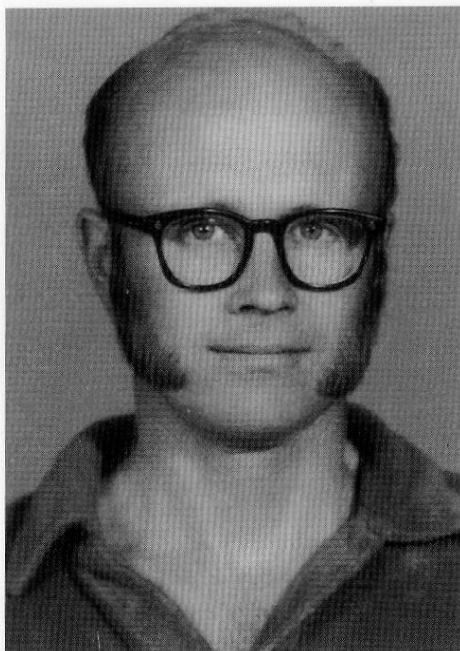
Those who knew Ken miss him terribly. But, his indelible legacy resonates today as ultra-precise atomic and molecular wave and pulse quantum optics continue to advance and provide heretofore unimaginable capability. Our quality of life depends on their metrology through the Quality and Finesse of the resonant oscillators that are the heartbeats of our technology.

Before being taken by Lou Gehrig’s disease, Ken began ultra-precise laser spectroscopy of unusual molecules such as  $\text{HO}_2$ , the radical cousin of the more common  $\text{H}_2\text{O}$ . Like Ken, such radical molecules affect us as much or more than better known ones. But also like Ken, they toil in obscurity, illuminated only by the purest light in the universe.

In 2005 the Nobel Prize in physics was awarded to Glauber, Hall, and Hensch<sup>††</sup> for laser optics and metrology.

<sup>†</sup> K. M. Evenson, J.S. Wells, F.R. Peterson, B.L. Danielson, G.W. Day, R.L. Barger and J.L. Hall, *Phys. Rev. Letters* 29, 1346(1972).

<sup>††</sup> *The Nobel Prize in Physics, 2005*. <http://nobelprize.org/>



PAULINIA, BRASIL 1976

THE SPEED OF LIGHT IS  
299,792,458 METERS PER SECOND!

*Kenneth M. Evenson – 1932-2002*



- <sup>i</sup> A. Einstein, *Annalen der Physik* 17,891(1905). (Translation by W. Perrett and G.B. Jeffery, *The Principle of Relativity*(with notes by A. Sommerfeld) (Methuen, London 1923), (republished by Dover, London 1952).
- <sup>ii</sup> W. G. Harter, *J. Mol. Spectrosc.* 210, 166(2001).
- <sup>iii</sup> W. G. Harter, J. Evans, R. Vega, and S. Wilson, *Am. J. Phys.* 53, 671(1985).
- <sup>iv</sup> W.G. Harter and T. C. Reimer, //www.uark.edu/ua/pirelli/html/poincare\_inv\_2.htm
- <sup>v</sup> D. E. Herschbach, (unpublished, 2005).
- <sup>vi</sup> H. Minkowski, *Mathematisch-Physikalische Klasse*, vol. 1, 53 (1908).
- <sup>vii</sup> H. A. Lorentz Koninklijke Akademie van Wetenschappen te Amsterdam. Section of Science. Proc. 6: 809-831 (1904).
- <sup>viii</sup> Albert Einstein "*Zur Elektrodynamik bewegter Körper.*" *Annalen der Physik* 18,639 (1905); *Annalen der Physik* 17,891(1905). (Translation: Perrett and Jeffery, *The Principle of Relativity*, (Methuen, London 1923), (Dover, 1952).
- <sup>ix</sup> Max Planck "*Zur Theorie des Gesetzes der Energieverteilung im Normal-spectrum.*" Deutsche Physikalische Gesellschaft. *Verhandlungen* 2: 237-245 (1900).
- <sup>x</sup> Louis de Broglie, *Nature* 112, 540 (1923); *Annalen der Physik* (10) 2 (1923).
- <sup>xi</sup> P. A. M. Dirac, "Forms of Relativistic Dynamics" *Rev. Mod. Physics*, 21: 392 (1949).
- <sup>xii</sup> Albert Einstein "*Über einen die Erzeugung und Verwandlung des Lichtes betreffenden heuristischen Gesichtspunkt.*" *Annalen der Physik* 17: 132-148 (1905). (Translation by A.B. Aarons and M.B. Peppard, *Am. J. Phys.* 33, 367(1965).)
- <sup>xiii</sup> E. Schrodinger, *Annalen der Physik* (4) 79 361 and 489 (1923); 80, 437 (1926); 81,109 (1926).
- <sup>xiv</sup> Schrodinger's protests about prevailing quantum mechanical interpretations are widely circulated. So far we have been unable to locate more solid references.
- <sup>xv</sup> L. C. Epstein, *Relativity Visualized*. (Insight Press 1981)
- <sup>xvi</sup> N. Bohr, *Zeitschrift für Physik*, 9, 1-2, (1922).
- <sup>xvii</sup> W. Heisenberg, *The Physical Principles of the Quantum Theory*, (Dover, New York, 1930).
- <sup>xviii</sup> P.A.M. Dirac, *Lectures on quantum mechanics*, (New York, Belfer Graduate School of Science, Yeshiva University, 1964). Dirac's first text in 1931 used  $\alpha$  and  $\beta$  to denote bra-ket duality.
- <sup>xix</sup> A. Einstein, "*I shall never believe that god plays dice with the universe*" Albert Einstein Archives, The Jewish National & University Library, The Hebrew University of Jerusalem (www.albert-einstein.org), Einstein Archives Online, Volume 15, #294, Letter to Cornelius Lanczos, March 21, 1942,http://www.alberteinstein.info/db/ViewDetails.do?DocumentID=30893.
- <sup>xx</sup> R. Feynman, *The Pleasure of Finding Things Out*, (Perseus Publishing, Cambridge, MA,1999) p. 8.
- <sup>xxi</sup> (unpublished) A huge energy shift is used for sake of geometric clarity. Atoms usually lose less than one part in  $10^9$  or  $10^{10}$  of their rest mass in optical emission. The atom in the example loses rest mass  $1/2 M_2c^2$  emitting a  $3/8 M_2c^2$  photon.
- <sup>xxii</sup> R. P. Feynman, R. Leighton, and M. Sands, *The Feynman Lectures* (Addison Wesley 1964) Our development owes a lot to Feynman's treatment cavity wave dispersion in Vol. II Ch. 24 and Vol. III Ch. 7.
- <sup>xxiii</sup> W. Rindler, *Essential Relativity-Special, General, and Cosmological*, Springer (New York 1977) p. 18. See also ref. 8, p. 111.

xxiv E.F.Taylor and J.A. Wheeler, *Spacetime Physics* (W. H. Freeman San Francisco 1966) p. 18.

## Acknowledgements

The author would like to thank Ronald F. Fox and Eric J. Heller for careful reading and suggestions regarding early versions of this work and Daniel Kennefick for information from the Einstein Centennial bibliography project. Also, we are grateful to Molly Longstreth and Usha Gupta for help with bibliographic search.

### Figure Captions

Fig. 1. Comparison of wave archetypes and related axioms of relativity.

(a) Pulse Wave (PW) peaks locate where a wave is. Their speed is  $c$  for all observers.

(b) Continuous Wave (CW) zeros locate where it is not. Their speed is  $c$  for all colors (or observers.)

Fig. 2. Pulse Wave (PW) as a sum of 12 Fourier CW's (a) PW parts: real  $\text{Re}\Psi$ , imaginary  $\text{Im}\Psi$ , and magnitude  $|\Psi|$ .

(b) CW phasor clocks plot real vs. imaginary parts of wave amplitude  $\Psi$ .

Fig. 3. Wave addition of counter propagating Fourier components.

(a) 2-PW Sum has binary sum has 4 values (0,0), (0,1), (1,0), (1,1) and diamond grid of peak paths on a plane of zeros.

(b) 2-CW Sum and interference has value continuum and square grid of zeros.

Fig. 4. "Fictitious" sources and their wave coordinate lattices in (a) Spacetime and (b) Per-spacetime.

CW lattices of phase-zero and group-node paths intermesh with PW lattices of "particle" or pulse wave paths.

Fig. 5. Co-propagating laser beams produce a collapsed wave lattice since all parts have same speed  $c$ .

Fig. 6. Laser lab view of 600THz CW and PW light waves in per-space-time (a-b) and space-time (c-d).

Fig. 7. Atom view of 600THz CW and PW light waves in per-spacetime (a-b) and space-time (c-d) boosted to  $u=3c/5$ .

Fig. 8. Wave phasor addition. (a) Each phasor in a wave array is a sum (b) of two component phasors.

(c) In phasor-relative views either  $A$  or else  $B$  is fixed. An evolving sum-and-difference rectangle is inscribed in the (dashed) circle of the phasor moving relative to the fixed one.

Fig. 9. Doppler shift b-matrix for a linear array of variously moving receiver-sources.

Fig. 10. (a) Euclidian mean geometry for counter-moving waves of frequency 1 and 4. (300THz units).

Fig. 10. (b) Geometry for the CW wave coordinate axes in Fig. 7.

Fig. 11. (a) Horizontal G-hyperbolas for proper frequency  $B=v$  and  $2B$  and vertical P-hyperbolas for proper wavevector  $k$ .

(b) Tangents for G-curves are loci for P-curves, and vice-versa.

Fig. 12. Dispersion hyperbolas for 2-CW interference (a) Laser lab view. (b) Atom frame view.

Fig. 13. Geometry of contact transformation between relativistic (a) Hamiltonian (b) Lagrangian.

Fig. 14. "True" paths carry extreme phase and fastest phase clocks. Light-cone has only stopped clocks.

Fig. 15. Quantum waves interfere constructively on "True" path but mostly cancel elsewhere.

Fig. 16. Trigonometric geometry (a) Unit circular area  $\phi=0.86$ . (b) Unit hyperbolic area  $\rho=0.99$ .

Fig. 17. Relativistic wave mechanics geometry. (a) Overview. (b) Details of contact transform tangents.

Fig. 18. Monochromatic (1-frequency) 2-CW wave space-time patterns.

Fig. 19. Dichromatic (2-frequency) 2-CW wave space-time patterns.

Fig. 20. (a-g) Elliptic polarization ellipses relate to galloping waves in Fig. 18. (h-i) Kepler anomalies.

Fig. 21. Cavity 2-CW modes. (a) Invariant "mass" hyperbolas. (b) COM frame. (c) ISOC frame.

Fig. 22. Optical cavity energy hyperbolas for mode number  $n=1-3$  and photon number  $Nn=0, 1, 2, \dots$

Fig. 23. Simulated spacetime photon counts for coherent (a-c) and photon-number states (d).

Fig. 24. Optical cavity model of (a) Emission, (b) Absorption, and (c) Compton scattering

Fig. 25. Compton scattering. (a) Vector sums on mass hyperbolas of low  $\omega_\ell$ , medium  $\omega_m$ , and high  $\omega_h$ .

(b-c) Feynman graphs. (d) Center of Momentum (COM) vector sums. (e-f) COM Feynman graphs.

Fig. 26. Compton nets are congruent Compton staircases of transitions. (a)  $f=2:1$  (b)  $f=\sqrt{2}:1$ .

Fig. 27. Optical wave frames by red-and-blue-chirped lasers (a) Varying acceleration (b) Constant  $g$ .

Fig. 28. Accelerated reference frames and their trajectories painted by  $e^{\pm\phi}$ -chirped coherent light.